

FINITE-DIFFERENCE MODEL OF CELL DEHYDRATION DURING CRYOPRESERVATION

A Thesis
Presented to
The Academic Faculty

by

Kevin A. Carnevale

In Partial Fulfillment
Of the Requirements for the Degree
Masters of Science in the
School of Mechanical Engineering

Georgia Institute of Technology

May, 2004

Finite-Difference Model of Cell Dehydration During Cryopreservation

Approved by:

Dr. Jens O. M. Karlsson, Advisor

Dr. Timothy M. Wick

Dr. H.S. Udaykumar

Date Approved 4/19/2004

ACKNOWLEDGMENT

I wish to express special appreciation to my advisor Dr. J.O.M. Karlsson for his unfaltering support, guidance, and insight. I wish to thank the members of my thesis committee: Dr. T. M. Wick, and Dr. H.S. Udaykumar for their recommendations and input regarding my work. I wish to thank Prof. Alex J. Fowler (U.Mass-Dartmouth) for his suggestions in obtaining a numerical solution to the highly nonlinear partial differential equation of our model. I wish to acknowledge that this work was funded from an NSF CAREER Award, BES-0242377.

I wish to thank my colleagues at the Biothermal Sciences Laboratory, Adam Higgins, Shannon Stott, Megan Sumpter, and Jonathan Barletta for their valuable discussions.

Finally, I wish to thank my parents and family for the support, love, and sacrifices they made that aided me through my education.

TABLE OF CONTENTS

Acknowledgements	iii
List of Tables	vi
List of Figures	vii
List of Variables	ix
Summary	xii
Chapter 1 Introduction	1
1.1 Background	1
1.2 Mathematical Modeling	4
1.3 Scope and Outline of Current Study	10
Chapter 2 Theoretical Background	13
2.1 Membrane-Limited Transport Model	13
2.2 Diffusion-Limited Transport Model	15
2.3 Constitutive Equations	16
2.3.1 Membrane Permeability	16
2.3.2 Cytoplasmic Viscosity	18
2.3.3 Chemical Potential	20
2.3.4 Supercooling	21
2.4 Dimensional Analysis	22
2.4.1 Characteristic Scales and Dimensionless Groups	22
2.4.2 Membrane-Limited Transport Model	24
2.4.3 Diffusion-Limited Transport Model	27
Chapter 3 Numerical Methods	31
3.1 Introduction	31
3.2 Spatial Discretization	31
3.2.1 Finite Difference Scheme	31
3.2.2 Discretization of Diffusion Equation	34
3.2.3 Discretization of Boundary Condition at $x = 0$	37
3.2.4 Discretization of Boundary Condition at $x = 1$	38
3.3 Temporal Discretization	40
3.4 Integration of Cell Properties	46
Chapter 4 Simulations with Constant Biophysical Properties	49

Chapter 5 Simulations with Temperature- and Concentration- Dependent Biophysical Properties	54
5.1 Comparison with Experimental Data	54
5.2 Simulations in Large Biot Number Regimes	57
Chapter 6: Parametric Analysis of Mass Transport Regimes During Cell Freezing	64
6.1 Nominal Values	64
6.2 Supercooling Predictions in the Four-Dimensional Parametric Space	65
Chapter 7: Discussion	77
Chapter 8: Conclusions/ Future Studies	85
Appendix A Code	87
References	110

LIST OF TABLES

Table 1	Biophysical properties of yeast cells (<i>S. cerevisiae</i>) (Levin, 1979)	55
Table 2	Biophysical parameters for hypothetical cell type (Kasharin and Karlsson, 1998)	57
Table 3	Physiologic range of cell biophysical properties and Cryopreservation conditions	64
Table 4	Ranges and nominal values of nondimensional parameters used in simulations	65
Table 5	Ranges of dimensionless parameters used in simulations Shown in Figures 11-16	68

LIST OF FIGURES

Figure 1	Illustration of ϕ_{sphere} containing NaCl and one water molecule.	20
Figure 2	Illustration of the nodal spacing.	32
Figure 3	Predicted volume fraction of intracellular water at the cell membrane, as a function of nondimensional time, for $Bi = 1000$ and $\Delta\tilde{\mu} = -0.01$. Shown are solutions obtained using our finite difference model (solid line) and using the finite element solver FEMLAB (dotted line).	51
Figure 4	Predicted volume fraction of intracellular water at the cell membrane, as a function of nondimensional time, for $Bi = 10,000$ and $\Delta\tilde{\mu} = -0.01$. Shown are solutions obtained using our finite difference model (solid line) and using the finite element solver FEMLAB (dotted line).	52
Figure 5	Maximum variation in intracellular salt content during cell dehydration with $Bi = 10^5$ and $\Delta\tilde{\mu} = -0.01$, simulated using our finite differences model with different grid spacings and time step sizes. The nondimensional time steps were $\Delta\tau = 10^{-2}$ (dash-double-dotted line); $\Delta\tau = 10^{-4}$ (dash-dotted line); $\Delta\tau = 10^{-6}$ (solid line); $\Delta\tau = 10^{-8}$ (dashed line); and $\Delta\tau = 10^{-10}$ (dotted line).	53
Figure 6	Comparison of numerical predictions (solid line) and experimental measurements (circles) of the normalized cell volume of yeast cells cooled at a rate of (a) $10^\circ\text{C}/\text{min}$, and (b) $100^\circ\text{C}/\text{min}$.	56
Figure 7	Predictions of intracellular water volume (normalized to its initial value) obtained using the finite-difference diffusion model (solid line) and Mazur's membrane-limited transport model (dotted line), for a hypothetical cell type with $\theta_M = 3 \times 10^{-2}$, $\theta_D = 4 \times 10^{-5}$. (a) Original finite-difference model; (b) Modified finite-difference model, including adaptive step size in diffusion-limited transport regime and new boundary conditions with provisions for non-uniform vitrification. Arrows indicate temperature at which $\delta t_D > \delta t_M$ (1) and temperature at which vitrification occurs at node $i = N - 1$ (2).	61
Figure 8	Predictions of intracellular water volume (normalized to its initial value) obtained using the finite-difference diffusion model (solid line) and Mazur's membrane-limited transport model (dotted line), for a hypothetical cell type with $\theta_M = 3 \times 10^{-2}$, $\theta_D = 4$. Arrows indicate temperature at which $\delta t_D > \delta t_M$ (1) and temperature at which vitrification occurs at node $i = N - 1$ (2).	62

Figure 9	Predicted variations in water volume fraction at nodes $i = 0$ (solid line), $i = N - 2$ (dotted line) and $i = N - 1$ (dashed line), for finite-difference simulation in Figure 8 ($\theta_M = 3 \times 10^{-2}$, $\theta_D = 4$).	63
Figure 10	Contour plot of the difference in nondimensional intracellular supercooling predictions between a membrane-limited model and the model under study (predicted supercooling was normalized relative to the characteristic temperature $T_c = 100$ K). Predictions are based on $\theta_D = 10^{-2}$ and $\varepsilon_D = 9$.	70
Figure 11	Contour plot of the difference in nondimensional intracellular supercooling predictions between a membrane-limited model and the model under study (normalized relative to the characteristic temperature). Predictions are based on $\theta_D = 10^{-1}$ and $\varepsilon_D =$ (a) 9, (b) 6, (c) 3.	71
Figure 12	Contour plot of the difference in nondimensional intracellular supercooling predictions between a membrane-limited model and the model under study (normalized relative to the characteristic temperature). Predictions are based on $\theta_D = 10^{-3}$ and $\varepsilon_D =$ (a) 9, (b) 6, (c) 3.	72
Figure 13	Contour plot of the difference in intracellular supercooling predictions between a membrane-limited model and the model under study (normalized to characteristic temperature). Predictions are based on $\theta_D = 10^{-5}$ and $\varepsilon_D =$ (a) 9, (b) 6, (c) 3.	73
Figure 14	Contour plot of the difference in intracellular supercooling predictions between a membrane-limited model and the model under study (normalized to T_c). Predictions are based on $\theta_D = 10^{-7}$ and $\varepsilon_D =$ (a) 9, (b) 6, (c) 3.	74
Figure 15	Contour plot of the difference in intracellular supercooling predicted by a membrane-limited model and the model under study. (normalized to T_c) Predictions are based on $\theta_D = 10^{-9}$ and $\varepsilon_D =$ (a) 9, (b) 6, (c) 3.	75
Figure 16	Contour plot of the difference in intracellular supercooling predictions between a membrane-limited model and the model under study (normalized to T_c). Predictions are based on $\theta_D = 10^{-11}$, $\varepsilon_D =$ (a) 9, (b) 6, (c) 3.	76

LIST OF SYMBOLS

α	= scaling factor
β	= ratio of Vogel-Fulcher critical temperature to glass transition temperature
ΔH_f	= molar specific heat of fusion of water
$\Delta \tilde{H}_f$	= nondimensional heat of fusion
$\Delta \mu$	= transmembrane chemical potential difference
$\Delta \tilde{\mu}$	= nondimensional transmembrane chemical potential difference
Δr	= distance between r_{outer} and r_{inner}
Δt^n	= real time step between the nondimensional time n and $n-1$
$\Delta \tau^n$	= nondimensional time step between nondimensional times n and $n-1$
Δx_i	= spacing between nodes i and $i-1$
Δx_{i+1}	= spacing between nodes $i+1$ and i
δt_D	= time scale for diffusion transport
δt_M	= time scale for membrane transport
δt_B	= time scale for freezing process
ε_M	= membrane Arrhenius number
ε_D	= diffusivity Arrhenius number
η	= cytoplasmic viscosity
$\tilde{\eta}$	= cytoplasmic viscosity
η_w	= temperature dependent water viscosity
γ	= dimension of problem
χ_w	= mole fraction of intracellular water
ϕ	= water volume fraction
ϕ_R	= water volume fraction at cell membrane
ϕ_i^n	= water volume fraction at node i and nondimensional time n
ϕ_{so}	= initial salt volume fraction
ϕ_{sphere}	= volume fraction of hydrated sodium ions
μ_{ice}	= chemical potential of extracellular ice
μ_w	= chemical potential of water
μ_o	= chemical potential of pure water
v_w	= molar specific volume of water
v_s	= molar specific volume of salt
σ_s	= salt dissociation constant
τ	= nondimensional time
τ^n	= nondimensional time after n time steps
θ_M	= characteristic parameter for the time scale of membrane transport
θ_D	= characteristic parameter for the time scale of diffusion transport
Φ^{n+1}	= vector of unknown water volume fractions at future time step
A	= cell surface area
\tilde{A}	= nondimensional cell surface area
A_o	= initial cell surface area
a_o	= apparent hydrodynamic radius of water

A_∞	=	limiting viscosity
B	=	cooling rate
Bi	=	Biot number
Bi_{eff}	=	effective Biot number
c_w	=	concentration of water
c_{w0}	=	initial water concentration
c_s	=	salt concentration
c_{s0}	=	initial salt concentration
D	=	diffusivity
D_o	=	dimensional diffusion coefficient at the cell center
D_R	=	dimensional diffusion coefficient at the cell membrane
D_c	=	characteristic diffusion coefficient
\tilde{D}	=	nondimensional diffusion coefficient
\tilde{D}_o	=	nondimensional diffusion coefficient at the cell center
\tilde{D}_i	=	nondimensional diffusion coefficient at node i
E	=	activation temperature
E_a	=	membrane activation energy
e_{mass}	=	mass conservation error
f	=	Lagrangian function
f_j	=	Lagrangian function evaluated at $x = x_j$
f_k	=	Lagrangian function evaluated at $x = x_k$
f_l	=	Lagrangian function evaluated at $x = x_l$
$g(x, \tau)$	=	right hand side of the discretized governing equation at time τ
h	=	effective number of water molecules in the hydration shell
i	=	spatial designation for nodal number
j	=	designation for first of three points fit by the Lagrange polynomial
J_w	=	molar water flux
k	=	designation for second of three points fit by the Lagrange polynomial
k_e	=	Einstein's shape factor for single spheres
k_B	=	Boltzmann's constant
l	=	designation for third of three points fit by the Lagrange polynomial
λ	=	hydrodynamic interaction constant
L_j	=	Lagrangian multiplier for $x = x_j$
L_k	=	Lagrangian multiplier for $x = x_k$
L_l	=	Lagrangian multiplier for $x = x_l$
L_p	=	membrane permeability
L_∞	=	limiting membrane permeability at infinite temperature
N	=	number of nodes
n	=	temporal designation for time step
P	=	matrix of coefficients
$P_{i,i}$	=	element in row i and column i of matrix P
Q	=	right hand side vector
Q_i	=	element in row i of the vector Q
$q(x, \tau)$	=	the diffusive terms of the right hand side of the discretized governing equation

R	=	dimensional cell radius
R_g	=	universal gas constant
R_o	=	initial cell radius
\tilde{R}	=	nondimensional cell radius
r	=	radial position in cell
r_{outer}	=	outer radius of a spherical subshell of the cell
r_{inner}	=	inner radius of a spherical subshell of the cell
T	=	temperature
T_g	=	glass transition temperature
T_o	=	equilibrium freezing temperature of water
T_{eq}	=	equilibrium freezing temperature of the supercooled liquid
ΔT	=	degree of supercooling
T_c	=	characteristic temperature interval
\tilde{T}	=	nondimensional temperature
\tilde{T}_g	=	nondimensional glass transition temperature
\tilde{T}_o	=	nondimensional pure water equilibrium temperature
t	=	time
t^n	=	real time after n nondimensional time steps
V	=	cell volume
V_o	=	initial cell volume
V_b	=	osmotically inactive volume
\tilde{V}	=	nondimensional cell volume
\tilde{V}_w	=	nondimensional water volume
\tilde{V}_s	=	nondimensional salt volume
\tilde{V}_{so}	=	initial nondimensional salt volume
\tilde{V}_b	=	ratio of inactive cell volume to initial cell volume
x	=	nondimensional location within cell
x_i	=	nondimensional location at node I
$y(x, \tau)$	=	the convective terms of the right hand side of the discretized governing equation

SUMMARY

A numerical model for describing the kinetics of intracellular water transport during cryopreservation was developed. As ice is formed outside the cell, depleting the extracellular liquid of water, the cell will experience an osmotic pressure difference across its membrane, which causes cell dehydration and concomitant shrinkage. Although Mazur (1963) has previously modeled this phenomenon as a two-compartment system with membrane limited transport, the assumption of well-mixed compartments breaks down at large Biot numbers. Therefore, we have developed a numerical solution to this moving-boundary problem, including diffusive transport in the intracellular liquid, in addition to the osmotically driven membrane flux. Our model uses a modified Crank-Nicolson scheme with a non-uniform Eulerian-Lagrangian grid, and is able to reproduce predictions from Mazur's model at low Biot numbers, while generating novel predictions at high Biot numbers. Given that cell damage may result from excessive water loss, our model can be used to predict freezing methods that minimize the probability of cell injury during the cryopreservation process.

CHAPTER 1

INTRODUCTION

1.1 Background

Cryobiology is the study of the biological response of organisms to low temperatures. Depending on the exact experimental conditions, extreme cold can be used to either destroy or preserve cells. By exploiting the deleterious effects of subzero temperatures to purposely damage cells, cryobiologists have applied cold to ablate tumors, treat tachyarrhythmias, act as an immunosuppressant, promote angiogenesis, and control myogenesis (Gage, 2004). On the other hand, the applications of cryogenic processing for cell preservation extend to cell transplantation, in vitro fertilization, preservation of cell lines for biological research or agricultural applications, and preservation of germplasm to maintain biodiversity. Cryopreservation has also been identified as a critical enabling technology for tissue engineering, where the ability to store tissue constructs for prolonged periods of time is a prerequisite for the mass-production, quality-control testing, distribution, and banking of tissue engineered products (Karlsson and Toner, 2000). It is clear that the potentially destructive effects of cryogenic processing must be avoided when freezing biological materials for purposes of cryopreservation. Given that the most abundant substance in biological materials is water, the biophysical response of cells to cryopreservation is determined primarily by phase transformations and transport of biological water.

During the freezing process, ice initially forms in the extracellular medium. As the extracellular ice grows, the amount of water in the remaining unfrozen solution is reduced, thereby increasing the extracellular solute concentration. This increase in solute

concentration imposes a chemical potential difference between the cytosol and unfrozen external solution, which acts as a driving force for transport of solutes into the cell and for diffusion of water out of the cell. The magnitude of the corresponding flux is determined by properties of the cell's plasma membrane, which acts as a barrier to transport. The membrane permeability to water and solutes has an Arrhenius-type temperature dependence. As a result of differences in the corresponding activation energies, the permeability of the cell membrane is significantly larger for water transport than for solute transport at subzero temperatures. Consequently, the cell membrane acts as if it were semipermeable, and the cellular response to an increase in extracellular tonicity caused by ice growth is primarily to express water through its plasma membrane via osmosis (Mazur, 1963; Levin, 1976).

The rate of the osmotically induced water efflux is limited by the permeability of the plasma membrane to water. Thus, because the freezing-induced extracellular hypertonicity increases with decreasing temperature, there is sufficient time available for maintaining equilibrium only if the rate of cooling is slow. On the other hand, if the time scale for the cooling process is short compared to the time scale for membrane transport, low temperatures are reached before significant dehydration can occur, and thus the cytoplasm attains nonequilibrium states. In such supercooled states, the actual temperature of the cytoplasm is less than its equilibrium freezing point temperature, resulting in a driving force for intracellular ice formation (IIF). Moreover, since ice formation is a stochastic process, the greater the amount of water inside the cell the greater the likelihood that ice nucleation will occur. This means that for rapid freezing

processes, during which a significant amount of water is retained within the cell, the likelihood of IIF will be greater than for a protocol which uses a slow freezing rate.

In 1972, Mazur *et al.* measured the survival of cells frozen as a function of cooling rate and found the post-thaw viability of cells to be poor for cells frozen with fast cooling rates and for cells frozen with very slow cooling rates, with the highest survival observed at an intermediate cooling rate (Mazur *et al.*, 1972). These authors speculated that the injury associated with high cooling rates was a consequence of IIF, while the injury associated with slow cooling rates was a consequence of excessive dehydration, which was thought to overexpose the cell to harmful concentrations of electrolyte and other solutes. The latter mechanism of injury is commonly referred to as “solution effects”.

In 1949, Polge *et al.* accidentally discovered that introduction of glycerol into the freezing media of rooster spermatozoa resulted in significant improvement in the recovery of viable cells after cryopreservation. Since then, many other chemicals have been found to exhibit cryoprotective properties, yet glycerol and dimethyl sulfoxide remain the most common cryoprotectant additives used to date. It is believed that these cryoprotectants reduce the intracellular concentration of water, thus reducing the rate at which the remaining water molecules can form damaging ice crystals, and that they act as a solvent to dilute the intracellular electrolytes when water is removed, thus protecting the cell from solution effects injuries (Mazur, 1984). On the other hand, when used in high concentrations, cryoprotectants can be cytotoxic.

1.2 Mathematical Modeling

To optimize a cryopreservation protocol, the values of all parameters required to fully describe the procedures for chemical and thermal processing must be established. Because these parameters can be numerous and interdependent, empirical optimization typically requires a factorial design with a prohibitively large number of candidate protocols to evaluate. Complicating matters is the fact that each cell species possesses distinct biophysical properties (membrane permeability, surface-to-volume ratio, cytoplasmic viscosity, etc.) characteristic of its biological function and structure; as a result, optimal values for the processing parameters (e.g. cooling rate) can vary by several orders of magnitude from cell type to cell type (Mazur, 1984). Thus, there have been efforts to develop mathematical models of the cell response to cryopreservation, to allow high-throughput evaluation of candidate preservation procedures using computer simulations, and to enable the rational design and optimization of protocols for cell and tissue cryopreservation (Karlsson *et al.*, 1996).

Because changes in the intracellular water content during freezing affect the likelihood of both IIF and solution effects damage, mathematical models of cryopreservation must include a description of the mass transfer process that governs the redistribution of intracellular water. This water transport process may be rate-limited either by the process of water permeation across the cell membrane or by the process of intracellular diffusion to the cell membrane. The mass transfer Biot number (Bi) can be used to quantify the relative magnitudes of the rates of membrane transport and diffusive transport within the cell. When $Bi \gg 1$, the water transport process is diffusion-limited, whereas transport is membrane-limited when $Bi \ll 1$. Most previous models of cell

dehydration have been developed under assumptions of membrane-limited transport, and are therefore valid only in low Biot number regimes.

Previous membrane-limited transport models have distinguished themselves by the manner in which they represent the cell's constituents and the mechanisms of membrane transport. In 1933, Jacobs presented a two-parameter approach for membrane transport, with one parameter describing the membrane permeability to water and another parameter describing the membrane permeability to solute (Jacobs, 1933). By including an osmotically inactive water volume, his work was able to account for the strong interactions of water with proteins and other macromolecules within the cell. Later, Kedem and Katchalsky added a third parameter to account for the co-transport of species, e.g. the coupled transport of water and solute through the same membrane channel (Kedem and Katchalsky, 1958). In 1963, Mazur proposed a model for membrane-limited water transport specifically tailored to the problem of cell freezing (Mazur, 1963). In this seminal work, freezing-induced cell dehydration was modeled subject to the assumptions that: (1) the membrane is permeable to water only; (2) the cytoplasmic membrane remains intact for the entire period of freezing; (3) the temperature of the cytosol is everywhere uniform; (4) the chemical potential difference across the cell membrane is proportional to the ratio of partial pressures; and (5) the rate of intracellular diffusion is much larger than the rate of transmembrane transport, resulting in a well-mixed intracellular compartment.

In membrane-limited models, it is assumed that the time scale for diffusion is significantly smaller than the time scale for membrane transport. In other words, the system is assumed to be in a regime in which the mass transfer Biot number is negligible.

However, this assumption is not always valid during cryopreservation. For instance, Levin *et al.* (1976) and Pushkar *et al.* (1976) have illustrated that erythrocytes are characterized by a large Biot number, due to their high membrane permeability. In another study, Kasharin and Karlsson (1998) have demonstrated that intracellular diffusion becomes the limiting transport mechanism at cryogenic temperatures, and have therefore argued that mass transfer during warming from the cryopreserved state will be diffusion-limited, even for cell types that are characterized by low Biot numbers during the freezing process.

As early as 1976, Levin presented the first diffusion-limited model of cell dehydration. He used a backward difference algorithm to predict transport in a one-dimensional, planar model of the cell. The cytoplasm was modeled as a pseudobinary solution consisting of a fictitious salt-protein solute in water. The osmotically inactive volume fraction of the cell was assumed to comprise only the hydrated salt-protein pseudo-species. Levin's model included a description of the Arrhenius-type temperature dependence of the membrane permeability, and estimated the value of the intracellular diffusion constant using the Stokes-Einstein relationship, with a crude model for the temperature- and concentration-dependence of the solution viscosity. In particular, the temperature-dependence of the diffusivity was derived from experimental data for the viscosity of supercooled water, which at the time was only available for temperatures down to -24°C (Hallet, 1963). The effect of solute concentration on cytoplasmic viscosity was estimated by modeling the hydrated salt-protein species as a hard-sphere suspension (Vand, 1948). It is possible that the inability of Levin's model to accurately

predict the cooling rate which will cause IIF in erythrocytes was due in part to the limited validity of these constitutive laws, especially at low temperatures.

In 1997, Batycky *et al.* modeled osmotically driven water transport in hepatocytes in the context of removal of a permeating solute (e.g., a cryoprotectant additive) at a constant, suprazero temperature. The permeating solute was allowed to diffuse within the cell cytosol, to penetrate the internal organelles, as well as to partition into the lipid phase of the cell and organelle membranes. Their model accounted for diffusive fluxes within the cell, but assumed a pseudo-steady state, thus limiting the validity of their analysis to small Biot number regimes. The osmotically inactive volume fraction of the cell was not explicitly considered to be a diffusing species, but was assumed to always be uniformly distributed throughout the cytoplasm. The biophysical properties of the cell, i.e. the membrane permeability and cytoplasmic diffusivity, were assumed to have constant values independent of temperature or solute concentration. The pseudo-steady state approximation allowed the system to be modeled using a lumped-parameter approach, resulting in an ordinary differential equation which was integrated using a Runge-Kutta algorithm.

Whereas the models of Mazur (1963), Levin (1976), and Batycky *et al.* (1997) have assumed the extracellular solution to have a spatially uniform composition, thus subjecting the cell to a homogeneous osmotic driving force, Jaeger and co-workers have modeled extracellular diffusion and investigated the response of cells to the resulting solute gradients along the cell surface (Jaeger *et al.*, 1999; Jaeger and Carin, 2002). Jaeger and colleagues used a finite element technique with interface-tracking schemes to handle the moving boundary of the cell, which was modeled with a two-dimensional

(cylindrical) geometry. They ignored the effect of the osmotically inactive volume fraction in their numerical simulations, because this effect was assumed to be small based on predictions from analytical solutions for the limiting case of vanishing Biot number. They did consider the Arrhenius-type temperature-dependence of the membrane permeability (Jaeger and Carin, 2002), but assumed the intra- and extracellular diffusivities to be constant and uniform (i.e., independent of temperature and concentration). The results presented were limited to low Biot number regimes in which no significant solute polarization was observed at the cell membrane.

Mao *et al.* (2003) used a finite-volume method to simulate intra- and extracellular diffusion during cell freezing, and, like Jaeger and Carin (2002) before them, tracked the evolution of the ice solidification front in order to investigate ice-cell interactions. Mao and co-workers analyzed a two-dimensional cell with cylindrical geometry and constant membrane permeability. They also assumed that the osmotically inactive volume fraction was negligible, and that the diffusivity was constant and uniform. Furthermore, their investigations were limited to low Biot numbers, resulting in negligible intracellular solute gradients, and predictions that matched those of a simple membrane-limited transport model (Mazur, 1963). However, unlike previous studies, the investigation of Mao *et al.* also relaxed the assumption of uniform temperature distributions, and took into account the coupled heat- and mass-transfer processes that govern the kinetics of extracellular ice growth (a Stefan problem). Their preliminary results suggest that kinetics of cell dehydration predicted using the nonisothermal model were significantly different from predictions obtained under the simplifying assumption of uniform temperature.

The most significant limitation of all previous investigations of mass transfer during cell freezing is the use of inadequate constitutive equations for the membrane permeability and cytoplasmic viscosity. Even though the Arrhenius equation has almost universally been used to model the permeability temperature-dependence in membrane-limited transport models since its introduction into the cryobiology literature by Levin *et al.* (1976), and the corresponding activation energy and reference permeability data are available for many cell types (e.g., McGrath, 1988), several of the published studies of diffusion-limited cell dehydration have made the simplifying assumption of constant membrane permeability (Batycky *et al.*, 1997; Jaeger *et al.*, 1999; Mao *et al.*, 2003). More significantly, all previous investigators, with the exception of Levin (1976), have assumed the intracellular diffusivity to be constant and independent of both temperature and concentration. Even though Levin considered both the concentration- and temperature-dependence of the cytoplasmic diffusivity, his constitutive model was based on data from a limited temperature range, and he was therefore unable to make predictions for temperatures below -30°C . With the publication in 1994 (Karlsson *et al.*, 1994) of a constitutive equation capable of estimating the diffusivity in the supercooled cytoplasm down to -149°C as a function of the intracellular concentration of water, salt, and glycerol (a common cryoprotectant), it has become possible to address these limitations. Karlsson and co-workers have demonstrated that during cooling, the intracellular diffusivity decreases faster than the membrane permeability, resulting in an increase in the Biot number during the course of the freezing process; for example, during freezing of oocytes, the Biot number becomes much larger than unity for temperatures below -60°C (Karlsson *et al.*, 1994). Thus, mass transfer becomes rate-

limited by diffusive transport at low temperatures, necessitating the use of diffusion-limited models of cell dehydration in this temperature range. Moreover, Kasharin and Karlsson (1998) have demonstrated that membrane-limited water transport models are unable to correctly predict the kinetics of cell dehydration during warming of cells from the cryopreserved state, because the Biot number is large during the initial phase of this process. Thus, there is a need for a diffusion-limited model of cell dehydration which incorporates realistic constitutive equations for all relevant biophysical properties, and which is capable of making predictions down to cryogenic temperatures.

1.3 Scope and Outline of Current Study

In the present work, we will develop a model of water transport in a system comprising a biological cell and extracellular ice. The model will incorporate membrane transport as well as intracellular diffusion, thus allowing simulation of cell dehydration at both small and large Biot numbers. In contrast to previous efforts, we will use realistic constitutive models for both the membrane permeability (using the Arrhenius temperature dependence first proposed by Levin *et al.*, 1976a) and the cytoplasmic diffusivity (using the phenomenological model developed by Karlsson *et al.*, 1994). Moreover, we will present results for cells of three-dimensional (spherical) geometry, which should result in improved accuracy over previously published planar and cylindrical models. Given that our present model does neglect both the osmotically inactive volume fraction and the effect of cryoprotectant additives, future extension of our work to include these factors is possible.

In Chapter 2, we present the governing equations for both membrane-limited and diffusion-limited cell dehydration driven by the presence of extracellular ice. Constitutive equations for the biophysical properties of the cell are also presented, including the cytoplasmic diffusivity and the membrane permeability. Nondimensional forms of the governing equations are derived, and four novel dimensionless groups are introduced to characterize the kinetics of cell dehydration.

In Chapter 3, a modified Crank-Nicolson differencing scheme is used together with a Lagrangian multiplier based central difference method to discretize the governing equations on a front-tracking, non-uniform, Lagrangian-Eulerian mesh. In Chapter 4, the numerical model of diffusion-limited transport is validated against predictions from a commercially available finite element solver, using simplifying assumptions for the system properties and driving force. Conservation of mass is also confirmed. Further validation studies are undertaken in Chapter 5, by implementing the realistic constitutive equations and generating numerical solutions for low Biot number regimes, which are then compared with the corresponding predictions obtained using a conventional membrane-limited water transport model.

In Chapter 6, a parametric analysis is undertaken. Numerical solutions of our finite difference model are presented for physiologically relevant ranges of the four characteristic nondimensional parameters identified in Chapter 2. Accordingly, qualitative and quantitative differences in the cell dehydration process are observed in different mass transfer regimes. In particular, regimes in which our predictions differ significantly from those obtained with a conventional membrane-limited model are evident.

Chapters 7 and 8 include a discussion of our findings, general conclusions, as well as suggestions for future studies.

CHAPTER 2

THEORETICAL BACKGROUND

2.1 Membrane-Limited Transport Model

In 1963, Mazur proposed a two-compartment, lumped parameter model to quantitatively describe the dehydration of cells during freezing. The intra- and extracellular compartments were assumed to be well-mixed, and separated by a semipermeable membrane which only admitted transport of water. In Mazur's membrane-limited transport model, the molar flux of water from the intracellular to the extracellular compartment was given by

$$J_w = \frac{L_p}{v_w^2} \Delta\mu \quad (1)$$

where L_p is the membrane water permeability, $\Delta\mu$ is the chemical potential difference across the membrane, and v_w is the molar specific volume of water. The water chemical potential difference is a result of depletion of extracellular water by ice formation, and thus

$$\Delta\mu = \mu_{ice} - \mu_w \quad (2)$$

where μ_{ice} is the chemical potential of extracellular ice, and μ_w is the chemical potential of water at the intracellular surface of the cell membrane. The water chemical potential is a function of the intracellular water concentration, c_w , which in membrane-limited transport models is assumed to be spatially uniform throughout the cell. Because c_w is uniform and water is the only species that can be transferred across the cell membrane, there is a one-to-one correspondence between the intracellular water concentration and the cell volume V :

$$c_w = \frac{(V_o - V_b)c_{wo}v_w - (V_o - V)}{(V - V_b)v_w} \quad (3)$$

where V_o and c_{wo} are the initial values of V and c_w , respectively, V_b is the osmotically inactive volume.

As water leaves the cell, the cell will shrink. The rate of change of the cell volume can be expressed as,

$$\frac{dV}{dt} = A \frac{dR}{dt} \quad (4)$$

where t is time; A , the surface area of the cell; and R , the cell radius. Because the intracellular fluid is incompressible, volume changes are caused only by the transmembrane water flux. Thus, continuity requires that

$$\frac{dR}{dt} = -J_w v_w \quad (5)$$

During the freezing process, the instantaneous rate of cooling is

$$B = -\frac{dT}{dt} \quad (6)$$

It is typically assumed that samples are sufficiently small that heat transfer is instantaneous, the temperature profile $T(t)$ is usually taken as a given, imposed by the chosen freezing protocol. Thus, the cooling rate B is known at every temperature; typically, linear temperature profiles are used, such that B is constant.

Combining Equations (1), (4), (5) and (6), one obtains Mazur's membrane-limited model of cell dehydration:

$$\frac{dV}{dT} = \frac{AL_p \Delta\mu}{Bv_w} \quad (7)$$

Constitutive equations for the permeability L_p and the driving force $\Delta\mu$ are given in Section 2.3. Given that $\Delta\mu$ is a function only of temperature and the intracellular water concentration, and that c_w can be determined from the cell volume using Equation (3), Equation (7) represents a nonlinear ordinary differential equation which can be integrated using standard numerical methods to obtain predictions of $V(T)$.

2.2 Diffusion-Limited Transport Model

To obtain a model capable of describing diffusion-limited cell dehydration, we will no longer assume that the intracellular compartment is well-mixed. Instead, intracellular water transport will be modeled using the radial diffusion equation:

$$\frac{\partial c_w}{\partial t} = \frac{1}{r^{\gamma-1}} \frac{\partial}{\partial r} \left(D r^{\gamma-1} \frac{\partial c_w}{\partial r} \right) \quad (8)$$

where γ is the dimension of the problem ($\gamma = 1, 2,$ or 3 , corresponding to planar, cylindrical, and spherical geometry, respectively), D is the diffusion coefficient, and r is the radial location. The diffusivity of an aqueous solution depends on both temperature and concentration (as described in Section 2.3.2); thus, for realistic conditions, D will vary with time and location.

At the interior surface of the cell membrane, water leaves the cell with a flux J_w , and is replenished by a diffusive flux from the cell interior. These fluxes will differ, as a result of the accumulation of water molecules that are continuously being “swept up” by the moving membrane. Continuity requirements thus yield the following boundary condition at the cell membrane:

$$-D \frac{\partial c_w}{\partial r} = J_w + c_w \frac{dR}{dt} \quad \text{at } r = R, \quad (9)$$

where the transmembrane water flux and the membrane velocity are given by Equations (1) and (5), respectively. Because, the cell geometry has been assumed to be symmetric, a zero-flux boundary condition is imposed at the cell center:

$$\frac{\partial c_w}{\partial r} = 0 \quad \text{at } r = 0 \quad (10)$$

2.3 Constitutive Equations

2.3.1 *Membrane Permeability*

The membrane permeability L_p must be estimated in order to obtain quantitative predictions using either membrane-limited or diffusion-limited water transport models. Thus, the following section will act as a foundation for understanding the transport properties of the cell membrane and the assumptions that will be made to model its behavior in the context of cryopreservation.

Molecules can cross the cell membrane by passively diffusing through the lipid bilayer, or by active or facilitated transport through membrane channels and pores made up of transmembrane proteins. For example, certain types of proteins can actively transport molecules against a transmembrane electrochemical potential by consuming energy. Another class of proteins facilitate molecular transport without consuming energy, for example by creating pores that allow molecules to cross the membrane. This mechanism is commonly referred to as facilitated transport. On the other hand, transport is classified as passive when a molecule simply diffuses down its concentration gradient through the lipid phase of the cell membrane (Alberts *et al.*, 2002).

Ellory and Willis (1981) have investigated the impact of low temperatures on the activity levels of these transport mechanisms. Specifically, they discovered that the

activity of pumping mechanisms in the human erythrocyte membrane decreased by three orders of magnitude over the temperature interval of 40 °C to 0 °C. Since this is a much larger decrease than that observed for passive transport, it is commonly assumed that active mechanisms of transport are negligible in temperature ranges relevant for cryobiology (Levin *et al.*, 1976a). Furthermore, it has been demonstrated that ion transport across membranes is relatively slow compared to the motion of water. As an example, sodium ions are transported across the cell membrane at a rate that is 10^8 times slower than the rate of water transport in the human erythrocyte (McGrath, 1988). Consequently, for the time scales typical of a cryopreservation protocol, the cell is presumed to be impermeable to ions unless circumstances lead to disruption of the membrane barrier. Thus, transmembrane transport of water via passive diffusion is the most significant mechanism for purposes of describing mass transfer during cryopreservation.

Zwolinski *et al.* (1949) discussed the diffusion of water through the hydrophobic membrane phospholipids from the point of view of absolute reaction rate theory. In their analysis, the process of water transport across a lipid bilayer membrane comprises three mechanisms: partitioning of water molecules from the aqueous phase into the lipid phase of the membrane, diffusion within the membrane, and the return from the lipid to the aqueous phase. Associated with the rate of each of these mechanisms is an activation energy. Levin has presented a model in which all three of the above impedances to water transport have been combined, yielding an apparent activation energy (Levin *et al.*, 1976a). Thus, the temperature-dependence of the membrane permeability to water can be described by the Arrhenius equation (Levin *et al.*, 1976a):

$$L_p = L_\infty e^{\frac{-E_a}{R_g T}} \quad (11)$$

where L_∞ is the limiting value of the membrane permeability at infinite temperature, E_a is the activation energy, and R_g is the universal gas constant.

2.3.2 Cytoplasmic Diffusivity

Predictions of the rate of intracellular diffusion requires knowledge of the diffusion constant for cytoplasmic water. The diffusivity can be determined from the Stokes-Einstein equation if the viscosity η of the intracellular solution is known:

$$D = \frac{k_B T}{6\pi a_o \eta} \quad (12)$$

where k_B is Boltzmann's constant; $a_o = 1.4 \times 10^{-10} \text{ m}$, is the apparent hydrodynamic radius of water. The cytoplasm is a complex suspension of organelles, proteins and other macromolecules in an aqueous solution of electrolytes and other solute species. For simplicity, we will approximate the intracellular liquid as a binary solution of water and salt (NaCl). Thus, we need to estimate the viscosity of this binary solution as a function of temperature and salt concentration.

Previous descriptions of the temperature-dependence of the viscosity of water at subzero temperatures have included Levin's 1976 phenomenological curve fit to viscosity measurements by Hallet (1963), and a power-law model proposed by Taborek (1986) based on his experimental data. Taborek's model is currently the most frequently used in the cryobiology literature; however, since it predicts that water vitrifies at -48°C , a temperature which is 85°C greater than the actual glass transition point of water, it is a poor model of the temperature-dependence of the viscosity of supercooled water.

Instead, this work will use a phenomenological viscosity model developed by Karlsson *et al.* (1994), which interpolates experimental data for temperatures ranging from -133°C to 20°C and solute concentrations from 0% to 100% *w/w* (Weast, 1976; Kresin and Korber, 1991; Luyet and Rasmussen, 1968). Accordingly, the temperature-dependence of water will be described using a Vogel-Fulcher form:

$$\eta_w = A_{\infty} e^{\frac{E}{T - \beta T_g}} \quad (13)$$

where A_{∞} is a pre-exponential coefficient, E is the activation temperature, T_g is the glass transition temperature, and β is the ratio of the Vogel-Fulcher critical temperature to glass transition temperature. For pure water, these parameters are (Karlsson *et al.*, 1994)

$$A_{\infty} = 2.711 \times 10^{-5} \text{ Pa s};$$

$$E = 614.823 \text{ K};$$

$$T_g = 139.92 \text{ K};$$

$$\beta = 0.88481;$$

In order to estimate the concentration-dependence of the viscosity of a water-NaCl solution, the liquid is modeled as a suspension of rigid salt spheres in a continuous fluid medium consisting of water. In 1948, Vand developed a mathematical model to predict the viscosity of such a suspension (Vand, 1948). By coupling the hydrodynamic equations governing incompressible flow around a rigid sphere with the effect of sphere-sphere interactions, Vand obtained the following equation describing the increase in suspension viscosity due to the presence of the hard spheres:

$$\eta = \eta_w e^{\frac{k_c \phi_{\text{sphere}}}{1 - \lambda \phi_{\text{sphere}}}} \quad (14)$$

where $k_e = 2.5$ is Einstein's shape factor for single spheres, $\lambda = 0.609375$ is the hydrodynamic interaction constant, and ϕ_{sphere} is the volume fraction of the rigid spheres. To estimate the value of ϕ_{sphere} , the hard spheres will be assumed to comprise hydrated salt ions as illustrated in Figure 1; thus,

$$\phi_{\text{sphere}} = c_s (\nu_s + h \nu_w) \quad (15)$$

where c_s is the salt concentration; ν_s , the molar specific volume of salt; h , the effective number of water molecules in the hydration shell. An estimate of the value of h is obtained by comparing the viscosity calculated using Equation (14) to measured viscosities of a water-NaCl solution at 20 °C; a good agreement is obtained for $h = 1$, and thus this value was adopted in the present study.

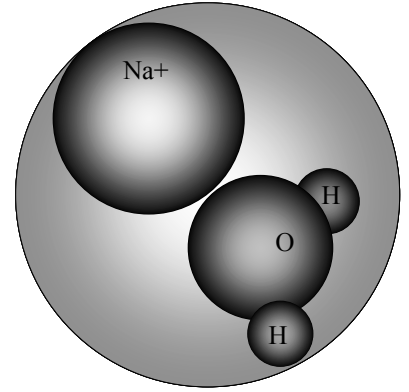


Figure 1: Illustration of ϕ_{sphere} containing NaCl and one water molecule.

2.3.3 Chemical Potential

With the assumption that the extracellular environment consists of ice and unfrozen aqueous solution in mutual equilibrium, the chemical potential of the extracellular water can be determined from the Clausius-Clapeyron relationship, yielding

$$\mu_{\text{ice}} = \mu_o + \Delta H_f \left(\frac{T}{T_o} - 1 \right) \quad (16)$$

where T_o is the equilibrium freezing temperature of water; μ_o , the chemical potential of water at T_o ; ΔH_f , the molar specific heat of fusion of water.

If one approximates the cytosol as an ideal solution, Raoult's law can be used to approximate the chemical potential of the intracellular water,

$$\mu_w = \mu_o + R_g T \ln(\chi_w) \quad (17)$$

where χ_w is the mole fraction of intracellular water, which can be computed as follows,

$$\chi_w = \frac{c_w}{c_w + \sigma_s c_s} \quad (18)$$

where $\sigma_s = 2$ and represents the salt dissociation constant.

2.3.4 Supercooling

Since the chemical potential of the intracellular water at a particular temperature will be greater than the chemical potential of the ice, there will exist a driving force for crystallization of the intracellular water. Thus, the probability of IIF will be strongly dependent on the degree of supercooling, defined as

$$\Delta T = T_{eq} - T \quad (19)$$

where T_{eq} is the equilibrium freezing point. The equilibrium freezing point depends on the water concentration, and can be estimated by noting that when $T = T_{eq}$, the chemical potential of the liquid water (Equation 17) must equal the chemical potential of ice (Equation 16). Thus, one obtains

$$T_{eq} = \frac{1}{\frac{1}{T_o} - \frac{\ln(\chi_w)R_g}{\Delta H_f}} \quad (20)$$

2.4 Dimensional Analysis

2.4.1 *Characteristic Scales and Dimensionless Groups*

If the cryopreservation procedure to be analyzed consists of a linear temperature profile with a constant rate B over a characteristic temperature interval T_c , then the characteristic time-scale (i.e., duration) of the whole process is

$$\delta t_B = \frac{T_c}{B} \quad (21)$$

During the freezing process, intracellular diffusion will occur with a characteristic time-scale

$$\delta t_D = \frac{R^2}{D_o} \quad (22)$$

where D_o is the diffusivity at the cell center ($r = 0$). Likewise, a characteristic time-scale for membrane transport can be defined:

$$\delta t_M = \frac{Rv_w}{L_p R_g T} \quad (23)$$

Kasharin and Karlsson (1998) have previously demonstrated that the extent of cell dehydration and the dominant mechanism of the water transport process are determined by the relative magnitudes of the three characteristic time-scales defined in Eqs. (21)-(23). In particular, the extent of membrane transport that occurs during the cooling process can be quantified by the ratio $\delta t_M/\delta t_B$, whereas the extent of diffusive transport during the freezing procedure is characterized by the ratio $\delta t_D/\delta t_B$.

To analyze these ratios, we define the following nondimensional variables:

$$\tilde{T} \equiv \frac{T}{T_c} \quad (24)$$

$$\tilde{R} \equiv \frac{R}{R_0} \quad (25)$$

where R_0 is the initial cell radius;

$$\tilde{T}_g \equiv \frac{T_g}{T_c} \quad (26)$$

$$\tilde{\eta} \equiv \frac{\eta}{\eta_w} \quad (27)$$

$$\tilde{D}_0 \equiv \frac{D_0}{D_c} \quad (28)$$

where D_c is a characteristic constant diffusivity, defined here as

$$D_c = \frac{k_B T_c}{6\pi a_0 A_\eta} \quad (29)$$

Given that both the diffusivity and the membrane permeability have a strong temperature-dependence, we will explicitly describe the effect of temperature on the characteristic time-scales by defining

$$\varepsilon_M \equiv \frac{E_a}{R_g T_c} \quad (30)$$

which is the nondimensional activation energy (Arrhenius number) for membrane transport, and similarly, a nondimensional activation energy for diffusion:

$$\varepsilon_D \equiv \frac{E}{T_c} \quad (31)$$

With the above definitions, the characteristic time-scale ratios can be expressed as follows:

$$\frac{\delta t_M}{\delta t_B} = \theta_M \cdot \frac{\tilde{R}}{\tilde{T}} \cdot e^{\varepsilon_M / \tilde{T}} \quad (32)$$

$$\frac{\delta t_D}{\delta t_B} = \theta_D \cdot \frac{\tilde{R}^2 \tilde{\eta}}{\tilde{T}} \cdot e^{\varepsilon_D / (\tilde{T} - \beta \tilde{T}_g)} \quad (33)$$

where we have defined two novel dimensionless groups,

$$\theta_M \equiv \frac{R_o B v_w}{L_\infty R_g T_c^2} \quad (34)$$

$$\theta_D \equiv \frac{R_o^2 B}{T_c D_c} \quad (35)$$

For a system in which the membrane permeability and diffusivity are independent of temperature and concentration, θ_M and θ_D characterize the extent of convective transport (i.e., membrane transport) and diffusive transport, respectively, on the time-scale of the cooling procedure. Thus, because cell dehydration requires both diffusion of intracellular water to the membrane and transport across the membrane, water loss during the freezing process will be negligible if either $\theta_M \gg 1$ or $\theta_D \gg 1$ (Kasharin and Karlsson, 1998). The dimensionless group θ_D is equivalent to the product of a Predvoditelev number and a Lewis number, while the ratio of θ_D to θ_M represents a Biot number.

2.4.2 Membrane-Limited Transport Model

Combining Equation (7) with Equations (2)-(3) and the constitutive relationships defined in Equation (11) and Equations (16)-(18), one obtains an ordinary, nonlinear differential equation in V :

$$\frac{dV}{dT} = \frac{L_\infty A R_g T}{B v_w^2} \cdot e^{-\frac{E_a}{R_g T}} \cdot \left[\frac{\Delta H_f}{R_g} \left(\frac{1}{T_o} - \frac{1}{T} \right) - \ln \left(\frac{V - V_b - c_{so} v_s \cdot (V_o - V_b)}{V - V_b - c_{so} \cdot (v_s - \sigma_s v_w) \cdot (V_o - V_b)} \right) \right] \quad (36)$$

where c_{so} is the initial concentration of intracellular salt. In order to write Equation (36) in nondimensional form, the following dimensionless quantities will be defined:

$$\tilde{T} \equiv \frac{T}{T_c} \quad (37)$$

$$\tilde{V} \equiv \frac{V}{V_o} \quad (38)$$

$$\tilde{V}_b \equiv \frac{V_b}{V_o} \quad (39)$$

$$\tilde{A} \equiv \frac{A}{A_o} \quad (40)$$

$$\tilde{T}_o \equiv \frac{T_o}{T_c} \quad (41)$$

$$\Delta\tilde{\mu} \equiv \frac{\Delta\mu}{R_g T_c} \quad (42)$$

$$\Delta\tilde{H}_f \equiv \frac{\Delta H_f}{R_g T_c} \quad (43)$$

where A_o is the initial surface area of the cell. The nondimensional driving force $\Delta\tilde{\mu}$ is a function of the variables \tilde{V} and \tilde{T} , and is dependent only on the dimensionless constants \tilde{V}_b , \tilde{T}_o , $\Delta\tilde{H}_f$, as well as the initial volume fraction of salt, $\phi_{so} = c_{so}v_s$, as shown below:

$$\Delta\tilde{\mu}(\tilde{V}, \tilde{T}) = \Delta\tilde{H}_f \cdot \left(\frac{\tilde{T}}{\tilde{T}_o} - 1 \right) - \tilde{T} \cdot \ln \left[\frac{\tilde{V} - \tilde{V}_b - \phi_{so} \cdot (1 - \tilde{V}_b)}{\tilde{V} - \tilde{V}_b - \phi_{so} \cdot (1 - \sigma_s \frac{v_w}{v_s}) \cdot (1 - \tilde{V}_b)} \right] \quad (44)$$

After substituting the above expressions into Equation (36), a nondimensional governing equation is obtained:

$$\frac{d\tilde{V}}{d\tilde{T}} = \frac{1}{\theta_M} \cdot e^{-\frac{\varepsilon_M}{\tilde{T}}} \cdot \gamma \tilde{V}^{\frac{\gamma-1}{\gamma}} \cdot \Delta\tilde{\mu}(\tilde{V}, \tilde{T}) \quad (45)$$

where we have made use of the fact that the surface area and volume of a γ -dimensional sphere are related by

$$\frac{A_o}{V_o} = \frac{\gamma}{R_o} \quad (46)$$

$$\tilde{A} = \tilde{V}^{\frac{\gamma-1}{\gamma}} \quad (47)$$

For purposes of comparison with the diffusion-limited water transport model, it is illustrative also to express the above governing equation in terms of the intracellular water concentration (where we will use the water volume fraction, $\phi = c_w v_w$, as a dimensionless concentration variable). Noting that the nondimensional cell volume can be determined from the water volume fraction by inverting Equation (3),

$$\tilde{V} = \frac{\phi_{so} + \tilde{V}_b(1 - \phi_{so} - \phi)}{1 - \phi} \quad (48)$$

one can rewrite the nondimensional chemical potential difference as a function of ϕ and \tilde{T} :

$$\Delta\tilde{\mu}(\phi, \tilde{T}) = \Delta\tilde{H}_f \cdot \left(\frac{\tilde{T}}{\tilde{T}_0} - 1 \right) - \tilde{T} \cdot \ln \left[\frac{\phi}{\phi + \sigma_s \frac{v_w}{v_s} (1 - \phi)} \right] \quad (49)$$

Because the osmotically inactive cell volume is neglected in our diffusion-limited model, we will also set $\tilde{V}_b = 0$ in the membrane-limited water transport model. Thus, substituting Equations (48)-(49) into Equation (45), one obtains a nondimensional differential equation in water volume fraction:

$$\frac{d\phi}{d\tilde{T}} = \frac{1}{\theta_M} \cdot e^{-\frac{\varepsilon_M}{\tilde{T}}} \cdot \frac{\gamma}{\phi_{s0}^{1/\gamma}} \cdot (1 - \phi)^{\frac{\gamma+1}{\gamma}} \cdot \Delta\tilde{\mu} \quad (50)$$

2.4.3 Diffusion-Limited Transport Model

To write the diffusion model (Equations 8-10) in nondimensional form, we will use the water volume fraction as a dimensionless concentration variable, and define a dimensionless position variable, x , and dimensionless time variable, τ , as follows:

$$x = \frac{r}{R} \quad (51)$$

$$d\tau = \frac{dt}{\delta t_D} \quad (52)$$

where Equation (52) is written in differential form because the characteristic time scale for diffusion as defined by Eq. (22) is time-varying. Because the definitions of both x and τ are time-dependent, transformation of the spatial and temporal derivatives in Equations (8)-(10) into nondimensional form requires the following identities:

$$\frac{\partial}{\partial r} = \frac{\partial x}{\partial r} \frac{\partial}{\partial x} + \frac{\partial \tau}{\partial r} \frac{\partial}{\partial \tau} \quad (53)$$

$$\frac{\partial}{\partial t} = \frac{\partial x}{\partial t} \frac{\partial}{\partial x} + \frac{\partial \tau}{\partial t} \frac{\partial}{\partial \tau} \quad (54)$$

From Equations (22), (52) and (53), one obtains

$$\frac{\partial x}{\partial r} = \frac{1}{R} \quad (55)$$

$$\frac{\partial \tau}{\partial r} = 0 \quad (56)$$

$$\frac{\partial x}{\partial t} = -\frac{D_o x}{R^3} \frac{dR}{d\tau} \quad (57)$$

Thus, the partial derivatives that appear in Equations (8)-(10) can be rewritten as follows:

$$\frac{\partial c_w}{\partial t} = \frac{D_o}{R^2} \frac{\partial c_w}{\partial \tau} - \frac{D_o x}{R^3} \frac{dR}{d\tau} \frac{\partial c_w}{\partial x} \quad (58)$$

$$\frac{\partial c_w}{\partial r} = \frac{1}{R} \frac{\partial c_w}{\partial x} \quad (59)$$

$$\frac{\partial^2 c_w}{\partial r^2} = \frac{1}{R^2} \frac{\partial^2 c_w}{\partial x^2} \quad (60)$$

$$\frac{\partial D}{\partial r} = \frac{1}{R} \frac{\partial D}{\partial x} \quad (61)$$

Equations (58)-(61) can be substituted into Equation (8) to yield

$$\frac{D_o}{R^2} \frac{\partial c_w}{\partial \tau} = \frac{D}{R^2} \frac{\partial^2 c_w}{\partial x^2} + \left[\frac{D_o x}{R^3} \frac{dR}{d\tau} + \frac{1}{R^2} \frac{\partial D}{\partial x} + \frac{D}{R^2} \frac{(\gamma - 1)}{x} \right] \cdot \frac{\partial c_w}{\partial x} \quad (62)$$

To complete the transformation to nondimensional form, we will replace the water concentration c_w by the corresponding volume fraction ϕ , and define the following dimensionless variables:

$$\tilde{D} = \frac{D}{D_o} \quad (63)$$

$$\tilde{R} = \frac{R}{R_o} \quad (64)$$

Thus, Equation (62) can be simplified to yield the nondimensional governing equation for intracellular transport:

$$\frac{\partial \phi}{\partial \tau} = \frac{x}{\tilde{R}} \frac{d\tilde{R}}{d\tau} \frac{\partial \phi}{\partial x} + \frac{1}{x^{\gamma-1}} \frac{\partial}{\partial x} \left(\tilde{D} x^{\gamma-1} \frac{\partial \phi}{\partial x} \right) \quad (65)$$

where the rate of change of the cell radius can be determined from Equation (5), which in nondimensional form becomes

$$\frac{d\tilde{R}}{d\tau} = \tilde{R}^2 \cdot \text{Bi} \cdot \Delta \tilde{\mu}(\phi_R, \tilde{T}) \quad (66)$$

where ϕ_R is the value of ϕ at the cell membrane ($x = 1$), and Bi is a time-varying Biot number, defined as follows:

$$\text{Bi} \equiv \frac{R_0 L_p R_g T_c}{D_0 v_w} \quad (67)$$

Similarly, Equation (9), the boundary condition at the cell membrane, becomes

$$\left. \frac{\partial \phi}{\partial x} \right|_{x=1} = \frac{1}{\tilde{D}_R \tilde{R}} (1 - \phi_R) \frac{d\tilde{R}}{d\tau} \quad (68)$$

where \tilde{D}_R is the nondimensional diffusivity \tilde{D} evaluated at the cell membrane ($x = 1$).

Likewise, the boundary condition at the cell center (Equation (10)) can be rewritten in nondimensional form, as follows:

$$\left. \frac{\partial \phi}{\partial x} \right|_{x=0} = 0 \quad (69)$$

For purposes of solving the diffusion equation subject to the above boundary conditions, it will be advantageous to combine Equation (69) with Equation (65) to yield the following form of the governing equation at the cell center:

$$\frac{\partial \phi}{\partial x} = \frac{\partial}{\partial x} \left(\tilde{D} \frac{\partial \phi}{\partial x} \right) \quad \text{for } x = 0 \quad (70)$$

Finally, in order to compare the diffusion-limited transport model with the nondimensional membrane-limited transport model as shown in Eq. (50), we will modify Eq. (65) to use nondimensional temperature instead of nondimensional time as the independent variable. This will require the following transformation

$$\frac{d\tilde{T}}{d\tau} = \frac{-BR_o^2 \tilde{R}^2}{D_o T_c} \quad (71)$$

which is obtained by combining Equations (6), (22) and (52). Thus, Equation (65) becomes:

$$\begin{aligned} \frac{\partial \phi}{\partial \tilde{T}} = & \frac{1}{\theta_M} \cdot e^{-\frac{\varepsilon_M}{\tilde{T}}} \cdot \Delta \tilde{\mu} \cdot \frac{x}{\tilde{R}} \cdot \frac{\partial \phi}{\partial x} \\ & - \frac{1}{\theta_D} \cdot e^{-\frac{\varepsilon_D}{\tilde{T} - \beta \tilde{T}_g}} \cdot \tilde{T} \cdot \frac{1}{x^{\gamma-1} \tilde{R}^2} \cdot \frac{\partial}{\partial x} \left(\frac{x^{\gamma-1}}{\tilde{\eta}} \cdot \frac{\partial \phi}{\partial x} \right) \end{aligned} \quad (72)$$

In Equation (72), the physical significance of the dimensionless groups θ_M , θ_D , ε_M , and ε_D becomes more clear; whereas the pair θ_M and ε_M determine the significance of the advective term representing membrane transport, the pair θ_D and ε_D determine the significance of the diffusive term. The nondimensional activation energies ε_M and ε_D determine, in large part, the temperature dependence of the behavior, while the dimensionless groups θ_M and θ_D demarcate different transport regimes under constant temperature conditions (i.e., they are indicative of the effect of temperature-independent factors on the respective transport mechanisms).

CHAPTER 3

NUMERICAL METHODS

3.1 Introduction

The diffusion-limited transport model that describes our system is a highly nonlinear partial differential equation with spatially varying, time dependent coefficients and complicated boundary conditions. As a result, an analytical solution is not tractable, and we have instead turned to numerical techniques in order to solve the problem. Thus we have discretized Equations (65), (68), and (69) using a Forward-Time, Centered Space (FTCS) scheme. A non-uniform, Eulerian-Lagrangian grid was used for spatial discretization, while a modified Crank-Nicolson method was used for temporal discretization.

3.2 Spatial Discretization

3.2.1 *Finite Difference Scheme*

Given that the nondimensional spatial coordinate x is defined such that $x = 0$ represents the cell center, and $x = 1$ the cell membrane, the discretization of the domain $x = [0,1]$ defines a spatial grid with nodes that move with the cell membrane such that the mesh is deformed during cell dehydration. Although this coordinate system is Lagrangian with respect to the cell membrane, the mesh does move relative to the intracellular fluid, given that the intracellular fluid is stationary (Batycky *et al.*, 1997) while the spatial grid is designed so that the relative spacing of the nodes will be fixed with respect to the nondimensional coordinate system. It is the Eulerian properties of the grid that give rise to the advective term in Equation (65).

As shown in Figure 2, a spatially non-uniform grid was defined, with the internodal distances give by,

$$\Delta x_i = x_i - x_{i-1} \quad \text{for } i = 1, \dots, N-1 \quad (73)$$

where N is the total number of nodes and the subscript i designates the node index. Numbering of the nodes follows the C^{++} syntax of referencing elements in a vector. Using this approach, $i = 0$ represents the cell center, and $i = N-1$ designates the node at the moving cell boundary. The spatial nodes can be distributed uniformly throughout the cell by requiring

$$\Delta x_i = \frac{1}{N-1} \quad \text{for } i = 1, \dots, N-1 \quad (74)$$

or nonuniformly by scaling the internodal spacing as follows

$$\Delta x_i = \alpha \Delta x_{i+1} \quad \text{for } i = 1, \dots, N-2 \quad (75)$$

Here, α is a scaling factor and is defined to be greater than one so that the spacing will be finer near the cell membrane. Given that $x_{N-1} = 1$ by definition, use of Equation (75) requires

$$\Delta x_{N-1} = \frac{\alpha - 1}{\alpha^{N+1} - 1} \quad (76)$$

Since the spatial grid is designed with the flexibility to be uniformly or

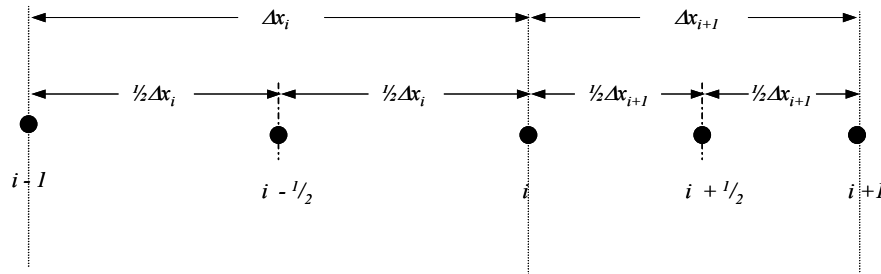


Figure 2. Illustration of the nodal spacing.

nonuniformly spaced, the numerical approximation of the spatial derivatives must be able to accommodate both. For uniform node spacing, a central difference scheme is typically used to obtain estimates of spatial derivatives to second-order accuracy. For our spatially non-uniform grid, we will estimate the spatial derivatives using a Lagrangian polynomial technique. In this method, if the value of a spatially varying quantity $f(x)$ (e.g. ϕ_w) is known at three consecutive nodes $x_j \leq x_k \leq x_l$, such that

$$f_j \equiv f(x = x_j) \quad (77)$$

$$f_k \equiv f(x = x_k) \quad (78)$$

$$f_l \equiv f(x = x_l) \quad (79)$$

then a smooth second-order function can be defined to interpolate between the known values:

$$f(x) = f_j L_j(x) + f_k L_k(x) + f_l L_l(x) \quad (80)$$

where, L_j , L_k , and L_l are the Lagrangian Multipliers:

$$L_j = \frac{(x - x_k)(x - x_l)}{(x_j - x_k)(x_j - x_l)} \quad (81)$$

$$L_k = \frac{(x - x_j)(x - x_l)}{(x_k - x_j)(x_k - x_l)} \quad (82)$$

$$L_l = \frac{(x - x_j)(x - x_k)}{(x_l - x_j)(x_l - x_k)} \quad (83)$$

The first derivative at x_k can then be approximated by differentiating Equation (80):

$$\left. \frac{df}{dx} \right|_k = f_j \frac{dL_j}{dx} + f_k \frac{dL_k}{dx} + f_l \frac{dL_l}{dx} \quad (84)$$

3.2.2 Discretization of Diffusion Equation

The right-hand side of the governing transport equation is a function of space and time:

$$g(x, \tau) = \frac{x}{\tilde{R}} \frac{d\tilde{R}}{d\tau} \frac{\partial \phi}{\partial x} + \frac{1}{x^{\gamma-1}} \frac{\partial}{\partial x} \left[\tilde{D} x^{\gamma-1} \frac{\partial \phi}{\partial x} \right] \quad (85)$$

Using a finite difference approach, Equation (85) will be discretized in space to yield an estimate of $g(x_i, \tau)$ for the interior nodes $i = 1, \dots, N-2$. The spatial discretization of the boundary conditions is described in Section 3.2.3 and 3.2.4. The Lagrangian polynomial method described above will be used to estimate the first-order and second-order spatial derivatives in Equation (85).

To estimate the first spatial derivative of the intracellular water volume fraction, $\frac{\partial \phi}{\partial x}$, we first determine the corresponding Lagrangian multipliers. By letting $j = i-1$, $k = i$, $l = i+1$, we obtain

$$x_j = x_{i-1} \quad (86)$$

$$x_k = \alpha \Delta x_{i+1} + x_{i-1} \quad (87)$$

$$x_l = \Delta x_{i+1} (\alpha + 1) + x_{i-1} \quad (88)$$

the Lagrangian multipliers become:

$$L_{i-1} = \frac{(x - \alpha \Delta x_{i+1} - x_{i-1})(x - \Delta x_{i+1} (\alpha + 1) - x_{i-1})}{\alpha \Delta x_{i+1}^2 (\alpha + 1)} \quad (89)$$

$$L_i = \frac{(x - x_{i-1})(x - \Delta x_{i+1} (\alpha + 1) - x_{i-1})}{\alpha \Delta x_{i+1}^2} \quad (90)$$

$$L_{i+1} = \frac{(x - x_{i-1})(x - \alpha \Delta x_{i+1} - x_{i-1})}{\Delta x_{i+1}^2 (\alpha + 1)} \quad (91)$$

Substituting these definitions into Equation (80) and subsequently differentiating will yield an estimate of the first derivative of the water volume fraction evaluated at $x = x_i$:

$$\left. \frac{d\phi}{dx} \right|_i = \frac{1}{\alpha(\alpha+1)\Delta x_{i+1}} \left[-\phi_{i-1} + (\alpha+1)(1-\alpha)\phi_i + \alpha^2\phi_{i+1} \right] \quad (92)$$

In order to discretize Equation (65), we also need to estimate the second derivative term

$$\frac{\partial}{\partial x} \left(\tilde{D}x^{\gamma-1} \frac{\partial \phi}{\partial x} \right) \quad (93)$$

This can be accomplished using the Lagrangian polynomial method, by defining

$$f(x) \equiv \tilde{D}x^{\gamma-1} \frac{\partial \phi}{\partial x} \quad (94)$$

In order to improve the accuracy of the estimate, we define new nodes halfway between $i-1$, i , and $i+1$, as shown in Figure 2; by convention these intermediate nodes are given fractional indices $i \pm 1/2$. Now we will discretize Equation (93) using Equation (84) and Equation (94), with $j = i-1/2$, $k = i$, $l = i+1/2$. Thus,

$$x_j = x_{i-1/2} \quad (95)$$

$$x_k = \frac{1}{2}\alpha\Delta x_{i+1} + x_{i-1/2} \quad (96)$$

$$x_l = \frac{1}{2}\Delta x_{i+1}(\alpha+1) + x_{i-1/2} \quad (97)$$

producing:

$$\left. \frac{df}{dx} \right|_i = \frac{2}{\alpha(\alpha+1)\Delta x_{i+1}} \left[-f_{i-1/2} + (\alpha+1)(1-\alpha)f_i + \alpha^2 f_{i+1/2} \right] \quad (98)$$

Evaluation of Equation (98) requires estimates of the quantities

$$f_i \equiv \tilde{D}_i x_i^{\gamma-1} \frac{\partial \phi}{\partial x} \Big|_i \quad (99)$$

$$f_{i-1/2} \equiv \tilde{D}_{i-1/2} x_{i-1/2}^{\gamma-1} \frac{\partial \phi}{\partial x} \Big|_{i-1/2} \quad (100)$$

$$f_{i+1/2} \equiv \tilde{D}_{i+1/2} x_{i+1/2}^{\gamma-1} \frac{\partial \phi}{\partial x} \Big|_{i+1/2} \quad (101)$$

Whereas the derivative $\frac{\partial \phi}{\partial x} \Big|_i$ in Equation (99) can be evaluated using Equation (92), the

derivatives $\frac{\partial \phi}{\partial x} \Big|_{i-1/2}$ and $\frac{\partial \phi}{\partial x} \Big|_{i+1/2}$ appearing in Equations (100) and (101), respectively,

were estimated from the known values of ϕ_{i-1} , ϕ_i , and ϕ_{i+1} as follows. The derivative

$\frac{\partial \phi}{\partial x} \Big|_{i+1/2}$ was evaluated using Equation (84) with $j = i$, $k = i+1/2$, $l = i+1$, such that

$$x_j = x_i \quad (102)$$

$$x_k = \frac{\Delta x_{i+1}}{2} + x_i \quad (103)$$

$$x_l = \Delta x_{i+1} + x_i \quad (104)$$

yielding

$$\frac{\partial \phi}{\partial x} \Big|_{i+1/2} = \left(\frac{\phi_{i+1} - \phi_i}{\Delta x_{i+1}} \right) \quad (105)$$

(note that because the points j , k , and l are evenly spaced by $\frac{1}{2}\Delta x_{i+1}$, the Lagrangian polynomial approximation reduces to a conventional central difference scheme). In a

similar fashion, the derivative $\frac{\partial \phi}{\partial x} \Big|_{i-1/2}$ was evaluated using Equation (84) with $j = i-1$,

$k = i-1/2$, $l = i$, such that

$$x_j = x_{i-1} \quad (106)$$

$$x_k = \frac{\alpha \Delta x_{i+1}}{2} + x_{i-1} \quad (107)$$

$$x_l = \alpha \Delta x_{i+1} + x_{i-1} \quad (108)$$

and

$$\left. \frac{\partial \phi}{\partial x} \right|_{i-1/2} = \left(\frac{\phi_i - \phi_{i-1}}{\alpha \Delta x_{i+1}} \right) \quad (109)$$

To complete the evaluation of Equations (100) and (101), the value of the nondimensional diffusivity must be estimated at the intermediate nodes $i - \frac{1}{2}$ and $i + \frac{1}{2}$. We followed the conventional approach of approximating these intermediate values by linear interpolation:

$$\tilde{D}_{i\pm 1/2} = \frac{1}{2} (\tilde{D}_i + \tilde{D}_{i\pm 1}) \quad (110)$$

3.2.3 Discretization of Boundary Condition at $x = 0$

In order to discretize Equation (70) at node $i = 0$ using FTCS, we define redundant nodes at $i = -1$ and $i = -\frac{1}{2}$, such that the nodes at $i = 0$ and $i = -1$ are spaced with an internodal distance of $\Delta x_0 = \Delta x_1$. Because of the even spacing of the nodes, the Lagrangian polynomial method will reduce to a conventional central differences approximation. In addition, by symmetry, $\phi_{-1} = \phi_1$ and $\phi_{-1/2} = \phi_{1/2}$, so that $\tilde{D}_{-1} = \tilde{D}_1$ and $\tilde{D}_{-1/2} = \tilde{D}_{1/2}$.

A central difference approximation of Equation (70) centered between the nodes $-\frac{1}{2}$ and $\frac{1}{2}$ yields

$$\left. \frac{df}{dx} \right|_0 = \frac{f_{1/2} - f_{-1/2}}{\Delta x_1} \quad (111)$$

where

$$f_{1/2} = \tilde{D}_{1/2} \left. \frac{\partial \phi}{\partial x} \right|_{1/2} \quad (112)$$

$$f_{-1/2} = \tilde{D}_{-1/2} \left. \frac{\partial \phi}{\partial x} \right|_{-1/2} \quad (113)$$

The derivative $\left. \frac{\partial \phi}{\partial x} \right|_{1/2}$ was evaluated using a central difference scheme centered between the nodes i and $i+1$, yielding

$$\left. \frac{\partial \phi}{\partial x} \right|_{1/2} = \frac{\phi_{i+1} - \phi_i}{\Delta x_{i+1}} \quad (114)$$

In a similar fashion, the derivative $\left. \frac{\partial \phi}{\partial x} \right|_{-1/2}$ was evaluated using a central difference scheme centered between the nodes $i-1$ and i , yielding

$$\left. \frac{\partial \phi}{\partial x} \right|_{-1/2} = \frac{\phi_i - \phi_{i-1}}{\Delta x_{i+1}} \quad (115)$$

3.2.4 Discretization of Boundary Condition at $x = 1$

The boundary condition at the cell membrane ($i = N-1$) requires special treatment. First, the spatial derivative associated with the advective term in Equation (65) will be evaluated with a backward difference scheme in order to simplify the treatment of the required fictitious nodes located beyond the cell membrane ($i = N, N-1/2$). The second derivative term will be evaluated as previously described, but with an internodal spacing between nodes N and $N-1$ of Δx_{N-1} . Because of the even spacing of the nodes, the Lagrangian polynomial method will reduce to a conventional central differences approximation.

According to this approach, Equation (68) can be discretized with a central difference approximation about node $N-1$ to obtain the relationship between the fictitious node N and the nodes $N-1$ and $N-2$.

$$\phi_N = (1 - \phi_{N-1}) \frac{2\Delta x}{\tilde{D}_R \tilde{R}} \frac{d\tilde{R}}{d\tau} + \phi_{N-2} \quad (116)$$

In addition, Equation (93) can be discretized with a central difference approximation centered between nodes $N-3/2$ and $N-1/2$, yielding

$$\left. \frac{df}{dx} \right|_{N-1} = \frac{f_{N-1/2} - f_{N-3/2}}{\Delta x_{N-1}} \quad (117)$$

where,

$$f_{N-3/2} = \tilde{D}_{N-3/2} \left(x_{N-3/2} - \frac{\Delta x_{N-1}}{2} \right)^{\gamma-1} \left. \frac{\partial \phi}{\partial x} \right|_{N-3/2} \quad (118)$$

$$f_{N-1/2} = \tilde{D}_{N-1/2} \left(x_{N-1/2} + \frac{\Delta x_{N-1}}{2} \right)^{\gamma-1} \left. \frac{\partial \phi}{\partial x} \right|_{N-1/2} \quad (119)$$

In order to avoid extrapolation of the diffusion coefficient and nodal location of the fictitious node, Equation (119) will be redefined as

$$f_{N-1/2} = \tilde{D}_{N-1} x_{N-1}^{\gamma-1} \left. \frac{\partial \phi}{\partial x} \right|_{N-1/2} \quad (120)$$

for simplicity. The derivative $\left. \frac{\partial \phi}{\partial x} \right|_{N-1/2}$ in Equation (120) was evaluated using a central

difference scheme centered between the nodes $N-1$ and N , yielding

$$\left. \frac{\partial \phi}{\partial x} \right|_{N-1/2} = \frac{\phi_N - \phi_{N-1}}{\Delta x_{N-1}} \quad (121)$$

In a similar fashion, the derivative $\left. \frac{\partial \phi}{\partial x} \right|_{N-3/2}$ required in Equation (118) was evaluated using a central difference scheme centered between the nodes $N-2$ and $N-1$, yielding

$$\left. \frac{\partial \phi}{\partial x} \right|_{N-3/2} = \frac{\phi_{N-1} - \phi_{N-2}}{\Delta x_{N-1}} \quad (122)$$

The other type of boundary condition that could be encountered at the cell membrane accounts for the possibility of nonuniform vitrification. This condition assumes that vitrification will occur initially at the intracellular membrane and that the resulting glassy state will act as a barrier to mass transport. This assumption is valid for a binary system of water and electrolyte, cooled monotonically, because the lowest concentration of water will occur at the intracellular membrane. As a consequence of the cytoplasmic transition into a vitreous state at the cell membrane, no water will be permitted to leave the cell, and thus the cell radius will not change with time (i.e., $\frac{d\tilde{R}}{d\tau} = 0$). Imparting these conditions into a numerical language would involve adjusting the boundary node to be adjacent to the glass front, and to redefine the boundary condition to be prohibitive of mass transport. The discretization technique of this new boundary condition makes use of Equations (70, 111-115).

3.3 Temporal Discretization

The nondimensional time step interval was defined as:

$$\Delta \tau_n = \tau_n - \tau_{n-1} \quad (123)$$

where the subscript n designates the time step. This time step can be of a constant size, or may vary. For example, when the time scale for membrane transport became smaller

than the time scale for diffusion transport ($\delta t_M < \delta t_D$); the nominal time step was be reduced by a factor ($\delta t_M/\delta t_D$), as described in Section 5.2.

In order to integrate the differential equation:

$$\left. \frac{\partial \phi}{\partial \tau} \right|_{x=x_i} = g(x, \tau) \quad (124)$$

a Crank-Nicolson scheme will be used. This scheme estimates the time-derivate in

Equation (124) using the trapezoidal rule:

$$\frac{\phi_i^{n+1} - \phi_i^n}{\Delta \tau_{n+1}} = \frac{1}{2} [g(x_i, \tau_n) + g(x_i, \tau_{n+1})] \quad (125)$$

where ϕ_i^n represents the water volume fraction at node i , at time step n . We now use the results of Section 3.2.2 to write the discretized form of Equation (85):

$$\begin{aligned} g(x_i, \tau_n) = & \frac{x_i}{\tilde{R}} \frac{d\tilde{R}}{d\tau} \left[\frac{\alpha^2 \phi_{i+1}^n + (\alpha + 1)(1 - \alpha)\phi_i^n - \phi_{i-1}^n}{\alpha(\alpha + 1)\Delta x_{i+1}} \right] \\ & + \frac{2}{\alpha(\alpha + 1)x_i^{\gamma-1}\Delta x_{i+1}^2} \phi_{i-1}^n \left(\frac{\tilde{D}_{i-1/2}^n \left(x_i - \frac{\alpha\Delta x_{i+1}}{2} \right)^{\gamma-1} - \tilde{D}_i^n x_i^{\gamma-1} (1 - \alpha)}{\alpha} \right) \\ & + \frac{2}{\alpha(\alpha + 1)x_i^{\gamma-1}\Delta x_{i+1}^2} \phi_i^n \cdot \\ & \left(\frac{-\tilde{D}_{i-1/2}^n \left(x_i - \frac{\alpha\Delta x_{i+1}}{2} \right)^{\gamma-1} + \tilde{D}_i^n x_i^{\gamma-1} (\alpha + 1)(1 - \alpha)^2 - \tilde{D}_{i+1/2}^n \alpha^3 \left(x_i + \frac{\Delta x_{i+1}}{2} \right)^{\gamma-1}}{\alpha} \right) \\ & + \frac{2}{\alpha(\alpha + 1)x_i^{\gamma-1}\Delta x_{i+1}^2} \phi_{i+1}^n \alpha \left[\tilde{D}_i^n x_i^{\gamma-1} (1 - \alpha) + \alpha D_{i+1/2}^n \left(x_i + \frac{\Delta x_{i+1}}{2} \right)^{\gamma-1} \right] \end{aligned} \quad (126)$$

Approximation of $g(x_i, \tau_{n+1})$ can be obtained in a similar manner. However, here we will evaluate all coefficients of ϕ_i^{n+1} at τ_n instead of τ_{n+1} , in order to avoid an iterative solution to the nonlinear differential equation. Thus,

$$\begin{aligned}
g(x_i, \tau_{n+1}) = & \frac{x_i}{\tilde{R}} \frac{d\tilde{R}}{d\tau} \left[\frac{\alpha^2 \phi_{i+1}^{n+1} + (\alpha + 1)(1 - \alpha) \phi_i^{n+1} - \phi_{i-1}^{n+1}}{\alpha(\alpha + 1) \Delta x_{i+1}} \right] \\
& + \frac{2}{\alpha(\alpha + 1) x_i^{\gamma-1} \Delta x_{i+1}^2} \phi_{i-1}^{n+1} \left(\frac{\tilde{D}_{i-1/2}^n \left(x_i - \frac{\alpha \Delta x_{i+1}}{2} \right)^{\gamma-1} - \tilde{D}_i^n x_i^{\gamma-1} (1 - \alpha)}{\alpha} \right) \\
& + \frac{2}{\alpha(\alpha + 1) x_i^{\gamma-1} \Delta x_{i+1}^2} \phi_i^{n+1} \cdot \\
& \left(\frac{-\tilde{D}_{i-1/2}^n \left(x_i - \frac{\alpha \Delta x_{i+1}}{2} \right)^{\gamma-1} + \tilde{D}_i^n x_i^{\gamma-1} (\alpha + 1)(1 - \alpha)^2 - \tilde{D}_{i+1/2}^n \alpha^3 \left(x_i + \frac{\Delta x_{i+1}}{2} \right)^{\gamma-1}}{\alpha} \right) \\
& + \frac{2}{\alpha(\alpha + 1) x_i^{\gamma-1} \Delta x_{i+1}^2} \phi_{i+1}^{n+1} \alpha \left[\tilde{D}_i^n x_i^{\gamma-1} (1 - \alpha) + \alpha D_{i+1/2}^n \left(x_i + \frac{\Delta x_{i+1}}{2} \right)^{\gamma-1} \right]
\end{aligned} \tag{127}$$

By bringing the implicit terms to the left hand side, a tridiagonal system of equations can be obtained of the form:

$$P\Phi^{n+1} = Q \tag{128}$$

where P is a matrix of coefficients, Φ^{n+1} is a vector of the ϕ_i^{n+1} terms, and Q is a vector which depends only on Φ^n and τ_n . By inspection of Equations (126-127), P is a tridiagonal matrix with

$$P_{i,i-1} = \frac{\Delta\tau_{n+1}}{2} \left(\frac{x}{\alpha(\alpha+1)\Delta x_{i+1}} \frac{d\tilde{R}}{d\tau} \right) - \frac{\Delta\tau_{n+1}}{\alpha(\alpha+1)x_i^{\gamma-1}\Delta x_{i+1}^2} \left(\frac{\tilde{D}_{i-1/2}^n \left(x_i - \frac{\alpha\Delta x_{i+1}}{2} \right)^{\gamma-1} - \tilde{D}_i^n x_i^{\gamma-1} (1-\alpha)}{\alpha} \right)$$

(129)

$$P_{i,i} = 1 + \frac{\Delta\tau_{n+1}}{2} \left(\frac{-x_i(1-\alpha)}{\alpha\Delta x_{i+1}} \frac{d\tilde{R}}{d\tau} \right) - \frac{\Delta\tau_{n+1}}{\alpha(\alpha+1)x_i^{\gamma-1}\Delta x_{i+1}^2} \cdot \left(\frac{-\tilde{D}_{i-1/2}^n \left(x_i - \frac{\alpha\Delta x_{i+1}}{2} \right)^{\gamma-1} + \tilde{D}_i^n x_i^{\gamma-1} (\alpha+1)(1-\alpha)^2 - \tilde{D}_{i+1/2}^n \alpha^3 \left(x_i + \frac{\Delta x_{i+1}}{2} \right)^{\gamma-1}}{\alpha} \right) \quad (130)$$

$$P_{i,i+1} = \frac{\Delta\tau_{n+1}}{2} \left(\frac{-x_i\alpha}{(\alpha+1)\Delta x_{i+1}} \frac{d\tilde{R}}{d\tau} \right) - \frac{\Delta\tau_{n+1}}{\alpha(\alpha+1)x_i^{\gamma-1}\Delta x_{i+1}^2} \alpha \left[\tilde{D}_i^n x_i^{\gamma-1} (1-\alpha) + \alpha D_{i+1/2}^n \left(x_i + \frac{\Delta x_{i+1}}{2} \right)^{\gamma-1} \right]$$

(131)

for $i= 1, \dots, N-2$. Likewise, inspection of Equations (126-127) yields the elements of the vector Q:

$$Q_i = \frac{\Delta\tau_{n+1}}{2} g(x_i, \tau_n) \quad (132)$$

for $i= 1, \dots, N-2$, where $g(x_i, \tau_n)$ is evaluated using Equation (126).

The coefficient matrix and right hand side vector for the boundary condition at $i=0$ are:

$$P_{0,0} = 1 + \frac{\Delta\tau_{n+1}}{\Delta x_{i+1}^{\gamma-1}} \tilde{D}_{i+1/2}^n \quad (133)$$

$$P_{0,1} = -\frac{\Delta\tau_{n+1}}{\Delta x_{i+1}^{\gamma-1}} \tilde{D}_{i+1/2}^n \quad (134)$$

$$Q_0 = \phi_i^n \left(1 - \frac{\Delta\tau_{n+1}}{\Delta x_{i+1}^{\gamma-1}} \tilde{D}_{i+1/2}^n \right) + \phi_{i+1}^n \left(\frac{\Delta\tau_{n+1}}{\Delta x_{i+1}^{\gamma-1}} \tilde{D}_{i+1/2}^n \right) \quad (135)$$

The temporal treatment of the boundary condition at the cell membrane requires special handling in order to avoid iterative solution strategies. One way that this is achieved is to evaluate the advective term explicitly so that the time derivative will assume a modified Crank-Nicolson scheme of the form:

$$\frac{1}{2} \frac{\phi_i^{n+1} - \phi_i^n}{\Delta\tau_{n+1}} = y(x_i, \tau_n) + \frac{1}{2} [q(x_i, \tau_n) + q(x_i, \tau_{n+1})] \quad (136)$$

where

$$y(x_i, \tau_n) = \frac{x_i}{\tilde{R}} \frac{d\tilde{R}}{d\tau} \left(\frac{\phi_i^n - \phi_{i-1}^n}{\Delta x_i} \right) \quad (137)$$

$$q(x_i, \tau_n) = \frac{\tilde{D}_i^n}{\Delta x_i^2} (\phi_{i+1}^n - \phi_i^n) - \frac{\tilde{D}_{i-1/2}^n \left(x_i - \frac{\Delta x_i}{2} \right)^{\gamma-1}}{x_i^{\gamma-1} \Delta x_i^2} (\phi_i^n - \phi_{i-1}^n) \quad (138)$$

$$q(x_i, \tau_{n+1}) = \frac{\tilde{D}_i^n}{\Delta x_i^2} (\phi_{i+1}^{n+1} - \phi_i^{n+1}) - \frac{\tilde{D}_{i-1/2}^n \left(x_i - \frac{\Delta x_i}{2} \right)^{\gamma-1}}{x_i^{\gamma-1} \Delta x_i^2} (\phi_i^{n+1} - \phi_{i-1}^{n+1}) \quad (139)$$

and where the factor of $\frac{1}{2}$ multiplying the time derivative accounts for the fact that the control volume at the cell membrane is smaller than the other control volumes throughout

the cell. Finally, the definitions for the water volume fraction at the fictitious point beyond the cell membrane will be defined as

$$\phi_{i+1}^n = (1 - \phi_i^n) \frac{2\Delta x_i}{\tilde{D}_i^n \tilde{R}} \frac{d\tilde{R}}{d\tau} + \phi_{i-1}^n \quad (140)$$

$$\phi_{i+1}^{n+1} = (1 - \phi_i^n) \frac{2\Delta x_i}{\tilde{D}_i^n \tilde{R}} \frac{d\tilde{R}}{d\tau} + \phi_{i-1}^{n+1} \quad (141)$$

in order to avoid iterative solution methods. Inserting these definitions into Equations (138) and (139) will yield

$$P_{N-1, N-2} = -\frac{\Delta\tau_{n+1}}{2x_i^{\gamma-1}\Delta x_{i+1}^2} \left(\tilde{D}_i^n x_i^{\gamma-1} + \tilde{D}_{i-1/2}^n \left(x_i - \frac{\Delta x_i}{2} \right)^{\gamma-1} \right) \quad (142)$$

$$P_{N-1, N-1} = \frac{1}{2} + \frac{\Delta\tau_{n+1}}{2x_i^{\gamma-1}\Delta x_{i+1}^2} \left(\tilde{D}_i^n x_i^{\gamma-1} + \tilde{D}_{i-1/2}^n \left(x_i - \frac{\Delta x_i}{2} \right)^{\gamma-1} \right) \quad (143)$$

$$\begin{aligned} Q_{N-1} = & \phi_i^n \left[\frac{1}{2} + \frac{\Delta\tau_{n+1}}{2x_i^{\gamma-1}\Delta x_{i+1}^2} \left(\tilde{D}_i^n x_i^{\gamma-1} + \tilde{D}_{i-1/2}^n \left(x_i - \frac{\Delta x_i}{2} \right)^{\gamma-1} \right) \right] \\ & + \phi_{i-1}^n \left[\frac{\Delta\tau_{n+1}}{2x_i^{\gamma-1}\Delta x_i^2} \left(\tilde{D}_{i-1/2}^n \left(x_i - \frac{\Delta x_i}{2} \right)^{\gamma-1} \right) \right] \\ & + \left[\phi_{i-1}^n + (1 - \phi_i^n) \frac{2\Delta x_i}{\tilde{R}\tilde{D}_i^n} \frac{d\tilde{R}}{d\tau} \right] \frac{\Delta\tau_{n+1}}{2x_i^{\gamma-1}\Delta x_i^2} \left(\tilde{D}_i^n x_i^{\gamma-1} \right) \\ & + \frac{\phi_i^n - \phi_{i-1}^n}{\Delta x_i} \frac{x_i \Delta\tau_{n+1}}{\tilde{R}} \frac{d\tilde{R}}{d\tau} + (1 - \phi_i^n) \frac{\Delta\tau_{n+1}}{\tilde{R}\Delta x_i} \frac{d\tilde{R}}{d\tau} \quad (144) \end{aligned}$$

These equations for the elements of the coefficient and right hand side matrix at the moving boundary will be redefined when vitrification at the cell membrane occurs (i.e., if ϕ_{sphere}). At the onset of glass transition, Equations (142) – (144) will be redefined as

$$P_{N-1,N-1} = 1 + \frac{\Delta\tau^{n+1}}{\Delta x_i^2} (\tilde{D}_{i-1}^n + \tilde{D}_i^n) \quad (145)$$

$$P_{N-1,N-2} = -\frac{\Delta\tau^{n+1}}{\Delta x_i^2} (\tilde{D}_{i-1}^n + \tilde{D}_i^n) \quad (146)$$

$$Q_{N-1} = \phi_i^n \left[1 - \frac{\Delta\tau^{n+1}}{\Delta x_i^2} (\tilde{D}_{i-1}^n + \tilde{D}_i^n) \right] + \phi_{i-1}^n \left[\frac{\Delta\tau^{n+1}}{\Delta x_i^2} (\tilde{D}_{i-1}^n + \tilde{D}_i^n) \right] \quad (147)$$

Once the matrices P and Q are assembled, solutions for the implicit water volume fractions will require inverting the coefficient matrix P . Since this matrix is tridiagonal, this process can be achieved efficiently using an LU decomposition algorithm (Faires and Burden, 1998).

3.4 Integration of Cell Properties

In order to estimate the cell radius \tilde{R} as a function of τ , Equation (66) was integrated between τ_0 and τ_n , yielding the following result:

$$1 - \frac{1}{\tilde{R}} = \int_0^{\tau_n} Bi \Delta \tilde{\mu} d\tau \quad (148)$$

where the Biot number Bi is defined in Equation (67). As a means to evaluate this integral, the trapezoidal rule will be used:

$$\tilde{R}_{n+1} = \left[\frac{1}{\tilde{R}_n} - \frac{\Delta\tau^{n+1}}{2} [(Bi_n \Delta \tilde{\mu}_n) + (Bi_{n+1} \Delta \tilde{\mu}_{n+1})] \right] \quad (149)$$

where all subscripts designate the time step.

As the cell constricts, the change in cell volume must be accounted for by water and salt volume fluxes. However, since the membrane is considered to be impermeable

to salt ions, mass conservation requires that the intracellular volume of salt is invariant with time. Violation of this mass conservation requirement will be defined as:

$$e_{mass} = \max_{\tau} \left[\frac{\tilde{V}_{so} - \tilde{V}_s}{\tilde{V}_{so}} \right] \quad (150)$$

where \tilde{V}_s is the intracellular nondimensional salt volume, and \tilde{V}_{so} is the initial intracellular nondimensional salt volume. For the binary system of water and NaCl, the nondimensional salt volume can be expressed as:

$$\tilde{V}_s = \tilde{V} - \tilde{V}_w \quad (151)$$

where

$$\tilde{V}_w = \frac{\int_0^R \phi_i A dr}{V_o} \quad (152)$$

and

$$\tilde{V} = \tilde{R}^3 \quad (153)$$

Evaluation of the water volume integral in Equation (152) was accomplished by subdividing the cell into subshells with an outer radius and inner radius defined as,

$$r_{outer} = r_i + \frac{\Delta r_{i+1}}{2} \quad (154)$$

$$r_{inner} = r_i - \frac{\alpha \Delta r_{i+1}}{2} \quad (155)$$

where r_i is the dimensional location of a node inside the cell (recall Equation 51) and dr_{i+1} is the dimensional distance between r_i and r_{i+1} . The amount of water contained within such a spherical shell is,

$$(V_w)_i = \phi_i \frac{4}{3} \pi (r_{outer}^3 - r_{inner}^3) \quad (156)$$

which can be nondimensionalized into the form:

$$\left(\tilde{V}_w\right)_i = \phi_i \tilde{R}^3 \left[\frac{3}{2} x_i^2 \Delta x_{i+1} (1 + \alpha) + \frac{3}{4} x_i \Delta x_{i+1}^2 (1 - \alpha^2) + \frac{1}{8} \Delta x_{i+1}^3 (1 + \alpha^3) \right] \text{ for } i = 1, \dots, N-2 \quad (157)$$

In order to account for the reduced control volume at the cell membrane, the outer and inner radii will be defined as,

$$r_{outer} = R \quad (158)$$

$$r_{inner} = R - \frac{\Delta r_i}{2} \quad (159)$$

Inserting these definitions into Equation (156) yields,

$$\left(\tilde{V}_w\right)_{N-1} = \phi_{N-1} \tilde{R}^3 \left[\frac{3}{2} \Delta x_{N-1} - \frac{3}{4} \Delta x_{N-1}^2 + \frac{1}{8} \Delta x_{N-1}^3 \right] \quad (160)$$

In a similar manner, the reduced control volume at the cell center can be accounted for by defining,

$$r_{outer} = \frac{\Delta r_{i+1}}{2} \quad (161)$$

$$r_{inner} = 0 \quad (162)$$

With these definitions, Equation (156) reduces to,

$$\tilde{V}_{w,0} = \phi_0 \tilde{R}^3 \frac{\Delta x_1^3}{8} \quad (163)$$

Finally, all these terms are summed to evaluate the total nondimensional water volume:

$$\begin{aligned} \tilde{V}_w = & \phi_0 \tilde{R}^3 \frac{\Delta x_1^3}{8} + \phi_{N-1} \tilde{R}^3 \left[\frac{3}{2} \Delta x_{N-1} - \frac{3}{4} \Delta x_{N-1}^2 + \frac{1}{8} \Delta x_{N-1}^3 \right] + \\ & \sum_{i=0}^{N-1} \phi_i \tilde{R}^3 \left[\frac{3}{2} x_i^2 \Delta x_{i+1} (1 + \alpha) + \frac{3}{4} x_i \Delta x_{i+1}^2 (1 - \alpha^2) + \frac{1}{8} \Delta x_{i+1}^3 (1 + \alpha^3) \right] \end{aligned} \quad (164)$$

CHAPTER 4

SIMULATIONS WITH CONSTANT BIOPHYSICAL PROPERTIES

Initial analysis of intracellular water diffusion was performed using constant biophysical properties for purposes of model validation. In particular, both the Biot number and the nondimensional chemical potential were assigned constant values in Equation (66), and the diffusivity was assumed to be spatially uniform ($\tilde{D} = 1$). Physically, these assumptions would require that the rates of diffusive transport and membrane transport differ only by a constant multiplicative factor, that the diffusivity be independent of solution composition, and that the extracellular chemical potential continuously decrease to accommodate a constant driving force as the cell dehydrates. Although these restrictions are not realistic, the simplifications allowed us to investigate the accuracy of our numerical model. By setting all parameters to a constant value, the complexity and nonlinearity of the system was reduced, thereby permitting the use of a commercially available multi-physics finite element solver (FEMLAB, Comsol AB, Stockholm, Sweden) for validation of our numerical model. We also examined the internal consistency of our predictions by evaluating the effect of node spacing and time step size on mass conservation.

We solved for the water volume fraction at each node of a spherical cell ($\gamma = 3$) as a function of nondimensional time by iteratively solving Equation (128), using Equations (129)-(135) with Equations (142)-(144) to evaluate the matrices P and Q , and Equations (66) and (149) to calculate variations of the cell radius. In the present set of simulations, we used a uniform grid ($\alpha = 1$), and initial conditions corresponding to a uniform distribution of intracellular water, with $\phi_i^0 = 0.95$ for $i = 0, \dots, N-1$. Because we

used a constant dimensionless chemical potential $\Delta\tilde{\mu} = -0.01$, it was possible for the intracellular water concentration to assume negative values for extended simulations; thus, simulations were halted if $\phi_{N-1}^n \leq 0$.

Initially, we compared our model predictions with those obtained using a commercial finite-element solver (FEMLAB) for the simplified system. Equations (65), (68), and (69) were implemented in FEMLAB after multiplying both sides of Equations (65) and (69) by x^2 to prevent a singularity at $x = 0$. In FEMLAB, a mesh with 15 elements of equal size was used. For our finite difference solution, we used a mesh with 1000 nodes, and a constant nondimensional time step $\Delta\tau = 10^{-6}$. Our predictions agreed reasonably well with predictions obtained using the FEMLAB solver for $\text{Bi} = 10^3$ (Figure 3) and $\text{Bi} = 10^4$ (Figure 4).

We also determined whether our numerical solution yielded results that were consistent with requirements of mass conservation. Given that the total volume of salt within the cell must remain constant during the dehydration process, we evaluated the magnitude of any artefactual variations in intracellular salt content using Equation (152), as a function of mesh size and time step. Representative results for $\text{Bi} = 10^5$ are shown in Figure 5. For $N \geq 100$, extensive violations of mass conservation (30%-100% error) were observed for time step sizes $\Delta\tau = 10^{-2}$ and $\Delta\tau = 10^{-4}$. For smaller time step sizes ($\Delta\tau \leq 10^{-6}$), the mass conservation error decreased with increasing number of nodes, and appeared to be independent of the magnitude of the nondimensional time step. For example, for $N = 1000$, the mass conservation errors were in the range 0.4%-1.4%, for $10^{-10} \leq \Delta\tau \leq 10^{-6}$, which is comparable to the performance reported in other studies of diffusion-limited cell dehydration (Levin, 1976; Mao et al., 2003).

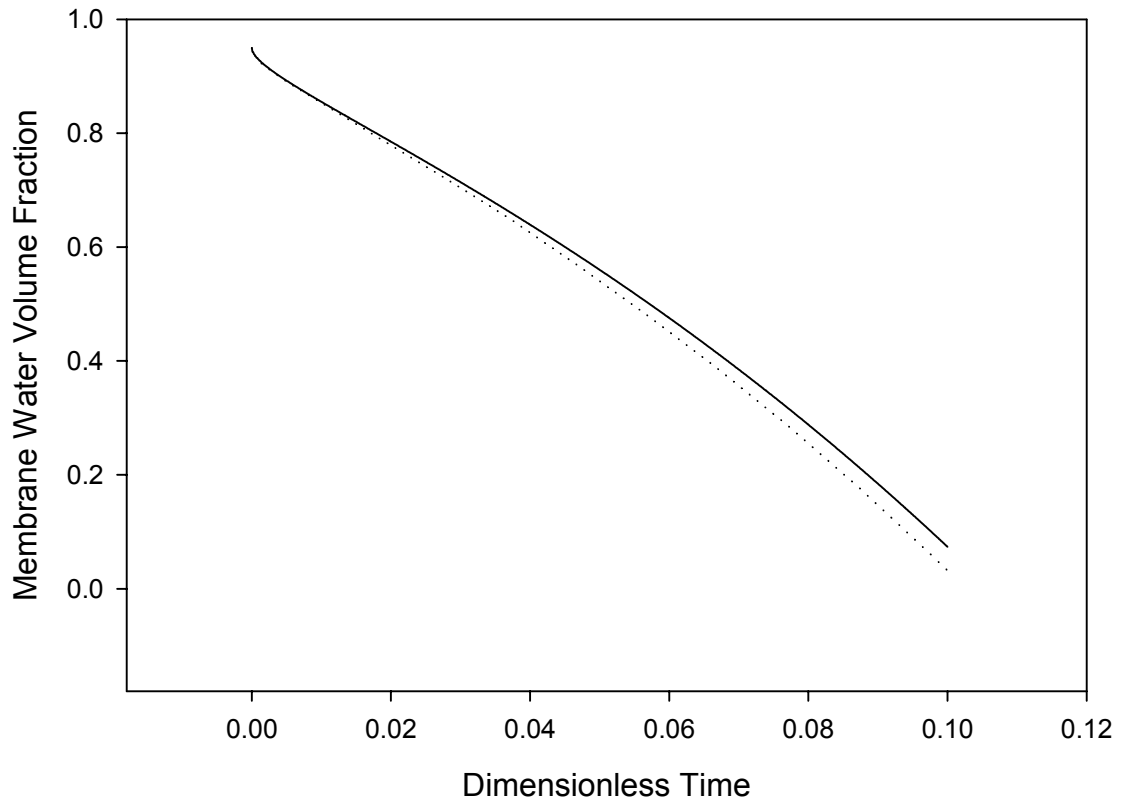


Figure 3. Predicted volume fraction of intracellular water at the cell membrane, as a function of nondimensional time, for $Bi = 1000$ and $\Delta\tilde{\mu} = -0.01$. Shown are solutions obtained using our finite difference model (solid line) and using the finite element solver FEMLAB (dotted line).

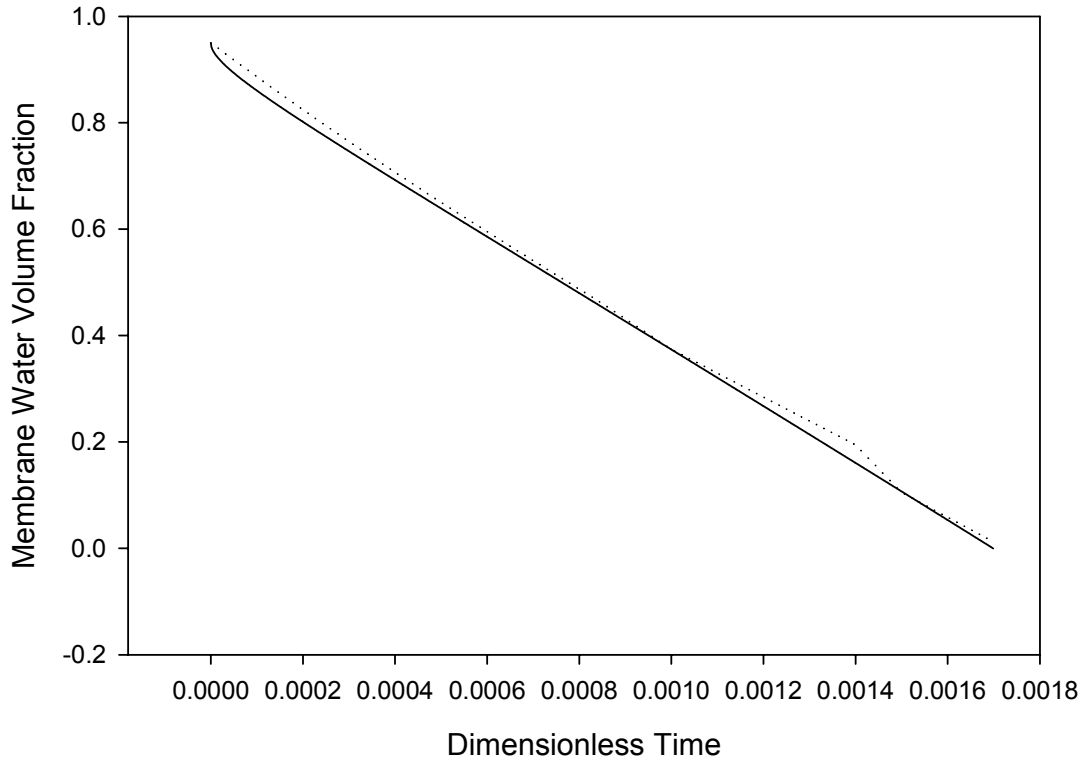


Figure 4. Predicted volume fraction of intracellular water at the cell membrane, as a function of nondimensional time, for $Bi = 10,000$ and $\Delta\tilde{\mu} = -0.01$. Shown are solutions obtained using our finite difference model (solid line) and using the finite element solver FEMLAB (dotted line).

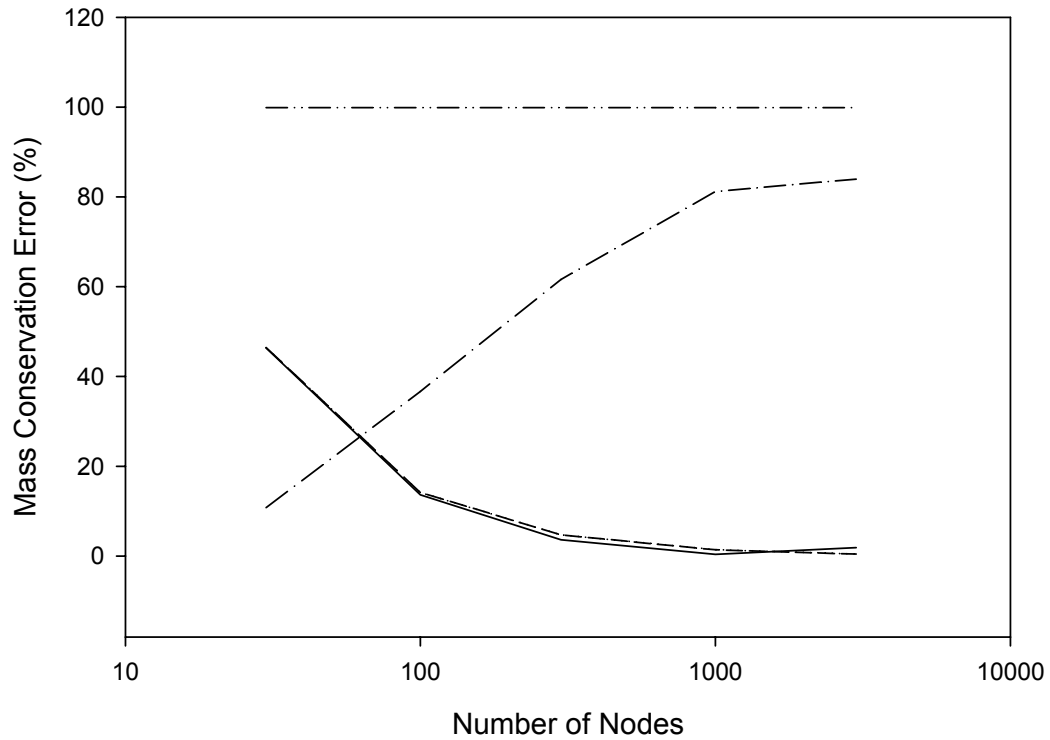


Figure 5. Maximum variation in intracellular salt content during cell dehydration with $Bi = 10^5$ and $\Delta\tilde{\mu} = -0.01$, simulated using our finite differences model with different grid spacings and time step sizes. The nondimensional time steps were $\Delta\tau = 10^{-2}$ (dash-double-dotted line); $\Delta\tau = 10^{-4}$ (dash-dotted line); $\Delta\tau = 10^{-6}$ (solid line); $\Delta\tau = 10^{-8}$ (dashed line); and $\Delta\tau = 10^{-10}$ (dotted line).

CHAPTER 5

SIMULATIONS WITH TEMPERATURE- AND CONCENTRATION- DEPENDENT BIOPHYSICAL PROPERTIES

5.1 Comparison with Experimental Data

In this chapter, the diffusivity, chemical potential, and permeability were calculated using the temperature- and concentration-dependent constitutive equations given in Section 2.3. Initially, we further validated our finite difference model by comparing its predictions to experimental measurements of cell volume changes during the dehydration of yeast (*S. cerevisiae*) cells published by Ushiyama *et al.* (1973).

We solved for the water volume fraction at each node of a spherical cell ($\gamma=3$) by iteratively solving the system of equations defined by Equation (128), using Equations (129)-(135) with Equations (66), (142)-(144), and (149) to evaluate the matrices P and Q . Variations in the cell biophysical properties were calculated using Equation (11) for the membrane permeability; Equations (12)-(15) for the diffusivity; Equations (16)-(18) for the chemical potentials. In order to evaluate these temperature-dependent parameters, we integrated Equation (71) using a forward difference scheme, to obtain the temperature at each time step. We checked for violations of mass conservation using Equation (150). In the present set of simulations, we used a linear cooling protocol with an initial temperature of 272.623 K, and a uniform initial concentration $c_{so} = 142 \text{ mol/m}^3$ ($\phi_i^0 = 0.9962$ for $i = 0, \dots, N-1$), corresponding to isotonic conditions.

We used published biophysical properties of yeast cells, shown in Table 1 (Levin, 1979). The corresponding nondimensional parameters, evaluated for $T_c = 30 \text{ K}$, are also shown in Table 1. For our finite difference solution, we used a uniform mesh ($\alpha = 1$) with

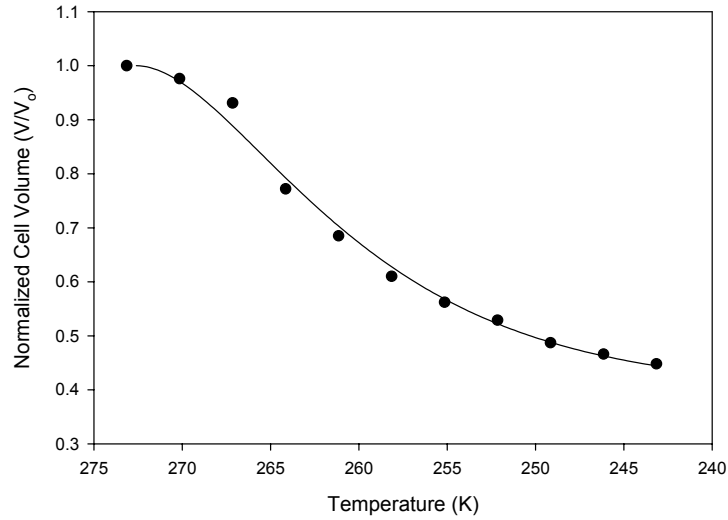
Table 1. Biophysical properties for yeast cell (*S. cerevisiae*) (Levin, 1979)

Cooling Rate	10 °C/min	100 °C/min
Cell radius (μm)	2.83	2.83
Activation energy ($J mol^{-1}$)	6.79×10^4	4.53×10^4
Limiting membrane permeability ($m Pa^{-1} s^{-1}$)	1.52×10^{-2}	2.73×10^{-6}
θ_D	2×10^{-6}	2×10^{-5}
θ_M	8×10^{-14}	4×10^{-9}
ε_D	20	20
ε_M	180	270

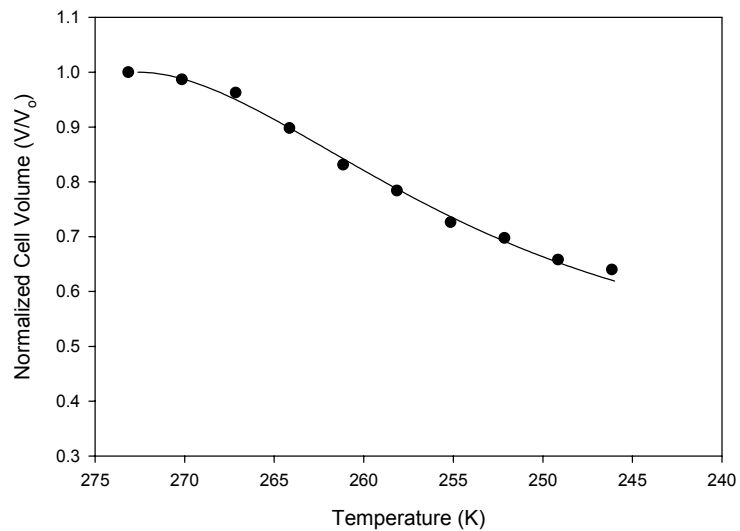
500 nodes, and a constant nondimensional time step of $\Delta\tau = 10^{-1}$ or $\Delta\tau = 10^{-2}$ to simulate freezing at the rates of 10 °C/min and 100 °C/min, respectively.

Our predictions for the kinetics of dehydration of yeast cells at 10 °C/min and 100 °C/min are shown in Figures 6(a) and 6(b), respectively. Evaluation of Equation (150) confirmed that mass conservation errors were smaller than 0.1% for these simulations. Although $\theta_D \gg \theta_M$ for both of these cases, the system is in fact in a membrane-limited transport regime, as a result of the temperature dependent factors ($\varepsilon_M \gg \varepsilon_D$). The maximum amount of solute polarization (quantified here by the difference between the water volume fraction at the membrane and cell center, normalized by the water volume fraction at the cell center) was only ~0% for both $B = 10$ °C/min and $B = 100$ °C/min. Because θ_D , θ_M and ε_M are all smaller for the slower cooling rate, the total amount of dehydration is greater for this case than for the faster cooling rate. Also shown in Figure 6 are experimental data of volume changes in yeast cells during freezing (Ushiyama *et al.*, 1973). As seen, our predictions agree reasonably well with the published experimental data, validating our model in the low Biot number regime. The accuracy of our model predictions are especially remarkable given the fact that the

osmotically inactive volume is neglected in the finite difference model (ie. $\tilde{V}_b = 0$), whereas yeast cells have an osmotically inactive volume $\tilde{V}_b = 0.24$ (Levin, 1979).



(a)



(b)

Figure 6. Comparison of numerical predictions (solid line) and experimental measurements (circles) of the normalized cell volume of yeast cells cooled at a rate of (a) 10°C/min, and (b) 100°C/min.

5.2 Simulations in Large Biot Number Regimes

In order to examine the behavior of our finite difference model under conditions of diffusion-limited transport, we simulated the response of a hypothetical cell type with the parameters shown in Table 2, which has been shown to enter large Biot number regimes at low temperatures (Kasharin and Karlsson, 1998). For purposes of comparison, we also obtained predictions for this cell type with Mazur's membrane-limited model, by numerically integrating Equation (45) using a fourth-order Runge-Kutta algorithm.

Initial predictions for the intracellular water volume (normalized to its initial value), obtained using the finite-difference model and the conventional membrane-limited transport model, are shown in Figure 7(a). In the finite difference calculation, we initially used a uniform grid ($\alpha = 1$) with 7750 nodes, and a constant step size $\Delta\tau = 10^{-4}$. Because this system is known to have a small Biot number for temperatures greater than $\sim 180\text{ K}$ (Kasharin and Karlsson, 1998), predictions of the finite difference model match those of the simple membrane-limited model in the initial stages of the simulation. However, the two models begin to diverge below $\sim 170\text{ K}$. Given that transition to a diffusion-limited regime ($Bi \gg 1$) should result in dehydration that is slower than

Table 2. Biophysical parameters for hypothetical cell type (Kasharin and Karlsson, 1998)

<i>Parameter</i>	<i>Symbol</i>	<i>Value</i>	<i>Units</i>
Cell radius	R_o	5×10^{-6}	m
Activation energy	E_a	1×10^4	$J\text{ mol}^{-1}$
Cooling Rate	B	200	$^{\circ}C/min$
Limiting membrane permeability	L_{∞}	1.362×10^{-13}	$m\text{ Pa}^{-1}\text{ s}^{-1}$
Characteristic Temperature Interval	T_c	100	K
	θ_D	4×10^{-5}	
	θ_M	3×10^{-2}	
	ε_D	6	
	ε_M	0.03	

predicted from a membrane-limited transport model (due to the additional resistance presented by the solute polarization layer), the finite-difference predictions for $T < 170\text{ K}$ in Figure 7(a) must be artefactual. Indeed the mass conservation error for this simulation was 14%.

To correct the problems evident in Figure 7(a), we recognized that they were caused by the fact that the diffusivity becomes vanishingly small as the temperature and intracellular water content decrease. Thus, with the nondimensional time variable defined using Equation (52), a constant nondimensional time step $\Delta\tau$ will correspond to an increasingly large time step Δt as D_o decreases. If the characteristic time-scale for membrane transport (δt_M ; Equation 23), is smaller than the time step used for integration, numerical problems will result. Therefore, we implemented an alternative nondimensionalization of time:

$$d\tau = \frac{dt}{\min(\delta t_M, \delta t_D)} \quad (165)$$

In practice, this was achieved by reducing the original nondimensional time step $\Delta\tau$ by a factor of $(\delta t_M/\delta t_D)$ whenever $\delta t_M < \delta t_D$. Furthermore, for conditions which resulted in vitrification (i.e. $\tilde{D} = 0$) of the intracellular solution near the membrane, we changed the boundary conditions as described in Equations (146)-(148), in order to prevent numerical difficulties associated with the vanishing diffusion constant.

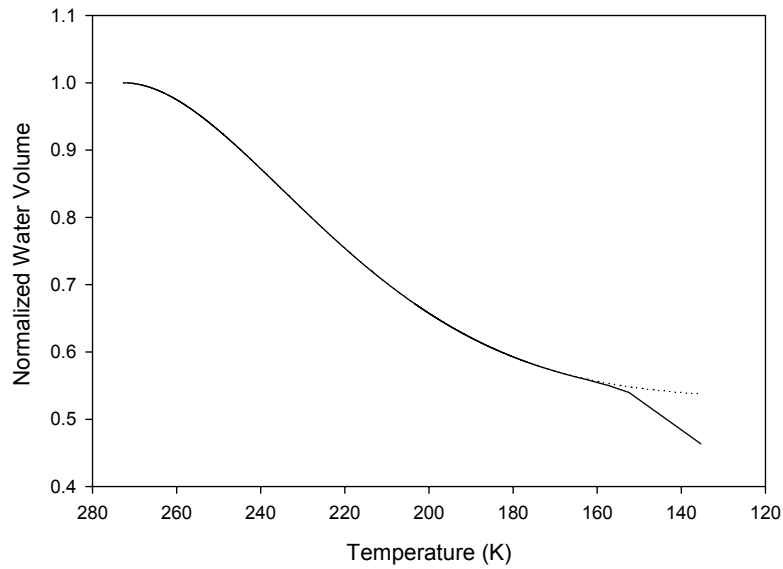
With the above modifications, using a nonuniform grid ($\alpha = 1.0148$) with 1000 nodes and a nominal time step $\Delta\tau = 10^{-5}$, predictions improved, as shown in Figure 7(b). For this simulation, errors in conservation of mass were less than 1%, and predicted water volumes do not decrease faster than Mazur's model. As indicated by arrows in Figure

7(b), the time step is rescaled as described above for $T < -105$ °C, inasmuch as $\delta t_M < \delta t_D$ in this temperature range. Moreover vitrification is predicted to occur in the solution at the interior surface of the cell membrane ($x=1$) at -126 °C, halting any further dehydration. Because the conventional membrane-limited transport model does not take into account the decrease in intracellular diffusivity with decreasing temperature and water content, it incorrectly predicts that cell shrinkage will continue below -126 °C.

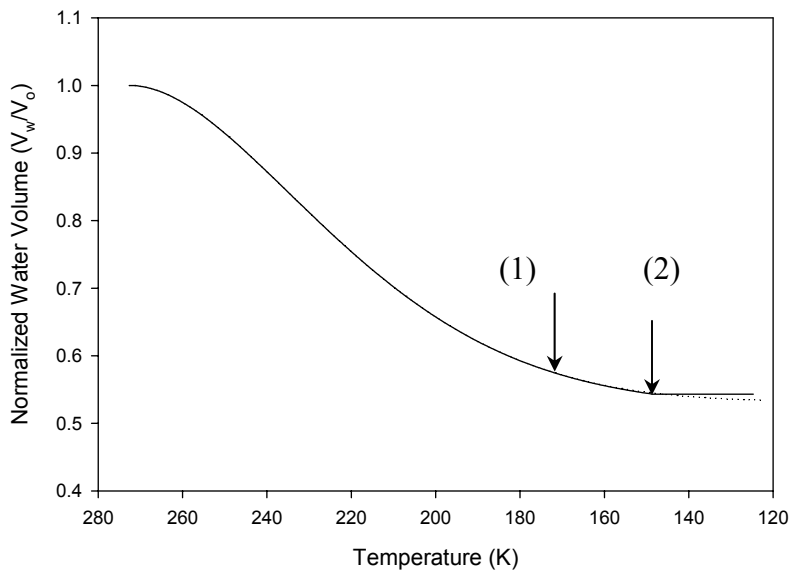
To further emphasize the differences in predictions from our model and the conventional membrane-limited transport model, we modified the parameters of the simulation to make $\theta_D > 1$, representing a highly diffusion-limited regime. By keeping θ_M and ε_M at the same values as those given in Table 2, predictions from Mazur's membrane-limited transport model will be identical to those shown in Figure 7. Thus, by increasing L_∞ by a factor of 10^5 while also increasing the cooling rate by a factor of 10^5 , the dimensionless group characterizing diffusion-limited transport will change from $\theta_D = 4 \times 10^{-5}$ to $\theta_D = 4$, while leaving θ_M unchanged. The corresponding predictions of our model, using a nonuniform grid ($\alpha = 1.0148$) with 1000 nodes and a nominal time step size $\Delta\tau = 10^{-6}$, are shown in Figure 8. For these conditions, the mass conservation error was less than 0.1%. As indicated by the arrow in Figure 8, mass transport occurs in a high Biot number regime ($\delta t_M < \delta t_D$) throughout the simulation, resulting in slower dehydration compared with predictions obtained using the membrane-limited model. Vitrification at the node closest to the cell membrane ($i = N - 1$) occurs at -85 °C, after which transport stops, leading to significant divergence from Mazur's model.

The kinetics of intracellular water transport in the previous simulation is shown in Figure 9, which describes the local changes in the water volume fraction at the cell center

$(x = 0)$ and near the cell membrane $(x = 1)$. Despite the fact that $\sim 30\%$ of the total cell water was lost, the water volume fraction at the cell center never changed during the simulation. Instead, most of the water was removed from the region near the cell membrane. Here, the water volume fraction was observed to drop sharply, causing a dramatic increase in the concentration of salt and leading to local vitrification. Subsequent to vitrification at the node $i = N - 1$, the water volume fraction increased at node $i = N - 2$ because the diffusive water flux from the cell interior was no longer depleted by the transmembrane flux. Eventually, the entire cell vitrified simultaneously at $T = 124 \text{ K}$, corresponding to the Vogel-Fulcher critical temperature (βT_g) . However, diffusion effectively stops well before the temperature reaches βT_g , because $\delta t_D \gg \delta t_B$ in this regime. Interestingly, $\delta t_M \ll \delta t_B$ in this temperature range, as evidenced by continued cell dehydration in the membrane-limited model predictions (Figure 8).



(a)



(b)

Figure 7. Predictions of intracellular water volume (normalized to its initial value) obtained using the finite-difference diffusion model (solid line) and Mazur's membrane-limited transport model (dotted line), for a hypothetical cell type with $\theta_M = 3 \times 10^{-2}$, $\theta_D = 4 \times 10^{-5}$. (a) Original finite-difference model; (b) Modified finite-difference model, including adaptive step size in diffusion-limited transport regime and new boundary conditions with provisions for non-uniform vitrification. Arrows indicate temperature at which $\delta t_D > \delta t_M$ (1) and temperature at which vitrification occurs at node $i = N - 1$ (2).

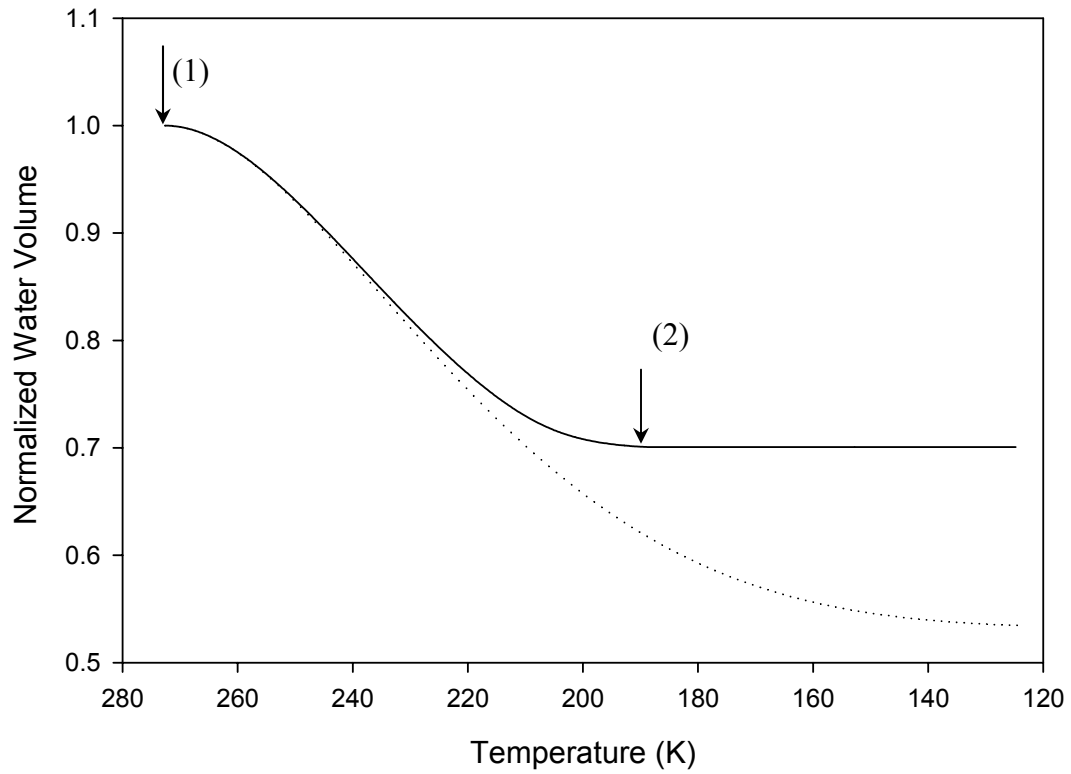


Figure 8. Predictions of intracellular water volume (normalized to its initial value) obtained using the finite-difference diffusion model (solid line) and Mazur's membrane-limited transport model (dotted line), for a hypothetical cell type with $\theta_M = 3 \times 10^{-2}$, $\theta_D = 4$. Arrows indicate temperature at which $\delta t_D > \delta t_M$ (1) and temperature at which vitrification occurs at node $i = N - 1$ (2).

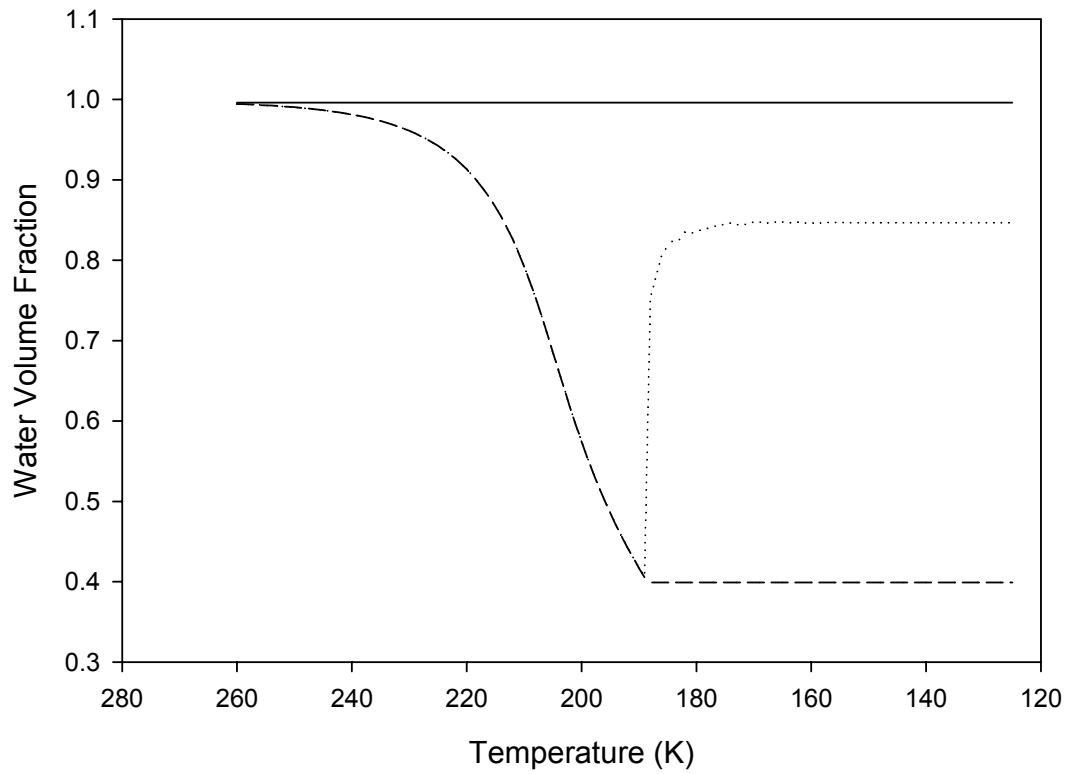


Figure 9. Predicted variations in water volume fraction at nodes $i = 0$ (solid line), $i = N - 2$ (dotted line) and $i = N - 1$ (dashed line), for finite-difference simulation in Figure 8 ($\theta_M = 3 \times 10^{-2}$, $\theta_D = 4$).

CHAPTER 6

PARAMETRIC ANALYSIS OF MASS TRANSPORT REGIMES DURING CELL FREEZING

6.1 Nominal Values

In this chapter, the effects of varying the nondimensional parameters θ_M , θ_D , ε_M , and ε_D were investigated in order to further explore mass transport regimes in which predictions from our diffusion model differed from those of the conventional membrane-limited transport model. When varying the parameters, each was perturbed about a nominal value, in a factorial design.

Nominal values for the characteristic transport parameters (θ_M , θ_D , ε_M , ε_D) were determined from physiological ranges of the cell biophysical properties and typical cryopreservation conditions. The ranges for the cooling rate, initial cell radius, and limiting permeability were obtained from a published compilation of properties for a variety of common cell types (McGrath, 1988), and are summarized in Table 3. Ranges for the Vogel-Fulcher viscosity coefficients were taken from estimations by Karlsson *et al.* (1994), and are also shown in Table 3. The characteristic temperature was defined to

Table 3. Physiological range of cell biophysical properties and cryopreservation conditions

<i>Parameter</i>	<i>Variable</i>	<i>Estimated</i>		<i>Units</i>
		<i>Lower Bound</i>	<i>Upper Bound</i>	
Cooling Rate	B	10^{-2}	10^1	$^{\circ}C/min$
Cell Radius	R_o	10^{-6}	10^{-4}	<i>m</i>
Limiting Permeability	L_{∞}	10^{-11}	10^1	<i>m/Pa s</i>
Activation Energy	E_a	10^4	10^5	<i>J/mol</i>
Vogel-Fulcher Coeff.	A_{η}	10^{-5}	10^{-3}	<i>Pa s</i>
Vogel-Fulcher Activation Temperature	E	600	750	<i>K</i>

be $T_c = 100\text{ K}$, which is on the order of the interval from the equilibrium freezing point of water ($0\text{ }^\circ\text{C}$) to its glass transition temperature ($-134\text{ }^\circ\text{C}$).

The physiologically relevant ranges of θ_M and θ_D were estimated from Equations (34) and (35) using the values in Table 3; within the calculated ranges, we chose nominal values $\theta_M = 10^{-11}$, $\theta_D = 10^{-3}$. The nominal value of ε_D was estimated based on the Vogel-Fulcher activation temperature of supercooled water, as predicted by (Karlsson *et al.*, 1994), yielding a nominal value $\varepsilon_D = 6$. Finally, the nominal value for ε_M was chosen to be the value that would result in 50% cellular dehydration for a hypothetical cell type characterized by the chosen nominal values of θ_M , θ_D , and ε_D ; this yielded a nominal Arrhenius number of $\varepsilon_M = 63.7$. The full ranges of the nondimensional parameters for physiologically relevant conditions are given in Table 4.

6.2 Supercooling Predictions in the Four-Dimensional Parametric Space

Intracellular supercooling is an important parameter which affects the probability of cell damage by IIF during cryopreservation (Karlsson *et al.*, 1993). In order to examine the benefit of our finite-difference diffusion model in predicting the cytoplasmic supercooling, we simulated the cell dehydration process over a range of values of the parameters θ_M , θ_D , ε_M , and ε_D . For purposes of comparison, we also obtained predictions with Mazur's membrane-limited model, by numerically integrating Equation (45) using a

Table 4. Ranges and nominal values of nondimensional parameters used in simulations

<i>Parameter</i>	<i>Nominal Value</i>	<i>Lower Bound</i>	<i>Upper Bound</i>
θ_M	10^{-11}	10^{-19}	10^{-2}
θ_D	10^{-3}	10^{-10}	10^3
ε_M	63.7	10	100
ε_D	6	6	7.5

fourth-order Runge-Kutta algorithm.

We solved for the water volume fraction at each node of a spherical cell ($\gamma=3$) by iteratively solving the system of equations defined by Equation (129), using Equations (130)-(136) with Equations (66), (143)-(148), and (150) to evaluate the matrices P and Q . Variations in the cell biophysical properties were calculated using Equation (11) for the membrane permeability; Equations (12)-(15) for the diffusivity; Equations (16) and (17) for the chemical potentials. In order to evaluate these temperature-dependent parameters, we integrated Equation (71) using a forward difference scheme, to obtain the temperature at each time step. We checked for violations of mass conservation using Equation (151). In the present set of simulations, we used a linear cooling protocol with an initial temperature of 272.623 K, and a uniform initial concentration $c_{so} = 142 \text{ mol/m}^3$ ($\phi_i^0 = 0.9962$ for $i = 0, \dots, N-1$), corresponding to isotonic conditions. The characteristic of supercooling at the cell center was calculated using Equations (19) and (20) at each time step.

We simulated the response of a hypothetical cell type with $\theta_D = 10^{-2}$ and $\varepsilon_D = 9$, corresponding to a transport regime rate-limited by diffusive transport. Even though these values are large compared to the nominal values, they are still within the physiological ranges defined in Table 4. Predictions for the maximum intracellular supercooling were obtained using the finite-difference model and using the conventional membrane-limited transport model; the absolute value of the difference between the two predictions (normalized with respect to T_c), is shown in Figure 10 for a range of values of θ_M and ε_M . In the finite difference calculations, we required the simulations to have a mass conservation error less than 1%. In the present set of simulations, this was

accomplished by using a uniform grid with 1000 nodes and a nominal time step size $\Delta\tau = 10^{-5}$. Twenty-five simulations were run for different combinations of values of θ_M and ε_M ; θ_M was varied over a range one order of magnitude above and below its nominal value, while ε_M was varied by $\pm 5\%$ of its nominal value. For small values of θ_M and ε_M , the supercooling predictions between the finite difference model and those of the simple membrane-limited model were found to disagree by as much as 37°C . However, the discrepancy between the models is observed to decrease to as little as 0.1°C for large θ_M and ε_M . Thus, despite the large values of the characteristic diffusion parameters θ_D and ε_D , there were regimes in the θ_M - ε_M plane in which predictions of the diffusion-limited and membrane-limited transport models agreed.

To further investigate the differences between supercooling predictions from the two models, we explored additional regimes in the four-dimensional parametric space, by repeating the above simulations for other values of θ_D and ε_D . The contour plots presented in Figures 11-16 were determined from combinations of values of the four nondimensional parameters, each of which was varied about its respective nominal value. In this analysis, 450 simulations were run, to obtain all combinations of all values of the four parameters listed in Table 5. We required that no numerical solutions have a violation of mass conservation exceeding 1%. This constraint was satisfied by using a uniform grid ($\alpha = 1$) with 500 nodes, and a nominal step size depending on the value of θ_D , as shown in Table 5. Avoiding violations in mass conservation with $\theta_D = 10^{-11}$ (Figure 16) was not possible. Initial analyses with this parametric value gave rise to mass conservation errors three-orders of magnitude larger than those obtained with all other values of θ_D . Furthermore, upon refining the spatial and temporal grids for the case of

Table 5. Ranges of dimensionless parameters used in simulations shown in Figures 11-16

$\Delta\tau$	θ_D	θ_M	ε_D	ε_M
10^{-6}	10^{-1}	10^{-12}	9	60.5
10^{-3}	10^{-3}	5×10^{-12}	6	62.1
10^{-2}	10^{-5}	10^{-11}	3	63.7
10^0	10^{-7}	5×10^{-11}		65.3
10^3	10^{-9}	10^{-10}		66.9
10^4	10^{-11}			

$\theta_D = 10^{-11}$, mass conservation errors became worse. Combined with the observation that the nondimensional water volume was predicted to increase with a fine internodal and temporal spacing, we believe that there are numerical problems in our solutions for this regime, and thus we do not consider the results presented in Figure 16 to be real. We did not further explore this issue, given that the value $\theta_D = 10^{-11}$ was outside the realistic range for this parameter as estimated by Table 4.

Differences in supercooling predictions between our model and the conventional membrane-limited model increased with increasing θ_D , increasing ε_D , decreasing θ_M , and decreasing ε_M . Although significant differences between the two modeling approaches were observed in some of the simulated regimes (e.g. Figure 11a), it should be noted that the present parametric analysis was restricted to a narrow range centered about a set of nominal values. Thus, behavior that is quantitatively and qualitatively different may be observed in regimes outside those simulated in Figures 11-15. For instance, erythrocytes ($\theta_M \cong 10^{-7}$, $\theta_D \cong 10^{-5}$, $\varepsilon_M \cong 19$, $\varepsilon_D \cong 6$) have been shown to exhibit extensive solute polarization (Levin, 1976) that would lead to large disagreements in supercooling predictions between a diffusion-limited and membrane-limited transport model. However, the values of θ_M and ε_M for erythrocytes both fall outside the window shown in

Figure 12(b). Thus, it may be necessary to complete further simulations in order to capture the behavior in all physiologically relevant transport regimes.

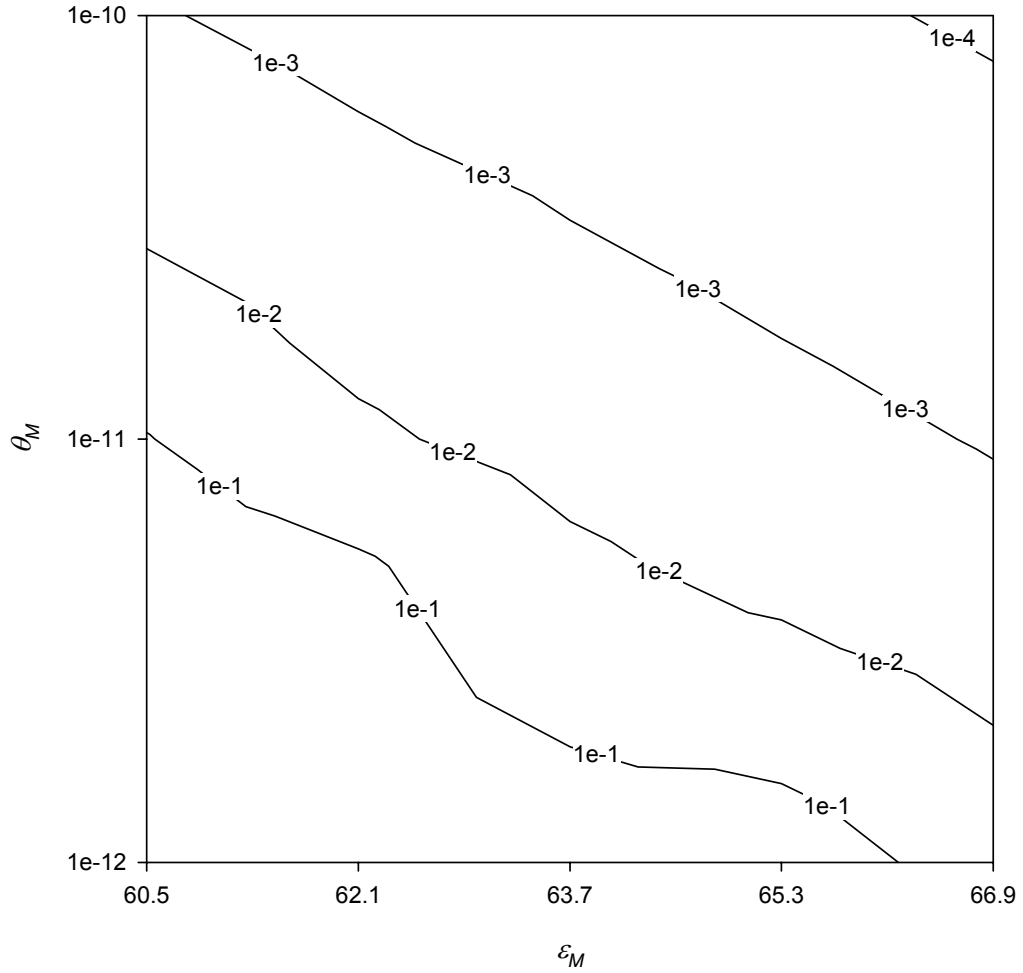


Figure 10. Contour plot of the difference in nondimensional intracellular supercooling predictions between a membrane-limited model and the model under study (predicted supercooling was normalized relative to the characteristic temperature $T_c = 100\text{ K}$). Predictions are based on $\theta_D = 10^{-2}$ and $\varepsilon_D = 9$.

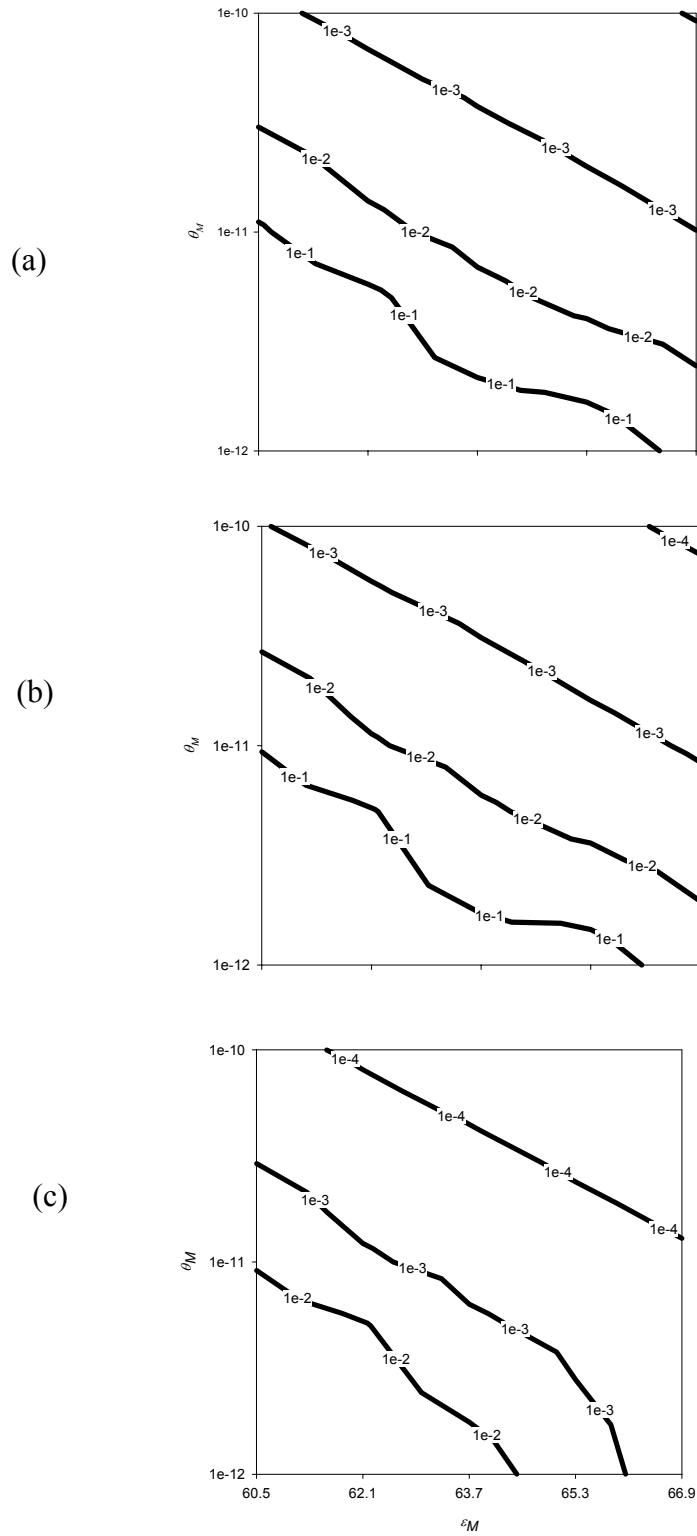


Figure 11. Contour plot of the difference in nondimensional intracellular supercooling predictions between a membrane-limited model and the model under study (normalized relative to the characteristic temperature). Predictions are based on $\theta_D = 10^{-1}$ and $\varepsilon_D =$ (a) 9, (b) 6, (c) 3.

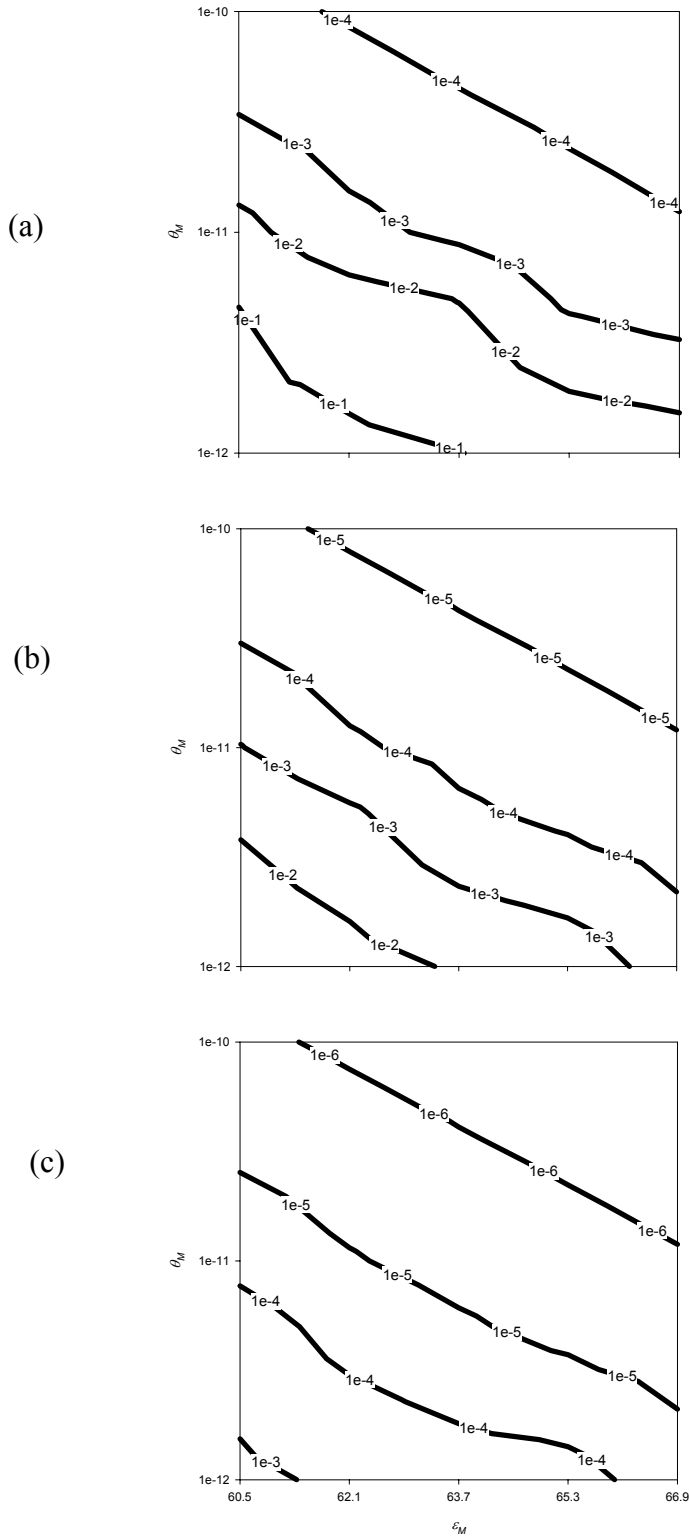


Figure 12. Contour plot of the difference in nondimensional intracellular supercooling predictions between a membrane-limited model and the model under study (normalized relative to the characteristic temperature). Predictions are based on $\theta_D = 10^{-3}$ and $\epsilon_D =$ (a) 9, (b) 6, (c) 3.

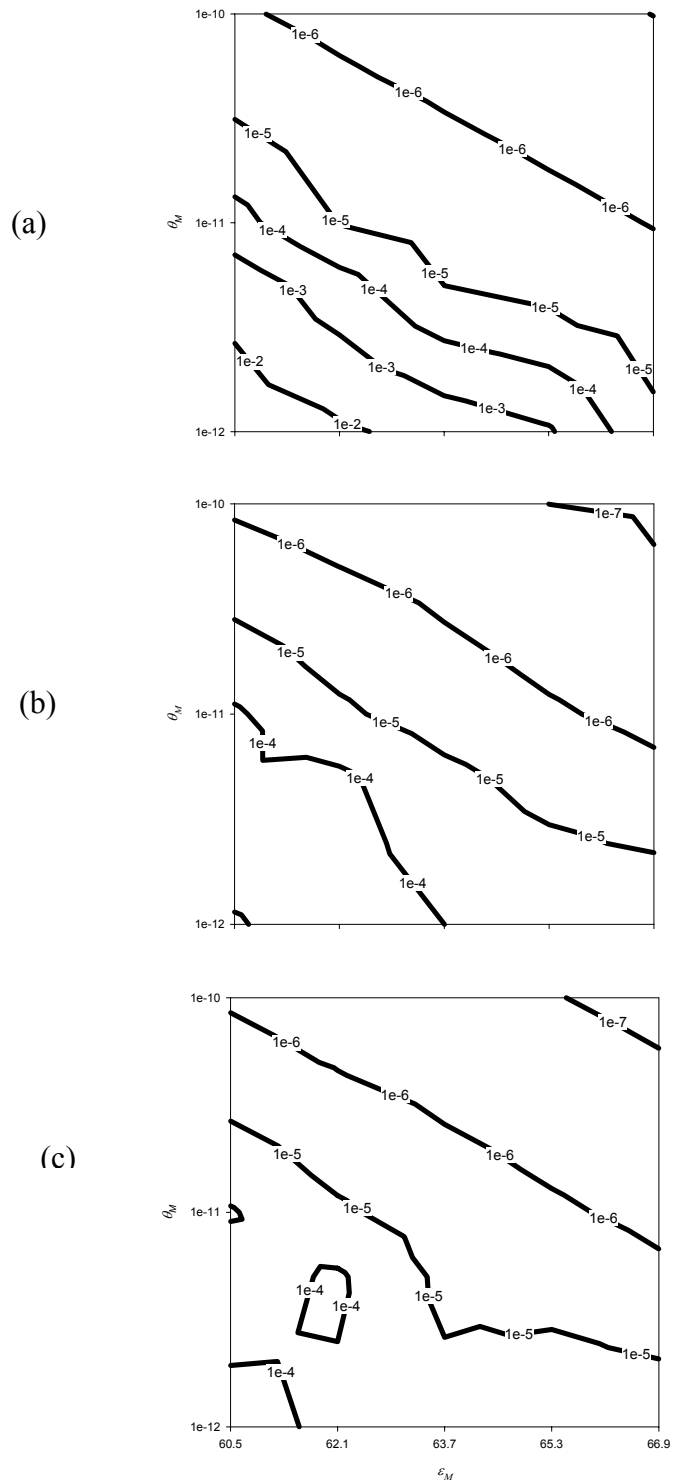


Figure 13. Contour plot of the difference in intracellular supercooling predictions between a membrane-limited model and the model under study (normalized to characteristic temperature). Predictions are based on $\theta_D = 10^{-5}$ and $\epsilon_D =$ (a) 9, (b) 6, (c) 3.

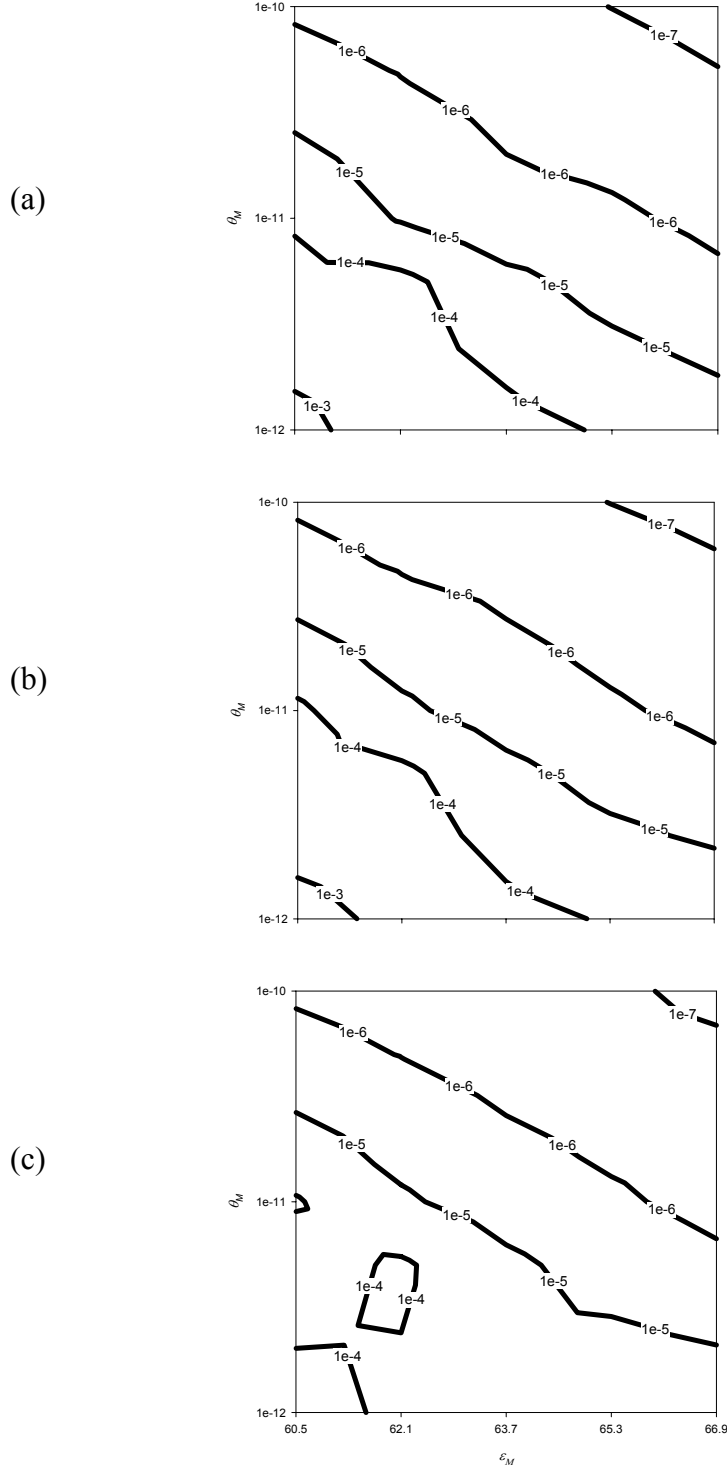


Figure 14. Contour plot of the difference in intracellular supercooling predictions between a membrane-limited model and the model under study (normalized to T_c). Predictions are based on $\theta_D = 10^{-7}$ and $\epsilon_D =$ (a) 9, (b) 6, (c) 3.

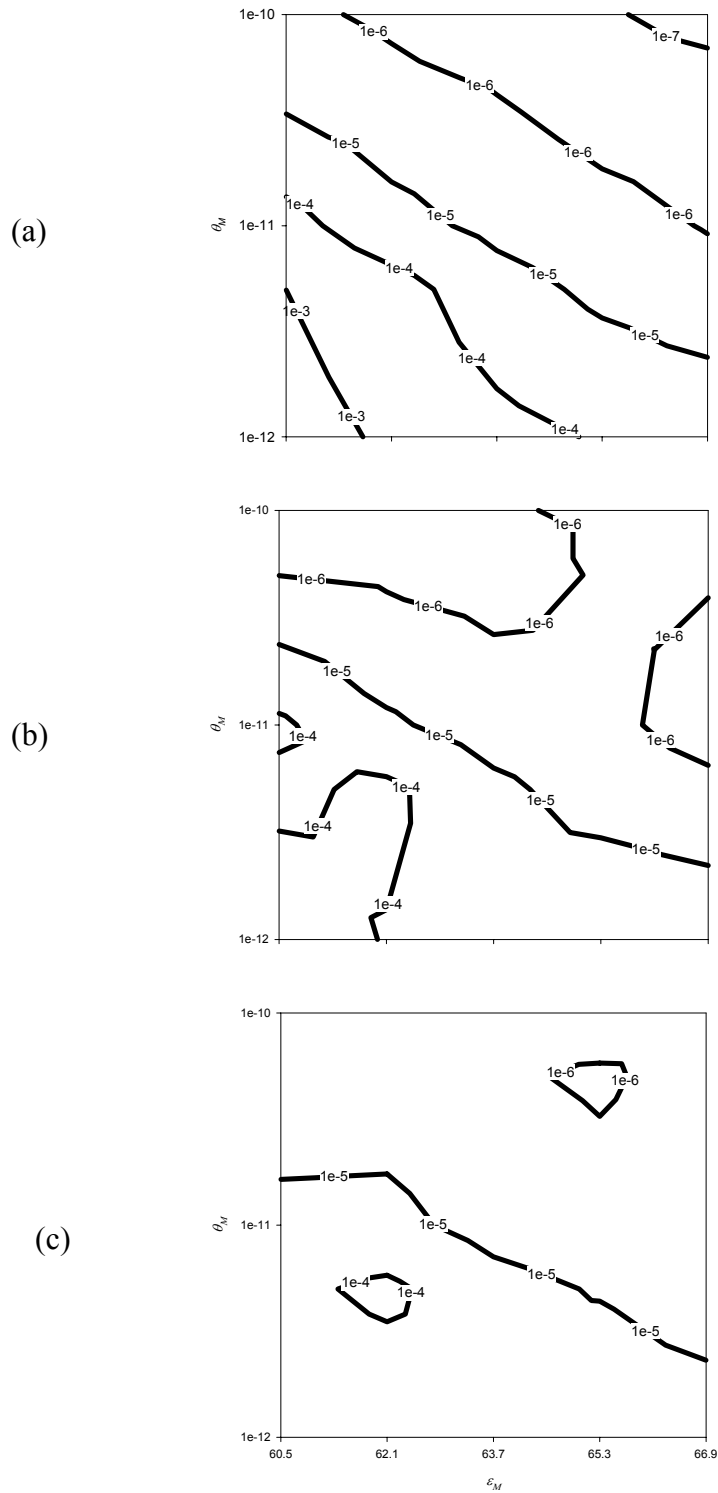


Figure 15. Contour plot of the difference in intracellular supercooling predicted by a membrane-limited model and the model under study. (normalized to T_c) Predictions are based on $\theta_D = 10^{-9}$ and $\epsilon_D =$ (a) 9, (b) 6, (c) 3.

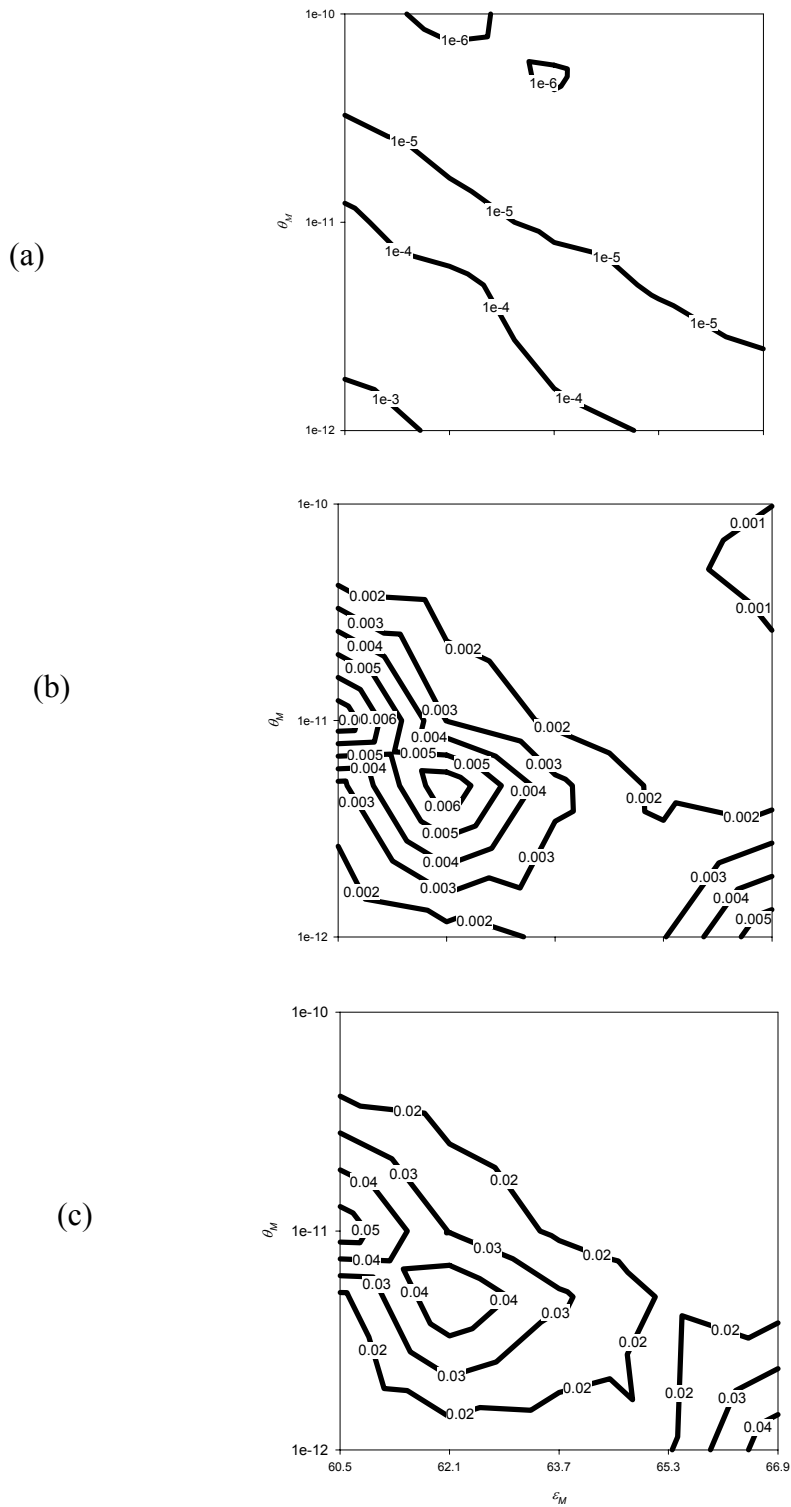


Figure 16. Contour plot of the difference in intracellular supercooling predictions between a membrane-limited model and the model under study (normalized to T_c). Predictions are based on $\theta_D = 10^{-11}$, $\epsilon_D =$ (a) 9, (b) 6, (c) 3.

CHAPTER 7

DISCUSSION

Diffusion-limited models of water transport during cryopreservation are scarce. To date, only Levin (1976), Mao *et al.* (2003), and Jaeger and co-workers (Jaeger *et al.*, 1999; Jaeger and Carin, 2002) have presented diffusion-limited models predicting the low temperature response of a cell to a chemically changing environment. Moreover, only Levin has investigated the effect of large Biot numbers, since both Mao *et al.* and Jaeger and co-workers have assumed constant biophysical properties in order to delineate the effects of cellular diffusion and the interactions with an advancing ice front. Even though Batycky *et al.* (1997) have presented a diffusion based model for osmotically driven intracellular transport, their study focused on the cell response during the removal of a semi-permeable species (e.g., a cryoprotectant chemical) near room temperature. Due to this limited availability of diffusion-limited models, the present study has been able to broaden the current understanding of the cellular response at large Biot numbers.

In our investigation, solutions to the temperature and spatial dependent cellular water volume fraction were obtained using numerical methods. The stability of a numerical technique is often determined with Fourier methods; however, Fourier methods assume periodic boundary conditions (Richtmyer and Morton, 1967; Tannehill *et al.* 1997) and since significant polarization occurs near the membrane, the boundary conditions must be explicitly considered when deriving the stability criterion. Thus Fourier methods cannot be applied. In order to include the boundary effects in the stability analysis, matrix methods are typically used (Tannehill *et al.*, 1997). Unfortunately, these methods can only be applied to linear systems (Quinney, 1987), and

thus a more empirical strategy has been used to evaluate the stability of the differencing scheme. This approach was based on the requirement that the total intracellular volume of salt be conserved during dehydration, consistent with the assumed semipermeable nature of the cell membrane.

Thus, all temporal and spatial grids used in simulates were defined with the intent of minimizing any violation of the required conservation of mass. For most investigations, the mass conservation error was constrained to within 1%; however, due to limitations of our solution algorithm as it is currently implemented, stability issues were occasionally encountered under extreme conditions (e.g., Figure 16). Despite the unavoidable numeric problems, our mass conservation errors compare well with those reported in other studies. In a previous study, Levin (1976) used a first-order accurate implicit backward difference scheme to integrate his partial differential equation, and reports mass conservation errors on the order of 0.1%. Mao *et al.* (2003) have used a second order accurate temporal scheme and report mass conservation errors as large as 10%. However, they explain that their results can be improved by mesh refinement. In addition, the computational domain used by Mao *et al.* comprised both the cell and an advancing ice front. Thus, the number of nodes actually used to discretized the cell radius was approximately 30 at the initial stages of the simulation, and decreased with the cell dehydration, inasmuch as their mesh was fixed.

The grid used in the present study and in Levin's investigation was designed such that the resolution of the mesh remains constant during the cell shrinkage (Levin, 1976) by using a Lagrangian-Eulerian approach. In contrast, a fixed Eulerian grid such as the one used by Mao *et al.* (2003) loses spatial resolution as the cell shrinks. Furthermore,

the work done here and by Levin use a nonuniform grid in order to improve spatial resolution near the membrane. Our use of a nonuniform, front-tracking Lagrangian-Eulerian grid proved to be a flexible solution which allowed simulation of cell dehydration over a large range of Biot numbers.

Estimation of the cell's biophysical properties is a critical prerequisite to the accurate modeling of the cell response to low temperatures. In 1976, Levin modeled the temperature dependence of the cytoplasmic viscosity by fitting a fourth-order polynomial to experimental viscosity data for pure water, which at the time had been measured down to -24°C (Hallet, 1963). For this reason, the minimum temperature simulated in Levin's work was only -30°C . Although, this limited temperature range was adequate for simulation of red blood cells, in which most transport occurs above -30°C , the viscosity model used by Levin would be unsuitable for use with most other cell types. In 1986, Taborek *et al.* presented a power law model of the viscosity of pure water. Unfortunately, the water viscosity was again only measured for temperatures down to -24°C , and extrapolation of the best fit power law model led to inaccuracies below this temperature; in particular, vitrification was predicted to occur at -48°C , approximately 85 K above the true glass transition point. However, until recently, the model of Taborek *et al.* has been the most frequently used in the cryobiology literature for the modeling of IIF (e.g., Toner *et al.*, 1990). Another approach to modeling the cell properties at subzero temperatures is to assume that they are constant (Mao *et al.*, 2003; Jaeger *et al.*, 1999). However, by neglecting the temperature-dependence of the membrane permeability and cytoplasmic viscosity, the calculated Biot number will decrease with decreasing temperature, in contrast with the results of previous studies,

which have found that the Biot number in fact increases with decreasing temperature (Karlsson *et al.*, 1994; Kasharin and Karlsson, 1998).

A major contribution of the present work was to model intracellular diffusion using an improved model of cytoplasmic viscosity. The constitutive equation employed here was based on the theoretical work of Karlsson *et al.* (1994). In their study, a phenomenological model of the viscosity of a ternary water-NaCl-glycerol solution was developed based on published experimental measurements. The empirical data used by Karlsson *et al.* included the concentration-dependence of the viscosity of water-glycerol solutions at 20°C (Weast, 1976), the temperature-dependence of the viscosity of an aqueous solution of 47% w/w glycerol (Kresin and Korber, 1991), and the measured glass transition temperature of water-glycerol solutions as a function of glycerol concentration (Luyet and Rasmussen, 1968). The resulting viscosity model has been validated against independent experimental data for temperatures down to -149°C (Karlsson *et al.* 1994; Karlsson, 2001). Karlsson *et al.* (1994) also accounted for the effect of salt ions using the theory developed by Vand (1948) to describe the perturbation of a liquid's viscosity by spherical particles suspended in the fluid. The range of temperatures and solution compositions for which the viscosity can be estimated using the model of Karlsson *et al.* is unprecedented in the cryobiology literature.

In the presence of cryoprotectants, the glass transition temperature is typically strongly dependent on cryoprotectant concentration; however, since the present study focuses on the behavior of a binary solution of water and NaCl, the glass transition temperature predicted using our viscosity model is constant. This simplifies the analysis, inasmuch as the whole cell will vitrify simultaneously. An exception to this is the

vitrification that will occur if a sufficient amount of water is removed at the cell boundary that only the hydrated salt “spheres” remain, form a glass shell. The approach we used to model the effects of this type of vitrification at the cell membrane is similar to techniques used to model the effect of skin formation that occurs at the surface of drying paint (Edwards, 1999), in which the interface velocity is set to zero upon solidification.

In modeling the external environment of the cell, the temperature and solute fields were assumed to be uniform. Inherent in this assumption is that the extracellular ice has enclosed the cell. Transmembrane temperature differences have been reported to rarely exceed 0.01 °C (Hua *et al.*, 1982). Moreover, it was assumed that the external solution was in equilibrium with the extracellular ice, which implies that the extracellular solution composition is uniform. However, according to the investigations of Jaeger and Carin (2002) and Mao *et al.* (2003), these assumptions might break down under certain conditions. For example, if the cell is initially remote to the ice front noticeable dehydration will not occur until the ice front meets the cell membrane (Jaeger and Carin, 2002). Furthermore, Mao *et al.* (2003) present data to show that at fast cooling rates, nonhomogenous solute temperature fields can have a significant effect on the amount of cell dehydration. Therefore, the present assumptions about the environmental conditions may not always be valid. Nonetheless, these assumptions are commonly used in modeling cell dehydration (Mazur, 1984; Levin, 1979).

It was assumed in this analysis that the intracellular solution was both ideal and dilute. In principle, this assumption will break down as the concentration of salt increases. However, empirically, the cells have been observed to obey Boyle-Van't Hoff's law, which is predicated on Raoult's law (Dick, 1959; Levin 1979); it has been

postulated that this apparent conformity with Raoult's law is possible because the effects of solution nonideality are lumped into an effective osmotically inactive volume (Levin *et al.*, 1976b; Levin *et al.*, 1977). Analyses that do incorporate solution nonideality explicitly indicate that the effect of this phenomenon is small (Mansoori, 1975; Levin *et al.*, 1977); however, recent analyses indicate that the effect of intracellular proteins on chemical potential may cause significant deviations from ideality under certain conditions (Elmoazzen *et al.*, 2002). Although deviations of Raoult's law are expected under some conditions, the simplifying assumptions about the temperature-dependence of the membrane permeability are likely to be a greater source of error in the membrane transport model (Levin, 1979; Levin *et al.*, 1976a). The validity of these and other assumptions has been discussed extensively by Mazur (1963) and Levin (1979).

In the present study, the kinetics of cell dehydration were characterized using dimensional analysis. The first attempts to identify scaling laws for the water transport process were by Mazur (1984). He found that the predicted temperature-dependence of the intracellular water volume during freezing remained the same when scaling the cooling rate inversely with the initial cell radius and in direct proportion with the membrane permeability. Thirumala and Devireddy (2003) applied this concept to predict the optimum cooling rate as a function of membrane activation energy. However, their analysis was incomplete in that they neglected to account for the effects of the initial solute concentration, discrepancies in reference temperatures used for permeability measurements, and cytoplasmic diffusion. In the present study, the identification of scaling laws was formalized by defining nondimensional quantities that fully characterize the kinetics of mass transport during cell freezing. In particular, the dimensionless

groups θ_M , θ_D , ε_M , and ε_D defined in Section 2.4.1 were found to play the most critical role. Parameters similar to θ_M and θ_D were first identified by Kasharin and Karlsson (1998); their definitions have been further refined here. In addition, Kasharin and Karlsson's preliminary analysis was extended to include an explicit description of the temperature-dependence of cellular dehydration during freezing, using Arrhenius numbers.

From the results of our investigation, it was apparent that the combinations of these nondimensional parameters that led to the most significant divergence from a membrane-limited model were also the values that resulted in the greatest amount of solute polarization. Kasharin and Karlsson (1998) gave evidence to support the fact that the membrane-limited model breaks down at temperatures near the glass transition point because the time scale for diffusion transport was larger than the time scale for membrane transport in this temperature range. Furthermore, they concluded that the impact of this effect would be more noticeable during warming than during cooling, because little transport occurs at low temperatures in the latter case.. Mao *et al.* (2003) didn't encounter solute polarization in their study of erythrocytes and instead attributed the observed discrepancies with predictions from the membrane-limited model to the effects of nonisothermal conditions. However, their investigation was in the regime of low Biot numbers and they thus did not expect to see any concentration gradients within the cell. On the other hand, in Levin's study of erythrocytes (1976), solute polarization as large as 50% was observed, and found to cause significant over prediction of water loss by the membrane-limited model.

The present study has made the simplifying assumption that the osmotically inactive cell volume is negligible. In contrast, Levin treated the osmotically inactive volume as a diffusing protein species associated with a very small diffusion coefficient. Thus, these cytoplasmic proteins would accumulate at the cell membrane as the cell constricts and greatly reduce the rate of water transport. This may partly explain why the degree of solute polarization observed by Levin was larger than that predicted by other investigations. Another model for the osmotically inactive volume is that presented by Batycky *et al.* (1997). In their analysis, the osmotically inactive volume was uniformly distributed throughout the cell. In effect, the intracellular protein distribution assumes a steady state, and thus these particles diffuse at an infinite speed. This approach is the direct opposite of Levin's. An alternative model which is physically plausible, involves the assumption that the osmotically inactive volume is distributed throughout the cell but behaves like a "sponge", creating intracellular convection (Frankel *et al.*, 1991) as the cell shrinks. Most assumptions of the intracellular structure treat the proteins as free molecules not tethered to the membrane. However, the tensegrity model of Wang *et al.* (1993) contradicts this common. According to Wang *et al.*, the cell comprises a meshwork of proteins, which reduces the effective water diffusivity and results in "sponge-like" behavior. Because it is not trivial to model the osmotically inactive volume, the present study has neglected this factor altogether, an approach that was also used by Mao *et al.* (2003) and Jaeger and coworkers (2002; 1999).

CHAPTER 8

CONCLUSIONS / FUTURE STUDIES

We have developed a model that predicts the cellular dehydration that results as a consequence of the freezing process. Our analysis represents an improvement over previous cell dehydration models by: (1) accounting for intracellular solute polarization, which is neglected in conventional, membrane-limited models; (2) incorporating realistic constitutive equations for the temperature- and concentration-dependent biophysical properties; (3) representing the cell geometry as a three-dimensional sphere instead of using simpler one- and two-dimensional geometries, and (4) using a numerical solution technique that affords stability and accuracy under a wide range of conditions.

Our model was validated in membrane-limited transport regimes, and found to give novel predictions in diffusion-limited transport regimes. We defined four nondimensional parameters that characterized the extent of cell dehydration and quantified the relative importance of diffusive and membrane transport processes. As a consequence of the complex nonlinear temperature-dependence of the cell dehydration process, we found that a single dimensionless parameter (e.g. the Biot number) would be insufficient to properly categorize the various mass transport regimes. Instead, the diffusion-limited and membrane-limited mass transport regimes are separated by a nonlinear relationship between the dimensionless parameters. From our parametric analysis, an effective Biot number could be defined:

$$Bi_{eff} = \frac{\theta_D^{0.3} e^{0.2\varepsilon_D}}{\theta_M e^{0.4\varepsilon_M}} \quad (166)$$

This expression represents a three-dimensional hypersurface corresponding to conditions under which the maximum supercooling predictions for the membrane- and diffusion-

limited transport models differed by approximately 1 K. Accordingly, if $Bi_{eff} \gg 1$, then a diffusion-limited model is needed to accurately simulate the cell behavior during freezing; conversely, if $Bi_{eff} \ll 1$, then the diffusion-limited and membrane-limited models yield comparable predictions.

Intracellular solute polarization is a characteristic of diffusion-limited transport. We found that slow diffusion leads to concentration gradients inside the cell and subsequent accumulation of salt at the cell membrane. We conclude that when these gradients are severe, the concentration of salt at the intracellular surface of the cell membrane can become sufficiently large to cause local vitrification. Whereas such local vitrification creates a glassy “shell” at the cell membrane, preventing further water efflux, the intracellular water is allowed to redistribute. The extent of redistribution depends on the temperature- and concentration-dependence of the cytoplasmic viscosity and the cooling rate; if the diffusivity decreases rapidly during cooling, intracellular concentration gradients will remain despite the lack of membrane transport.

The present study served to develop computation tools for accurately modeling the cell dehydration response during the cryopreservation process. Future extensions of the model will include incorporation of the effects of the osmotically inactive volume, and of cryoprotectant chemicals. In addition, applications to tissue preservation will require predictions of the cellular response to the mechanical environment presented by the extracellular matrix, as well as the effect of cell-cell interactions.

APPENDIX A

SOURCE CODE

```

/*          Cell Dehydration Code,  created by: Kevin Carnevale          */
/*          written in Microsoft Visual Studio C++          */

```

```

#include <stdio.h>
#include <stdlib.h>
#include <math.h>
#include <time.h>
#include <definitions.h>

```

```

int main(void)

```

```

{
/* Define Variables *****/

```

- start, finish and elapsed are variables that will be used to determine the clock cycles of the cpu during the run of the simulation.
- GasConst, vH2O, vNaCl, To, Ti, CoolRt, Linf, Ea, Hf, Ro, cso, A, E, betaTg, ao, Boltz, are all physical parameters/properties, the definitions of which are described in the "Input Values" section.
- dRdt is the time rate of change of the nondimensional radius
- Biot is the time varying Biot number defined using the initial cell radius (Needed for calculating dRdt.
- Bi_cond is the condition for converting time nondimensionalization from a diffusion based to a permeability based. In such a change, the Biot number must be defined in terms of the dimensional radius at the present time, or RRo, where R is the nondimensional radius.
- Lp is the membrane permeability
- dm_u is the transmembrane chemical potential difference.
- T is temperature.
- D0 is the dimensional diffusivity at the cell center.
- Teq is the equilibrium temperature of the supercooled cytoplasm.
- delTs is the amount of supercooling.
- Vwater is the intracellular water volume.
- Vsalt is the intracellular salt volume.
- R is the nondimensional cell radius.
- r is the nondimensional intracellular radial position (xR)
- td and tm are the time constants for diffusion and membrane transport, respectively
- *ptemp, *plp, *pbi, *pdmu, *pD0, *pdRdt, *pTeq, *pvw, *pvs are the pointers to temperature, permeability, Biot number (Biot), chemical potential, diffusivity at cell center, time rate of change of cell radius, equilibrium temperature of supercooled cytoplasm, water volume and salt volume, respectively.
- w is the scaling factor for nodal spacing.
- dtau is the nondimensional time step.
- dtauo is the starting value of the nondimensional time step. This value is used when reducing the time step according to a permeability nondimensionalization of time.
- tau is the nondimensional time.
- real_time is the dimensional time.

- N is the number of nodes
- *pN is the pointer to the location of the number of nodes.
- No is the total number of nodes. This value is important when nonuniform vitrification occurs and N is reduced to be the node that lies on the boundary of this glass front, therefore, No just keeps the original information.
- Data1, Data2, and resume_data are all data files. Data1 and Data2 are defined to collect information at certain intervals during the simulation. Typically Data2 records the water volume fraction of each node, and Data1 records certain other properties like, radius, water volume, salt volume, biot number, chemical potential, etc. resume_data is a file that records the information required to resume the simulation from Tstop.
- Tstop is a user defined temperature to stop the simulation prematurely. This value is used to when the user wishes to stop the simulation and resume its work at some later time. In such a case the simulation will run up to Tstop, and resume from Tstop at the later point in time.
- Dat1rec is the first temperature at which data should be recorded to Data1.
- chngrec1 is the temperature interval from Dat1rec at which data should be recorded to Data1.
- Dat2rec is the first temperature at which data should be recorded to Data2.
- chngrec2 is the temperature interval from Dat2rec at which data should be recorded to Data1.
- rec2flagchng is a variable that reduces chngrec2 if a certain temperature is reached or if nonuniform vitrification is encountered. Since Data2 usually records nodal information, there could be a lot of information to save, therefore chngrec2 is typically coarse; however, to obtain a finer saving period this value is used.
- interval is the interval at which nodal information is saved. Since there may be a large number of nodes, it may be unnecessary to save all nodal information, and thus this value is used to define the interval of saving.
- resume is a value that defines if the simulation should start from the beginning or start from Tstop.
- invR (inverse of the nondimensional radius), term, and hold are all variables used in the integration of dRdt.
- stop is a variable that will end the simulation if $T < Tstop$, or $T < BetaTg$.
- *pstop is a pointer to the address of stop.
- i is a looping parameter
- flag is either 0 or 1, and is used to notify the program if non uniform vitrification has occurred.
- *pflag is a pointer to the address of flag.

```

clock_t start, finish;
double elapsed;
double GasConst, vH2O, vNaCl, To, Ti, CoolRt, Linf, Ea, Hf, Ro, cso, A, E,
        betaTg, ao, Boltz;
double dRdt, Biot, Bi_cond, Lp, dmu, T, D0, Teq, delTs, Vwater, Vsalt;

```

```

double R, r, td, tm
double *ptemp, *plp, *pbi, *pdmu, *pD0, *pdRdt, *pTeq, *pvw, *pvs;
double w, dtau, dtauo, tau, real_time,
int N, *pN, No
FILE *CellDehydr_v20_data1;
FILE *CellDehydr_v20_data2;
FILE *resume_data_20;
double Tstop;
double Dat1rec, chngrec1
double Dat2rec;
int chngrec2, rec2flagchng, interval, resume;
double invR, term, hold,
double stop, *pstop;
int i;
int flag, *pflag;

```

```

/* Allocate Memory for Matrices *****/

```

- The set of equations being solved is a tridiagonal system that can be written in the form $AX = B$. The lower diagonal of the tridiagonal matrix is defined as the matrix lower, the upper diagonal as upper, and the main diagonal as main. B is the right hand side vector (RHS), and X is the water volume fraction (phi). *pl, *pu, *pm, *pr, *pp, are the pointers to the first element of these vectors.
- The diffusivity is given a vector, since it is spatially varying, with *pdiff the pointer to the first element of D.
- x is a vector the location of each node, and *px is a pointer to the first element of x.
- dx is a vector of the distance between nodes, and *pdx is a pointer to the first element of dx.

```

/* Matrices for use in this program AX = B */
double *lower, *upper, *main, *RHS, *phi;
double *pl, *pu, *pm, *pr, *pp;

```

```

/* Matrix for Diffusivity */
double *D;
double *pdiff;

```

```

/* Matrix of Nodal Spacing dx */
double *dx, *x;
double *pdx, *px;

```

```

/* Input Values *****/
/* The user enters in the physical parameters defined below. */

```

```

resume = 0;          /* Enter 0 to start new simulation 1 to resume */

GasConst = 8.314;   /* J mol-1 K-1 Universal Gas Const. */
vH2O = 1.8e-5;      /* m3 mol-1 Specific Vol of Water */
vNaCl = 2.699e-5;   /* m3 mol-1 Specific Vol of Salt */
cso = 142.;         /* mol m-3 Isotonic Salt Conc. */
To = 273.15;        /* K Equilibrium Freezing Temp */
Ti = 272.623;       /* K Initial Temp */
Hf = 6016.52;       /* J mol-1 Heat of Fusion */
ao = 1.4e-10;       /* m Hydrodynamic water radius */
Boltz = 1.380e-23; /* J K-1 Boltzman Constant */
betaTg = 123.80;    /* K Vogel-Fulcher Parameter */

Ea = 5.2960e4;      /* J mol-1 Activation Energy */
A = 2.711e-5;       /* Pa s Preexponential Coefficient */
E = 614.823;        /* K Vogel-Fulcher Activation enrgy*/
CoolRt = 6.e2;      /* K min-1 Cooling Rate */
Linf = 1.5656e-2;   /* m Pa-1 s-1 Limiting Permeability */
Ro = 7.2314e-5;     /* m Initial Cell Radius */

N = 500;            /* Number of Nodes */
w = 1.0;            /* Scaling Factor for nodal spacing */
dtau = 1.e-4;       /* Nondimensional Time Step */

Tstop = 0.;         /* Temperature to Stop Simulation */
Dat1rec = 272.6;    /* 1st temp at which data will be sent to data1 */
Dat2rec = 260;      /* 1st temp at which data will be sent to data2 */
interval = 1;       /* For saving nodal information */
chn grec1 = 0.2;    /* Value at which to reduce Dat1rec */
chn grec2 = 20;     /* Value at which to reduce Dat2rec */
rec2flagchn g = 5; /* Value to change chn grec2 to once flag = 0 */
chn gdtau = 1e-10; /* Value to change dtau after first node vitrif */

```

```

/* Declare Variables *****/

```

- Memory is being allocated for the files, and the pointers are assigned to the addresses of the variables that they point to.
- start is assigned the value of the current clock cycle.
- The if statement for resume, will open resume_data to be read, if the simulation is being resumed from Tstop.

```

start = clock();
Data1 = fopen("Data1.dat","w");
Data2 = fopen("Data2.dat","w");
if (resume == 1)
{ resume_data = fopen("resume_data.dat", "r");
}
pN = &N;
ptemp = &T;
plp = &Lp;
pbi = &Biot;
pdmu = &dmu;
pD0 = &D0;
pdRdt = &dRdt;
pTeq = &Teq;
pvw = &Vwater;
pvs = &Vsalt;
pstop = &stop;
pflag = &flag;

```

/* Allocate Memory for Matrices *****/

- Here memory is allocated from the matrices. The command malloc is used to define a vector space of the size in parenthesis.
- Also the pointers are assigned the address of the first element of these vectors.

```

lower = (double *)malloc(N*sizeof(double));
upper = (double *)malloc(N*sizeof(double));
main = (double *)malloc(N*sizeof(double));
RHS = (double *)malloc(N*sizeof(double));
phi = (double *)malloc(N*sizeof(double));

```

/* Define the pointers */

```

pl = &lower[0];
pu = &upper[0];
pm = &main[0];
pr = &RHS[0];
pp = &phi[0];

```

```

D = (double *)malloc(N*sizeof(double));
pdiff = &D[0];

```

```

dx = (double *)malloc((N-1)*sizeof(double));
x = (double *)malloc(N*sizeof(double));
pdx = &dx[0];

```



```
px = &x[0];
```

```
/* Initial Calculation Conditions *****/
```

```
stop = 1;  
flag = 1;  
No = N;  
dtau = dtau;  
CoolRt = -CoolRt/60.;
```

- Process of determining the nodal spacing
- First, if $w = 1$, then the grid spacing is uniform, with a distance of $1/(N-1)$.
- Otherwise, the equation for the grid spacing at the cell membrane takes the form of $dx = (1-w) / (1 - w^{(N-1)})$ which is a geometric series estimation of $L = dx * (\text{summation from } k=0:N-2 \text{ of } w^k)$. $L = 1$.
- The nodal spacing for each node thereafter takes the form $dx(i) = w * dx(i+1)$
- Once the spatial grid is determined, the x location of each node is found by summing the dx's

```
if (w==1)  
{  
    dx[N-2] = 1./(N-1);  
}  
else  
{  
    dx[N-2] = (1-w)/(1-pwr(w,N-1));  
}
```

```
for (i=N-3; i>=0; i=i-1)  
{  
    dx[i] = w*dx[i+1];  
}
```

```
x[0] = 0;  
x[N-1] = 1;  
for (i=1; i<N-1; i++)  
{  
    x[i] = x[i-1] + dx[i-1];  
}
```

- Other initial values.
- Nondimensional radius is initially 1.
- If the simulation is being resumed, these values will not be defined with initial values, but will be read from the resume_data file.

```
if (resume == 0)  
{
```

```

k = 0;
tau = 0;
real_time = 0;
R = 1.;
invR = 1.;
term = 0.;
resflag = 1;
}
else
{
fscanf(resume_data_20, "%lf %lf %i", &tau, &real_time, &k);
fscanf(resume_data_20, "%lf %lf %lf", &term, &R, &dRdt);
resflag = 0;
}

```

/ Initial Conditions Inside Cell *****/*

- In this section the initial conditions within the cell are calculated, factors like, initial water volume fraction, Biot #, chemical potential, Water Volume, Salt Volume, Diffusion Coefficient, Supercooling and time rate of radius change.
- PostProc is a function that calculates the Water and Salt Volumes.
- Diffusivity is a function that calculates the viscosity and diffusion coefficients of each node within the cell.
- Cell Props is a function that calculates temperature, permeability, biot number, and chemical potential.

```

if (resume == 0)
{
    /* Set all nodes to have the initial water volume fraction */
    for (i=0; i<N; i++)
    {
        phi[i] = 1. - cso*vNaCl;
    }

    /* Volume Calculations */
    PostProc(pvw, pvs, R, pdx, px, pp, N, w);

    /* Cell Properties */
    Diffusivity(pdifff, pD0, pp, pflag, pstop, pN, Ti, vH2O, vNaCl, pdRdt, A,
        E, ao, Boltz, betaTg, plev, pdim);

    CellProps(ptemp,plp,pbi,pdmu,Ti,CoolRt,real_time,Linf,Ea,
        GasConst,Ro,D0,vNaCl,vH2O,Hf,To,R,phi[N-1], pTeq, phi[0]);

    dRdt = pwr(R,2)*Biot*dmu;
}

```

```

        delTs = Teq - Ti;
    }

/* Resumed Conditions Inside Cell *****/
- This reads the values for temperature, permeability, biot number, chemical
  potential, dimensional diffusivity at the cell center, water volume fraction, and
  diffusivity from the previously run simulation.
- It then uses PostProc to determine the Water and Salt Volumes from this
  information.

    else
    {
        fscanf(resume_data_20, "%lf %lf", &T, &Lp);
        fscanf(resume_data_20, "%lf %lf %lf", &Biot, &dmu, &D0);
        for (i=0; i<N; i++)
        { fscanf(resume_data_20, "%lf %lf", &phi[i], &D[i]);
        }
        fclose(resume_data_20);
        PostProc(pvw, pvs, R, pdx, px, pp, N, w);
    }

/* Print Starting Values to File *****/

    fprintf(Data1, "Nodes (%i) w (%lf) dtau (%e) \n", N, w, dtau);
    fprintf(Data1, "Linf %e B %e Ea %e \n", Linf, CoolRt, Ea);
    fprintf(Data1, "A %e E %e Ro %e \n", A, E, Ro);
    fprintf(Data1, "Temp Vsalt Vw Biot dtau delTs \n");
    fprintf(Data1, "%lf %.11lf %.11lf %e %e %lf \n", T, Vsalt, Vwater, Biot, dtau,
        delTs);

/* Assemble Matrices A & B of AX = B *****/
- ModTrapMethod is a function that evaluates the descritized equations. (See
  Chapter 3).
- The matrix A consists of the coefficients of the phi(n+1) terms, and the right
  handside matrix B consists of the phi(n) and any other constant terms.

    do
    {

        ModTrapMethod(pm, pl, pu, pr, N, pdx, px, pdiff, pp, dtau, dRdt, R, w, flag);

/* Solve the Tridiagonal Matrix *****/

- Solution of the resulting tridiagonal matrix involves using an LU decomposition.
  Here, in order to conserve memory, the lower, upper, main, and phi matrices were
  recycled.

```

- The LU decomp method used puts the main diagonal ones in the L matrix. (See Below)

$$\begin{bmatrix} m_0 & u_0 & 0 & 0 \\ l_0 & m_1 & u_1 & 0 \\ 0 & l_1 & m_2 & u_2 \\ 0 & 0 & l_2 & m_3 \end{bmatrix} = \begin{bmatrix} 1 & 0 & 0 & 0 \\ l'_0 & 1 & 0 & 0 \\ 0 & l'_1 & 1 & 0 \\ 0 & 0 & l'_2 & 1 \end{bmatrix} \begin{bmatrix} m'_0 & u'_0 & 0 & 0 \\ 0 & m'_1 & u'_1 & 0 \\ 0 & 0 & m'_2 & u'_2 \\ 0 & 0 & 0 & m'_3 \end{bmatrix}$$

- So that,

$$\begin{aligned}
 u'_i &= u_i \\
 l'_i &= l_i / m'_i \\
 m'_i &= m_i - l'_i u'_{i-1}
 \end{aligned}$$

```
phi[0] = RHS[0];
```

```
for (i=1; i<N; i++)
{
    lower[i-1] = lower[i-1]/main[i-1];
    main[i] = main[i] - lower[i-1]*upper[i-1];

    phi[i] = RHS[i] - lower[i-1]*phi[i-1];
}
```

```
phi[N-1] = (1./main[N-1])*phi[N-1];
for (i=N-2; i>=0; i=i-1)
{

    phi[i] = (1./main[i])*(phi[i] - upper[i]*phi[i+1]);
}
```

```
/* Update Values *****/
```

- Integration of dRdt using Trapezoidal Method
- Integration of time using Euler method.

```
tau += dtau;
real_time += dtau*( (pwr(Ro,2)*pwr(R,2)) / D0 );
```

```
hold = Biot*dmu;
```

```
Diffusivity(pdif, pD0, pp, pflag, pstop, pN, T, vH2O, vNaCl, pdRdt, A, E, ao,
    Boltz, betaTg, plev, pdim);
```

```
CellProps(ptemp,plp,pbi,pdmu,Ti,CoolRt,real_time,Linf,Ea,GasConst,Ro,D0,vNa
    Cl,vH2O,Hf,To,R,phi[N-1], pTeq, phi[0]);
```

```

if (flag == 1)
{
term += (dtau/2.)*(hold + Biot*dmu);
invR = 1. - term;
R = 1. / invR ;
dRdt = pwr(R,2)*Biot*dmu;
}

delTs = Teq - T;
td = (pwr(Ro*R,2))/(D0);
tm = (R*Ro*vH2O)/(Linf*exp(-Ea/(GasConst*T))*GasConst*T);
Bi_cond = R*Biot;

if (Bi_cond > 1)
{
    dtau = dtauo/Bi_cond;
}

/* Post Processing *****/

PostProc(pvw, pvs, R, pdx, px, pp, N, w);

/* Data Storage *****/

/* Record Data to Data1 */
if (T < Dat1rec)
{

    fprintf(Data1,"%lf %.11lf %lf %.11lf %i %0.11lf\n",T, Vsalt, delTs,
            phi[0], Vwater);
    Dat1rec = Dat1rec - chngrec1;

    /* Print Status to Screen */
    printf("tau = %6.4lf  T = %lf  dtau = %e Vw = %0.8lf\n", tau, T, dtau,
            Vwater);
}

/* Record Data to Data2 */
if (T < Dat2rec)
{

    fprintf(Data2, "%lf\n", T);
    for (i=0; i<No; i=i+interval)
    {
        fprintf(Data2,"%e ", phi[i]);
    }
}

```

```

    }
    fprintf(Data2, "\n");

    for(i=0; i<No; i=i+interval)
    {
        r = x[i]*R;
        fprintf(Data2, "%e    ", r);
    }
    fprintf(Data2, "\n");

    if (flag==0 || T < 180)
    {
        chngrec2 = rec2flagchng;
    }

    Dat2rec = Dat2rec - chngrec2;
}

/* Record Data to resume */
if (T<= Tstop)
{
    resume_data = fopen("resume_data.dat", "w");

    fprintf(resume_data, "%0.8e %0.8e %i\n", tau, real_time, k);
    fprintf(resume_data, "%0.8e %0.8e %0.8e \n", term, R, dRdt);
    fprintf(resume_data, "%0.8e %0.8e \n", T, Lp);
    fprintf(resume_data, "%0.8e %0.8e %0.8e \n", Biot, dm_u, D0);
    for (i=0; i<N; i++)
    {
        fprintf(resume_data, "%0.8e %0.8e \n", phi[i], D[i]);
    }
}

/*****

if (T <= Tstop)
{
    stop = 0;
}

} while (stop == 1);

/* End *****/

fclose(Data1);
fclose(Data2);
fclose(resume_data);

```

```
free(pl);
free(pm);
free(pu);
free(pr);
free(pp);
free(pdx);
free(pdifff);
free(px);

finish = clock();
elapsed = ((double)(finish-start)) / CLOCKS_PER_SEC ;
printf("elapsed clock time: %lf\n", elapsed);
printf("\nType 1 then ENTER to continue ");
scanf("\n");
return 0;
}
```

```

/*                                     Function: PostProc                                     */

#include <stdio.h>
#include <stdlib.h>
#include <math.h>
#include <definitions.h>

int PostProc(double *vw, double *vs, double Rbar, double *pdx, double *loc, double
*pp, int n, double w)
{

/* Define Variables *****/
- This function takes in the pointers to the water volume and salt volume, because it
will change these values by the end of the program. Since it is changing the values
it needs to know the location of the variable to change.
- Other numbers that variables called are the nondimensional radius, the number of
nodes, and the scaling factor. These values are constants to the this function and
won't be changed, so they don't need a pointer.
- On the other hand, the matrices for nodal spacing (dx), nodal location (loc), and
water volume fraction (pp) must send a pointer to the starting value of these
matrices in order to read all the matrix values.
- All these pointer issues are just syntax of C++.

    double x, dx;
    int k;

/* Nondimensional Volume of Water Inside Cell *****/

- The water volume was calculated by visualizing each nodal point as a subshell of
the entire spherical cell, and summing up all these small volumes.
- The calculation is based on  $V_{shell} = (4/3)\pi(r_o^3 - r_i^3)$  where  $r_o = r + dr/2$ , and  $r_i = r -
wdr/2$ , with  $r = xR$  and  $dr = Rdx$ 

    /* Water volume shell at membrane */
    dx = *(pdx+n-2);
    *vw = pwr(Rbar,3)* ( *(pp+n-1)*( (3./2.)*dx - (3./4.)*pwr(dx,2) +
        (1./8.)*pwr(dx,3) ) );

    /* Water volume shell at Cell Center */
    dx = *pdx;
    *vw += pwr(Rbar,3)*( *pp*(1./8.)*pwr(dx,3) );

    for (k=1; k<n-1; k++)
    {
        x = *(loc + k);

```



```

dx = *(pdx + k);
*vw += *(pp+k)*pwr(Rbar,3)*( (3./2.)*pwr(x,2)*dx*(1+w) +
(3./4.)*x*pwr(dx,2)*(1-pwr(w,2)) +
(1./8.)*pwr(dx,3)*(1+pwr(w,3)) );
}

```

/* Nondimensional Volume of Salt Inside Cell *****/
- For the binary system, $R^3 = V_w + V_s$ in nondimensional units.

```

*vs = pwr(Rbar,3) - *vw;

```

```

return 0;

```

```

}

```

```

/*                                     Function: Diffusivity                                     */

#include <stdio.h>
#include <stdlib.h>
#include <math.h>
#include <definitions.h>

int Diffusivity(double *diff, double *pDo, double *phiw, int *flag, double *stop, int
*N, double temp, double vw, double vs, double *rdot, double A, double E, double ao,
double Boltz, double betaTg)
{
    /* Define Variables */

    double phi_sphere, phis, visc, visc_bin, h, pi, visc_lev, visc_w, visc_w_20;
    int j,n;

        h = 1.0;
        pi = 3.141593;
        n = *N;

/* Check for temperature less than vitrification temp */
- If the temperature is less than the vitrification temperature we want the simulation
to stop. Therefore, this if statement will change stop and make the simulation end.
It will not end immediately, instead it will continue running through the update
variables and data storage sections, but once it gets to the while condition at the
end, it will stop.

    if (temp < betaTg)
    {
        *stop = 0;
        printf("Temperature below vitrification: %lf K \n", temp);
    }

/* Viscosity of Binary solution of "free" water and CPA for ya = 0 */
    visc_bin = A*exp(E / (temp - betaTg));

    for (j=0; j<n; j++)
    {
        /* Salt Volume Fraction and Phisphere */
        phis = 1.0 - *(phiw + j);
        phi_sphere = phis*( 1.0 + h*( vw/vs ) );

/* Check for water depletion */
- This condition will check to see if nonuniform vitrification has occurred.
- For a binary solution, the only condition that would result in nonuniform
vitrification is when Phisphere becomes greater than one. (Note: when CPA's are

```

used, betaTg will vary with Temp and concentration, and therefore location, and is thus another condition to check

- Nonuniform vitrification has been handled here by setting the nondimensional diffusion coefficient at that vitrified node to be zero.
- Furthermore, if vitrification occurs at the membrane boundary then water transport across the membrane will be stopped and thus the cell radius won't change. Thus dRdt is set to zero.
- Finally, to make the boundary become this new vitreous location, the last node is assigned the value of the node that vitrified. (Thus N-1, becomes the adjacent node that isn't vitrified and the boundary condition will apply to it.)

```

if (phi_sphere > 1)
{
    *(diff+j) = 0;
    if (j==n-1)
    {
        *rdot = 0;
        *flag = 0;
    }
    if(j<*N)
    {
        *N = j;
    }
    printf("Free water less than hydrated salt at T = %lf %i \n",
        temp,j);
}

```

- When Φ_{sphere} is not greater than one, the function will proceed to calculate the dimensional viscosity, dimensional diffusion coefficient at the cell center (j=0), and nondimensional diffusion coefficients for all nodes.

```

else
{
    visc = visc_bin*exp( (2.5*phi_sphere) / (1.0 -
        0.609375*phi_sphere) );

    if (j==0)
    {
        *pDo = (Boltz*temp)/(6.0*pi*ao*visc);
    }

    *(diff+j) = ((Boltz*temp)/(6.0*pi*ao*visc)) / *pDo;
}
}
return 0;
}

```

```

/*                                     Function: CellProps                                     */

#include <stdio.h>
#include <stdlib.h>
#include <math.h>
#include <definitions.h>

int CellProps(double *temp, double *lp, double *bi, double *delu, double ti, double B,
double realtime, double lmf, double ea, double GC, double ro, double DO, double vs,
double vw, double hf, double to, double rbar, double memphiw, double *Teq, double
centphiw)
{

    double Concw, Concs, sigmaS, molefractw, WatConc, SaltConc, CentMoleFract;
    sigmaS = 2.;

    WatConc = centphiw/vw;
    SaltConc = (1-centphiw)/vs;
    CentMoleFract = WatConc / (WatConc + sigmaS*SaltConc);
    *Teq = 1 / ( (1/to) - GC*log(CentMoleFract)/hf );

    Concw = memphiw/vw;
    Concs = (1-memphiw)/vs;
    molefractw = Concw / (Concw + sigmaS*Concs);

    *temp = ti + B*realtime;
    *lp = lmf*exp(-ea/(GC**temp));
    *bi = (ro**lp*GC**temp) / (DO*vw);
    *delu = (hf/(GC**temp))* ( *temp/to) - 1 ) - log(molefractw);

    return 0;
}

```

```

/*          Function: ModTrapMethod          */

#include <stdio.h>
#include <stdlib.h>
#include <math.h>
#include <definitions.h>

int ModTrapMethod(double *m, double *l, double *u, double *rhs, int N, double
*pdx, double *px, double *pdiff, double *pphi, double dtau, double dRdt, double R,
double w, int flag)
{
/* Define Variables *****/

- x is the nodal location
- A, B, and C, are variables to condense the main equations and facilitate debugging.
-  $D_i = x^2 D_i^n$ 
-  $D_{plus} = (x + dx/2)^2 D_{i+1/2}^n$ 
-  $D_{minus} = (x - wdx/2)^2 D_{i-1/2}^n$ 

    double x, A, B, C, Di, Dplus, Dminus, dx;
    int i;

    /* Internal node discretization */
- This uses the equations from Chapter 3, to determine the lower, main, upper (l,m,u)
  diagonals of A, and the right hand side matrix.

    for (i=1; i<N-1; i++)
    {
        x = *(px + i);
        dx = *(pdx + i);

        Dplus = 0.5*( *(pdiff+i) + *(pdiff+i+1) )*pwr((x+0.5*dx),2) ;
        Dminus = 0.5*( *(pdiff+i) + *(pdiff+i-1) )*pwr((x-0.5*w*dx),2);
        Di = *(pdiff+i)*pwr(x,2);

        A = (Dminus - Di*(1-w)) / w;
        B = ( -Dminus + (w+1)*pwr((1-w),2)*Di - pwr(w,3)*Dplus ) / w;
        C = w*( (1-w)*Di + w*Dplus);

        /* the phi(i-1,n+1) term */
        *(l+i-1) = 0.5*dtau*( (x*dRdt)/(dx*R*w*(w+1)) -
            (2*A)/(w*(w+1)*pwr(x,2)*pwr(dx,2)) );

        /* the phi(i,n+1) term */

```

$$*(m+i) = 1. + 0.5*dtau*((-x*dRdt*(1-w))/(dx*R*w) - (2*B)/(w*(w+1)*pwr(x,2)*pwr(dx,2)));$$

/* the phi(i+1,n+1) term */

$$*(u+i) = 0.5*dtau*((-x*dRdt*w)/(dx*R*(w+1)) - (2*C)/(w*(w+1)*pwr(x,2)*pwr(dx,2)));$$

/* the rhs terms */

$$*(rhs+i) = *(pphi+i)*(1. + 0.5*dtau*((x*dRdt*(1-w))/(dx*R*w) + (2*B)/(w*(w+1)*pwr(x,2)*pwr(dx,2))));$$

$$*(rhs+i) += *(pphi+i+1)*(0.5*dtau*((x*dRdt*w)/(dx*R*(w+1)) + (2*C)/(w*(w+1)*pwr(x,2)*pwr(dx,2))));$$

$$*(rhs+i) += *(pphi+i-1)*(0.5*dtau*((-x*dRdt)/(dx*R*w*(w+1)) + (2*A)/(w*(w+1)*pwr(x,2)*pwr(dx,2))));$$

}

/* Boundary Conditions */

/* Boundary Condition at x = 0 */

$$x = 0;$$

$$i = 0;$$

$$dx = *(pdx+i);$$

/* for phi(i,n+1) */

$$*(m+i) = 1. + dtau*(0.5*(*(pdiff+i) + *(pdiff+i+1)))/(pwr(dx,2));$$

/* for phi(i+1, n+1) */

$$*(u+i) = -dtau*(0.5*(*(pdiff+i) + *(pdiff+i+1)))/(pwr(dx,2));$$

/* the rhs terms */

$$*(rhs+i) = *(pphi+i)*(1. - dtau*(0.5*(*(pdiff+i) + *(pdiff+i+1)))/(pwr(dx,2)));$$

$$*(rhs+i) += *(pphi+i+1)*(dtau*(0.5*(*(pdiff+i) + *(pdiff+i+1)))/(pwr(dx,2)));$$

/* Boundary Condition at x = 1 */

- There are two possible boundary conditions accounted for here. The first is for normal fluctuation of the cell membrane, the other is for nonuniform vitrification.

$$x = 1.;$$

$$i = N-1;$$

if (flag==1)

{

$$dx = *(pdx+i-1);$$

$$Dplus = *(pdiff+i)*pwr(x,2);$$

$$Dminus = 0.5*(*(pdiff+i) + *(pdiff+i-1)) * pwr((x-0.5*dx),2);$$

```

*(l+i-1) = -0.5*dtau*(Dplus + Dminus)/(pwr(x,2)*pwr(dx,2));
*(m+i) = 0.5 + 0.5*dtau*(Dplus + Dminus)/(pwr(x,2)*pwr(dx,2));

*(rhs+i) = *(pphi+i)*(0.5 - 0.5*dtau*(Dplus +
    Dminus)/(pwr(x,2)*pwr(dx,2)));
*(rhs+i) += *(pphi+i-1)*(0.5*dtau*(Dminus)/(pwr(x,2)*pwr(dx,2)));
*(rhs+i) += *(pphi+i-1)*(dtau* *(pdiff+i))/(2*pwr(dx,2)) + (1. -
    *(pphi+i))* (dtau*dRdt)/(R*dx);
*(rhs+i) += (*(pphi+i) - *(pphi+i-1))*(dtau*x*dRdt)/(dx*R);
*(rhs+i) += (1. - *(pphi+i))*(dRdt*dtau)/(R*dx);
}

else
{
dx = *(pdx+i);

*(m+i) = 1 + ( (dtau/pwr(dx,2))* ( *(pdiff+i) + *(pdiff+i-1) ) );
*(l+i-1) = - ( (dtau/pwr(dx,2))* ( *(pdiff+i) + *(pdiff+i-1) ) );

*(rhs+i) = *(pphi+i)*(1 - ( dtau/pwr(dx,2))* ( *(pdiff+i) + *(pdiff+i-1) ) );
*(rhs+i) += *(pphi+i-1)*( (dtau/pwr(dx,2))* ( *(pdiff+i) + *(pdiff+i-1) ) );

}

return 0;
}

```

```
/*                                Function: pwr                                */
- This function calculates the power of a to the b. In the calculation below, b must be
  an integer and positive.
```

```
#include <stdio.h>
#include <stdlib.h>
#include <math.h>
```

```
double pwr( double a, double b)
{
    double answer;
    int j;

    answer = a;
    for (j=1; j<b; j++)
    {
        answer = answer*a;
    }
}
```

- Even though it is more versatile, the below exponential expression that can calculate the power of a to the b requires more clock cycles to evaluate than the above. Furthermore, since the binary analysis does not have decimal exponents (ie $b=0.5$), the below exponential power calculation is not used. This exponential expression is left in case in the addition of cryoprotectants a more complicated power calculation is needed.

```
answer = exp(b*log(a));

return answer;
}
```



```

/*                                     Header File: definitions                                     */

#ifndef definitions
#define definitions

int PostProc(double *vw, double *vs, double Rbar, double *pdx, double *loc, double
*pp, int n, double w);

int Diffusivity(double *diff, double *pDo, double *phiw, int *flag, double *stop, int
*N, double temp, double vw, double vs, double *rdot, double A, double E, double ao,
double Boltz, double betaTg);

int CellProps(double *temp, double *lp, double *bi, double *delu, double ti, double B,
double realtime, double linf, double ea, double GC, double ro, double DO, double vs,
double vw, double hf, double to, double rbar, double memphiw, double *Teq, double
centphiw);

int ModTrapMethod(double *m, double *l, double *u, double *rhs, int N, double
*pdx, double *px, double *pdiff, double *pphi, double dtau, double dRdt, double R,
double w, int flag);

double pwr( double a, double b);

#endif

```

REFERENCES

- Alberts B., Johnson A., Lewis J., Raff M., Roberts K., and Walter P. Molecular Biology of the Cell Fourth Edition. Garland Science, New York, 2002.
- Batycky R.P., Hammerstedt R., and Edwards D.A. Osmotically driven intracellular transport phenomena. *Philosophical Transactions: Mathematical, Physical and Engineering Sciences* **355**: 2459-2488, 1997.
- Dick D.A.T. Cell Water. Butterworth, London, 1959.
- Edwards D.A. Skinning during desorption of polymers: an asymptotic analysis. *SIAM Journal of Applied Mathematics* **59**: 1134-1155, 1999.
- Ellory J.C., and Willis J.S. Phasing out the sodium pump. In "Effects of Low Temperatures on Biological Membranes" (G.J. Morris and A. Clarke, eds.), pp. 107-119. Academic Press, 1981.
- Elmoazzen H.Y., Elliott J.A.W., and McGann L.E. The effect of temperature on membrane hydraulic conductivity. *Cryobiology* **45**: 68-79, 2002.
- Faires J.D., and Burden R. Numerical Methods Second Edition. Brooks/Cole Publishing Company, California, 1998.
- Frankel I., Mancini F., and Brenner H. Sedimentation, diffusion, and Taylor dispersion of a flexible fluctuating macromolecule: The Debye-Bueche model revisited. *The Journal of Chemical Physics* **95**: 8636-8646, 1991.
- Gage A. Selective Cryotherapy. *Cell Preservation Technology* **2**: 3-14, 2004.
- Hallett J., The temperature dependence of the viscosity of supercooled water. *Proceedings of the Physical Society* **82**: 1046-1050, 1963.
- Weast, R.C. *Handbook of Chemistry and Physics*, 57th ed. (CRC, Cleveland, 1976).
- Hua T, Cravalho G, Jiang L. The temperature difference across the cell membrane during freezing and its effect on water transport. *Cryoletters* **3**: 255-264, 1982.
- Jacobs M.H. The simultaneous measurement of cell permeability to water and to dissolved substances. *Journal of Cellular and Comparative Physiology* **2**: 427-444 (1932-1933).
- Jaeger M., Carin M., Medale M., and Tryggvason G. The osmotic migration of cells in a solute gradient. *Biophysical Journal* **77**: 1257-1267, 1999.

- Jaeger M., and Carin M. The front-tracking ALE method: application to a model of the freezing of cell suspensions. *Journal of Computational Physics* **179**: 704-735, 2002.
- Karlsson J.K., Cravalho E.G., and Toner M. A model of diffusion-limited ice growth inside biological cells during freezing. *Journal of Applied Physics* **75**: 4442-4455, 1994.
- Karlsson J.K., Eroglu A., Toth T.L., Cravalho E.G., and Toner M. Fertilization and development of mouse oocytes cryopreserved using a theoretically optimized protocol. *Human Reproduction* **11**: 1296-1305, 1996.
- Karlsson J.K., Toner M. Cryopreservation. In "Principles of tissue engineering" (R.P. Lanza eds.) pp. 293-307. Academic Press, San Diego, 2000.
- Karlsson J.O.M. A theoretical model of intracellular devitrification. *Cryobiology* **42**: 154-169, 2001.
- Kasharin A.V., and Karlsson J.K. Analysis of mass transport during warming of cryopreserved cells. *Annals of the New York Academy of Sciences* **858**: 163-174, 1998.
- Kedem O., and Katchalsky A. Thermodynamic analysis of the permeability of biological membranes to non-electrolytes. *Biochimica et Biophysica Acta*. **27**: 229-246, 1958.
- Kresin M., and Körber Ch. Influence of additives on crystallization kinetics: Comparison between theory and measurements in aqueous solutions. *Journal of Chemical Physics* **95**: 5249-5255, 1991.
- Levin R.L. Kinetics of water transport in biomaterials during freezing. Sc.D. thesis Department of Mechanical Engineering, MIT, June 1976.
- Levin R.L., Cravalho E.G., and Huggins C.E. A membrane model describing the effect of temperature on the water conductivity of erythrocyte membranes at subzero temperatures. *Cryobiology* **13**: 415-429, 1976a.
- Levin R.L., Cravalho E.G., and Huggins C.E. The effect of hydration on the water content of human erythrocytes. *Biophysical Journal* **16**: 1411-1426, 1976b.
- Levin R.L., Cravalho E.G., and Huggins C.E. The effect of solution nonideality on RBC volume regulation. *Biochimica et Biophysica Acta* **465**: 179-190, 1977.
- Levin R.L. Water permeability of yeast cells at sub-zero temperatures. *Journal of Membrane Biology* **46**: 91-124, 1979.

- Luyet B., Rasmussen D. Study by differential thermal analysis of the temperatures of instability of rapidly cooled solutions of glycerol, ethylene glycol, sucrose and glucose. *Biodynamica* **10**: 167-191, 1968.
- Mansoori G.A. Kinetics of water loss from cells at subzero centigrade temperatures. *Cryobiology* **12**: 34-45, 1975.
- Mao L., Udaykumar H.S., and Karlsson J.O.M. Simulation of micro-scale interaction between ice and biological cells. *International Journal of Heat and Mass Transfer* **46**: 5123-5136, 2003.
- Mazur P. Kinetics of water loss from cells at subzero temperatures and the likelihood of intracellular freezing. *Journal of General Physiology* **47**: 347-369, 1963.
- Mazur P., Leibo S.P., and Chu E.H.Y. A two-factor hypothesis of freezing injury-evidence from Chinese hamster tissue culture cells. *Experimental Cell Research* **71**: 345-355, 1972.
- Mazur P. Freezing of living cells: Mechanisms and implications. *American Journal of Physiology* **247**: C125-C142, 1984.
- McGrath J.J. Membrane transport properties. *Low Temperature Biotechnology. Emerging Application and Engineering Contributions*, pp. 273-331, 1988.
- Polge C., Smith A.U., and Parkes A.S. Revival of spermatozoa after vitrification and dehydration at low temperatures. *Nature (London)* **164**: 666, 1949.
- Pushkar N.S., Itkin Y.A., Bronstein V.L., Gordiyenko E.A., and Kozmin Y.V. On the problem of dehydration and intracellular crystallization during freezing of cell suspensions. *Cryobiology* **13**: 147-152, 1976.
- Quinney D. *An Introduction to the Numerical Solution of Differential Equations*, Research Studies Press, Letchworth, pp. 163-196, 1987.
- Richtmyer R.D., and Morton K.W. *Difference Methods for Initial-Value Problems*, Interscience Publishers, New York, 1967.
- Taborek P., Kleiman R.N., and Bishop D.J. Power-law behavior in the viscosity of supercooled liquids. *Physical Review B* **34**: 1835-1840, 1986.
- Tannehill J.C., Anderson D.A., and Pletcher R.H. *Computational Fluid Mechanics and Heat Transfer*, Taylor and Francis, Washington, 1997.
- Thirumala S., and Devireddy R.V. A graphical method for determining the optimal cryopreservation rate of an arbitrary biological system. *Proceedings of the 2003*

Summer Bioengineering Conference, pages 663-664, Key Biscayne, FL, June 25-29, 2003.

- Toner M., Cravalho E.G., Karel M. Thermodynamics and kinetics of intracellular ice formation during freezing of biological cells. *Journal of Applied Physics* **67**: 1582-1592, 1990. (erratum: *Journal of Applied Physics* **70**: 4653, 1991)
- Ushiyama M., Cravalho E.G., Diller K.R. Huggins C.E. Intracellular water content of *Saccharomyces cerevisiae* during freezing at constant cooling rates. *Cryobiology* **10**: 517-518, 1973.
- Vand V. Viscosity of solutions and suspensions. *Journal of Physical Chemistry* **52**: 277-299, 1948.
- Wang N., Butler J.P., and Ingber D.E. Mechanotransduction across the cell surface and through the cytoskeleton. *Science* **260**: 1124-1127, 1993.
- Zwolinski B. J., Eyring H., and Reese C.E. Diffusion and membrane permeability. *Journal of Physical Chemistry* **53**: 1426-2453, 1949.